Thermal Modelling Of Ultrarelativistic Heavy Ion Collisions Conserving Strangeness Exactly

by

Mark Marais

A thesis submitted in fulfilment of the
requirements for the Ph.D degree
in the Department of Physics
University of Cape Town
South Africa

2002

Thermal Modelling of Ultrarelativistic Heavy Ion Collisions Conserving Strangeness Exactly

Mark Marais

Department of Physics, University of Cape Town
Rondebosch 7700, South Africa

Abstract

Thermal modelling of particle production in ultrarelativistic heavy-ion collisions incorporating appropriate conservation principles with respect to the relevant quantum numbers, has been highly successful in determining chemical freeze-out conditions across a wide range of beam energies. This is done for heavy-ion collisions in the broad range of energy from SIS/GSI through AGS/BNL up to SPS/CERN and RHIC/BNL, assuming that particles can be described by a hadron gas in thermal and chemical equilibrium. The role of strangeness conservation and strangeness equilibration is a central feature in our considerations. Fits to the data from collaborations at the above facilities, and, comparisons with analysis done by other authors, are made. Energy dependence of the chemical freeze-out parameters is studied and, recently proposed criteria for freeze-out in terms of energy per particle and total baryon density are investigated. The chemical freeze-out trajectory is compared with the phase boundary between the hadron gas phase and the quark-gluon plasma in the temperature versus baryochemical potential plane.

Research supported by The National Research Foundation (NRF)

There is no excellent beauty
that hath not some strangeness
in the proportion.

Francis Bacon
Essays "Of Beauty"

Preface

The material presented divides naturally into three components. The first part, Chapters 1 to 3, presents the conceptual and theoretical framework of high-energy collisions and the hadron gas model, assuming thermal and chemical equilibrium. Formulations of the partition function are developed in Chapter 3 to include exact conservation of strangeness. Expressions for particle number calculations are obtained from the partition functions for all particles in the hadronic spectrum. In Chapter 4 results from the model are discussed and compared to results from other groups. Chapter 5 incorporates the idea of exact strangeness conservation into a (bag) model used to construct phase transition curves which are compared with the chemical freeze-out points in terms of the temperature, T, and, a baryochemical potential, μ_B. In the final part, Chapter 6, selected topics; freeze-out and hadronization, are reviewed.

Chapter 1 introduces us to the quark-gluon plasma; from conception to creation in ultrarelativistic, heavy-ion collisions, to detection. A review and conceptual perspective is given of the development of a thermodynamical picture of high-energy collisions. The basic assumptions of a thermal model are presented and the different formulisms which are available for describing such a model are discussed. Signatures for the detection of the plasma are discussed. The chapter closes with a brief look at current and future experimental programmes.

Chapter 2 reviews the current status of strangeness and strangeness enhancement in the composition of secondaries as a possible signal for quark-gluon plasma formation.

Chapter 3 develops a thermal model based on the grand canonical approach but, with strangeness being treated exactly. Exact strangeness conservation in heavy-ion collisions is discussed in detail. Partition functions for the full hadronic spectrum are explicitly constructed. Expressions for particle number production, $\langle N \rangle$, are derived from the partition functions using well established techniques. Model parameters are defined and (minimization) procedures to be used in the next chapter are discussed.

The fourth chapter presents the results of the model calculations applied to recent heavy-ion

experiments at the SIS, AGS, SPS and RHIC. The effect of different mass cut-offs as well as a strangeness equilibration factor, γ_s, introduced in the previous chapter, is examined in detail. Comparisons are made with analysis done by other groups of the results obtained for (chemical) freeze-out in terms of the model parameters and a chisquared value, χ^2. Special emphasis is placed on plotting the freeze-out points in the $T - \mu_B$ plane, and, comparing it to freeze-out curves satisfying recently proposed criteria in terms of the energy per particle, and also, the total baryon density.

In Chapter 5 the chemical freeze-out points and theoretical freeze-out curves discussed in the previous chapter, are compared with phase transition curves obtained by developing a model based on ideas of the M.I.T.-bag model. Perturbative QCD corrections are included.

Chapter 6 briefly reviews freeze-out and hadronization in conjunction with final remarks reiterating some of the salient features investigated in earlier chapters.

Appendix A deals with canonical corrections to the grand-canonical formulism in its pure form. This is discussed in the case of a free point-like p, $\overline{p}$ gas as well as in the case of heavy-ion collisions. The limits in which the canonical and grand canonical formulisms become equivalent are discussed.

Appendix B presents a geometrical model for calculating the baryon number, B, and charge, Q, in the case of a central collision between two nuclei of different sizes where the smaller nucleus burrows a hole through the larger.

And, finally, Appendix C derives the form of the single-particle partition function taking resonance widths or, lifetimes, into account.

Contents

List of Figures

List of Tables

Chapter 1

The Fireball: A Quark-Gluon Plasma?

" The structures that can be formed from the interaction of elementary quarks and gluons are, at this time, the most fundamental and represent the frontier of challenges to the human understanding of nature." [1]

1.1 Introduction

The exciting possibility of producing a completely new form of matter and probing key challenges in physics and the evolution of the early universe, has driven the quest to explore nuclear matter under extreme high conditions of energy density and temperature in relativistic high-energy, heavy-ion collisions.

The aim is to create this new state of matter, namely, a quark-gluon plasma (QGP), in the laboratory and thereby recreate the scenario which, according to present theory, occurred in the first few microseconds in the cosmic fireball created in the big-bang.

Hadrons, particles subject to strong nuclear forces, such as protons and neutrons in the nuclei of atoms, are made up of quarks and gluons. By compressing nuclei so that their individual protons and neutrons fuse or overlap, releasing their quark and gluon content, an enormous amount of energy is dumped into a very small volume and it should be possible to create a much greater volume, compared to typical hadron volumes, in which we find a completely new form of matter, namely, a "soup" or plasma of free quarks and gluons. The short time during which this would occur is on the scale of a fermi (3.3×10^{-24} seconds).

The deconfinement or, release of the quarks and gluons and, thus, the phase transition from hadronic matter to a plasma state, is an almost inevitable consequence of quantum chromo-

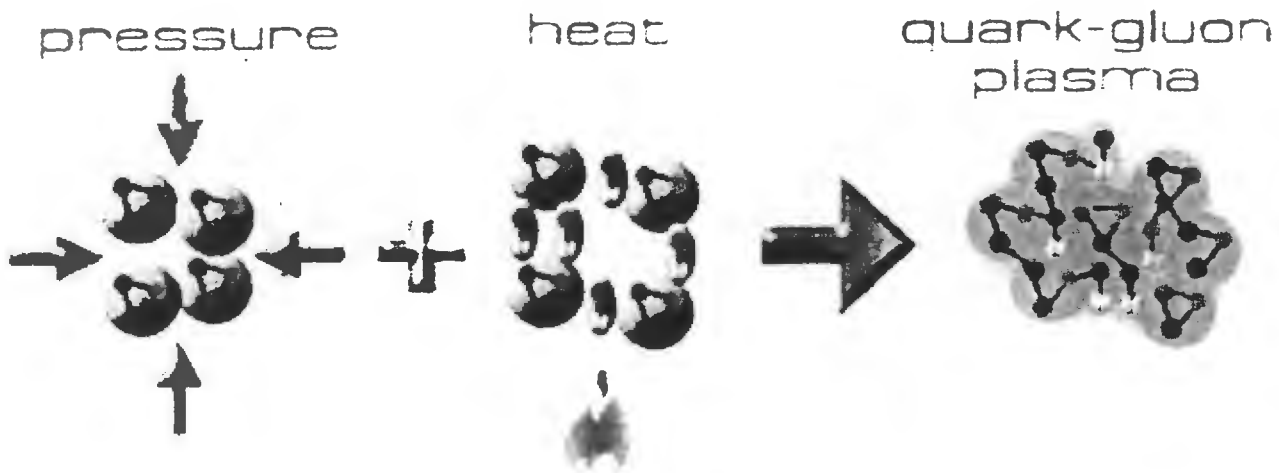

Figure 1.1: *A diagrammatic reprsentation of the phase transition from hadrons to quarks [2].*

dynamics (QCD), the theory of strong interactions which describes the interactions between quarks and gluons. QCD predicts that strongly interacting matter will form a hadron gas at low temperatures and a plasma of quarks and gluons at high temperatures [3]-[6]. Between these two phases is a transition or intermediate phase where colour becomes deconfined and chiral symmetry is restored. The quarks become massless in the final plasma phase.

The QGP, if created, will expand rapidly in an explosive fireball and simultaneously cool before "freezing" or condensing back into confined hadron states like protons and neutrons and a host of many others. The process whereby the quarks and gluons clump or group together into hadrons is known as hadronization.

The normal nucleon density (ρ_0) and energy density (ε_0) of a nucleus is; $\rho_0 \approx 0.14 \frac{\text{nucleons}}{\text{fm}^3}$ and $\varepsilon_0 \approx 130 \frac{\text{MeV}}{\text{fm}^3}$, and, taking the radius of a proton to be ≈ 0.8 fm, the energy density of a proton is $\varepsilon_p \approx 440$ MeV/fm^3. When a nucleus is put into a state where the nucleon density becomes 10 to 15 times greater than ρ_0 and the energy density becomes 15 to 20 times greater than ε_0 or, in a state in which the temperature exceeds a certain critical value (T_c), a phase transition to a QGP is expected to occur [7].

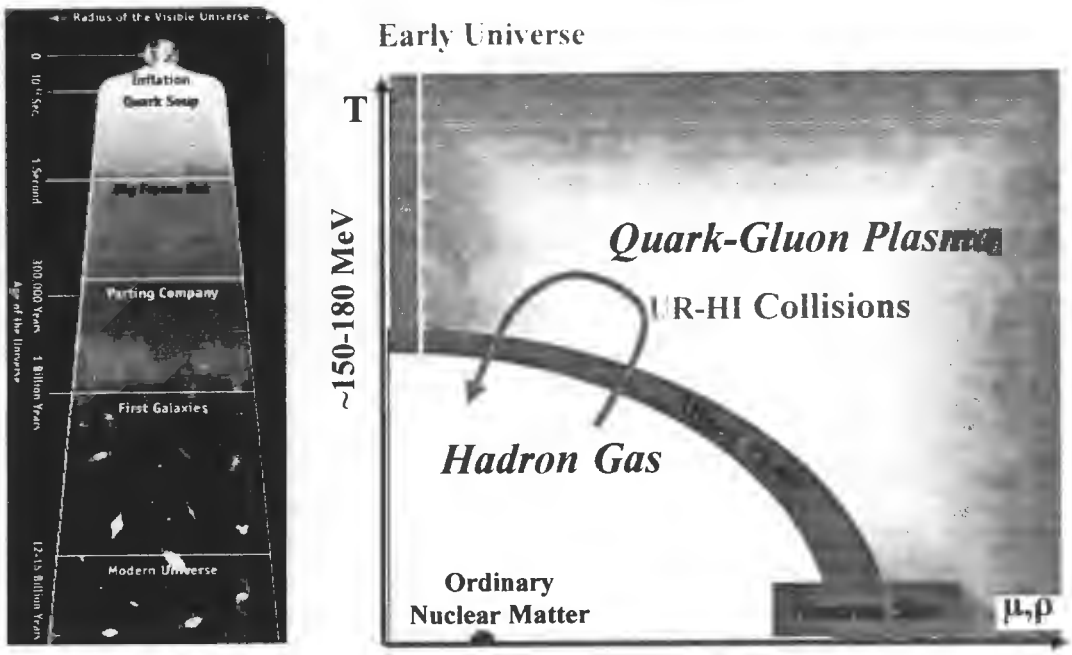

Figure 1.2: *Phase diagram of hadronic matter depicting the transition from hadrons to quarks [8].*

The only way we have today of reaching such extreme conditions in the laboratory or, of exceeding the temperatures governing the early universe 40 microseconds after its birth [9], is with ultrarelativistic nucleus-nucleus collisions [7] using larger atomic nuclei such as gold or lead nuclei. Large amounts of beam energy are directed into a very compact collision zone [10] by colliding two beams of projectile particles head-on or, by directing a relativistic beam at a solid target. Under the extreme high conditions of energy density and/or temperature created in the collision, the hadronic matter in the ensuing fireball could undergo the phase transition to a QGP (a weakly interacting Fermi and Bose gas [11]).

Experiments performed at accelerators, such as at Brookhaven (New York), CERN (European Organization for Nuclear Research - Geneva) and GSI (Gesellschaft für Schwerionenforschung - Darmstadt), yield information about particle numbers produced at certain projectile energies and targets.

The conditions necessary for the existence of the plasma are possibly satisfied in the core of neutron stars where the energy density may be as high as $10-20$ times that of ordinary nuclear matter [12]. A schematic representation depicting the different phases of hadronic matter is shown in Figure 1.2. Shown in the figure is the phase boundary between the QGP and the

hadron gas phase (HG) in terms of temperature and baryon density.

In the quest for the QGP key issues of fundamental importance in making, identifying and probing the QGP in the laboratory include: the mechanism whereby quarks are confined in hadrons, understanding the nature of the phase transition, chiral symmetry breaking/restoration, the process of hadronization and, testing the predictions of (lattice) QCD.

1.2 Existence of Fireballs

The idea of a "fireball" - a region in space where, after a collision, the energy of the longitudinal motion is largely transferred to transverse degrees of freedom [11] or, a cluster of highly excited hadronic matter sticking together for a very short period of time and where the hadron gas phases move with collective motion [13, 14], had begun with Heisenberg's claim in 1936 [15] that a single elementary hadron-hadron collision can give rise to multiple secondary particle production (eleven years before the discovery of the pion!). The first Hydrogen bubble chamber pictures proved Heisenberg correct. Thus, in a single nucleus-nucleus collision a domain in space will arise from which many secondary particles will emanate. This region of production can be thought of as the "fireball".

The fireball can be characterized by the following physical variables:

- energy density,
- baryon number density and,
- total volume.

1.3 Relativistic Collisions

In a nucleus-nucleus collision in the centre-of-mass (c.m.) system the two colliding nuclei approaching each other with relativistic velocities are highly Lorentz contracted ("pancake-shaped"). They overlap either partially as in a peripheral collision or, totally as in a central collision.

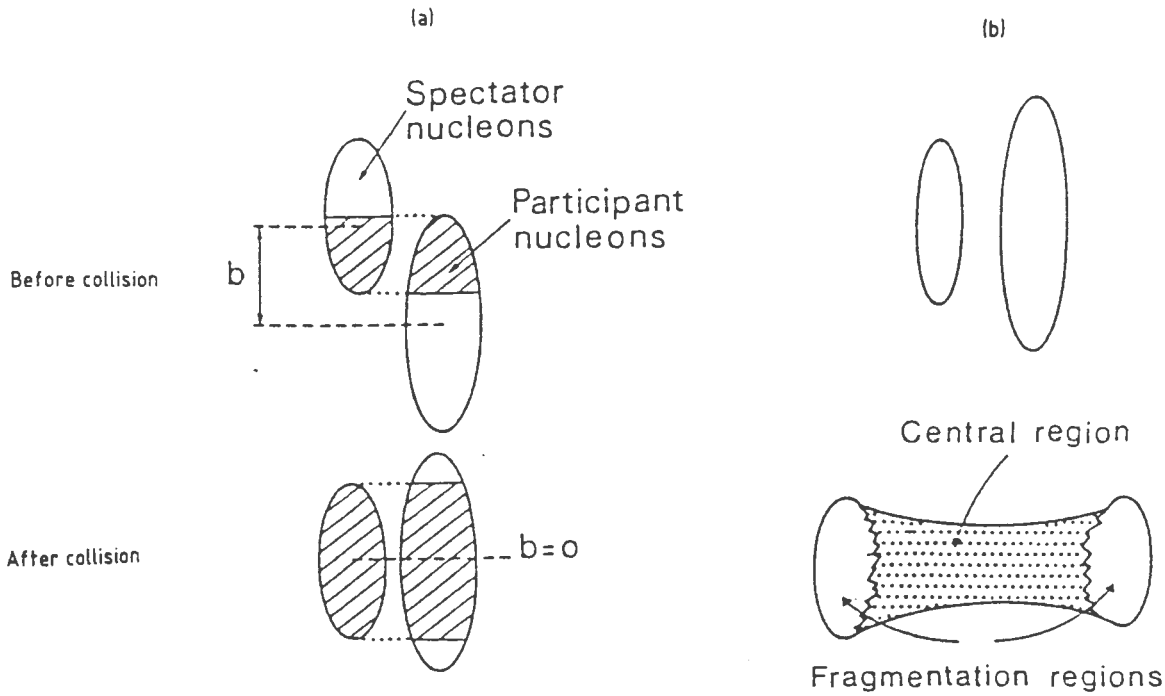

Figure 1.3: *The spatial evolution of a heavy-ion collision in a) a peripheral and b) a central collision [7].*

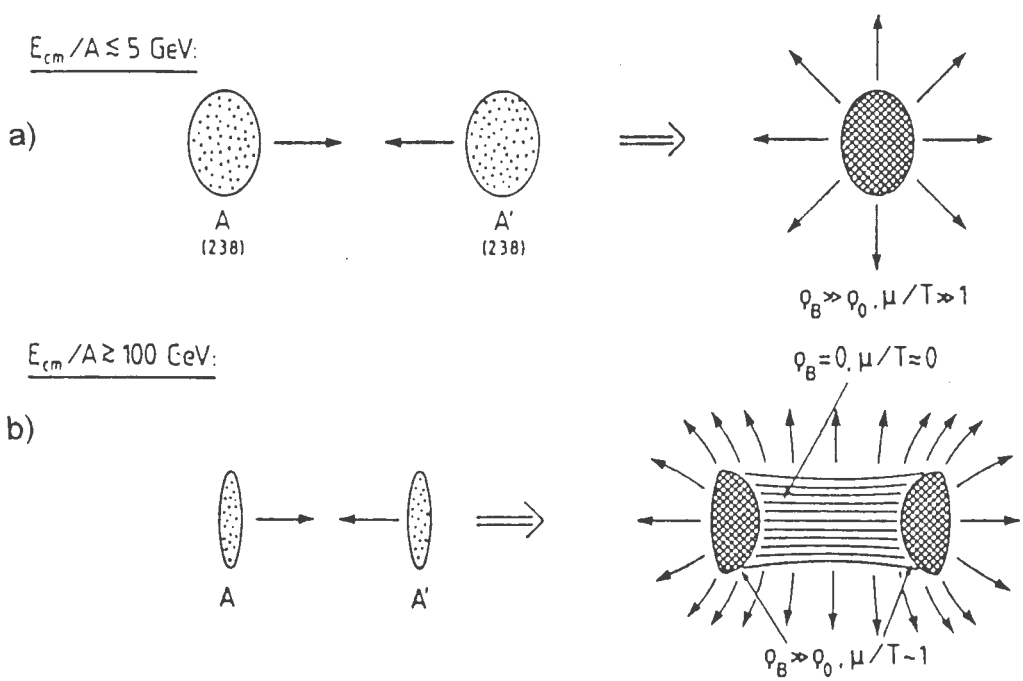

Figure 1.4: *The spatial evolution of a heavy-ion collision in a) the stopping regime and b) the transparent regime [10].*

Figure 1.4 illustrates the difference between a peripheral collision and a central collision. In the former, the nuclei overlap partially with an impact parameter, b (the distance between the centres of the nuclei in the collisions), which can be about as large as the sum of both their transverse radii. Some nucleons of both nuclei do not participate in the collision and are known as spectator nucleons [7]. In central collisions spectator nucleons arise when one of the colliding nuclei is smaller than the other. The smaller nucleus burrows a hole through the larger one and the nucleons at the outer edges of the larger nucleus which do not participate in the collision are, thus, spectator nucleons. An example of this is the collision between a gold nucleus and a smaller silicon nucleus.

Peripheral and central collisions can be distinguished experimentally by measuring the energy released in the collision or the multiplicity of the secondary particles or, both. Both the average energy released and the average multiplicity of the produced particles in the collision are proportional to the number of participating nucleons [7].

It is also important to distinguish between coherent collisions, in which each nucleus interacts as a whole and there is a collective effect of the nucleons, and incoherent collisions, in which there is no collective effect and the collision is a succession of nucleon-nucleon interactions. For the same beam energy the amount of energy in the centre-of-mass frame depends on the degree of coherence in the collision. The greater this is, the greater the energy will be.

Coherent collisions are modelled using either thermodynamics or hydrodynamics whereas incoherent collisions are modelled mainly with the Lund model [16] or the Dual Parton model [17, 18].

In the c.m. frame for the collision between two nuclei they are either stopped completely, thereby using up all the kinetic energy, or, for extremely high-energy ultrarelativistic collisions; the two nuclei now much more Lorentz contracted, essentially pass through each other - a feature known as nuclear transparency which is expected to show its first effects around c.m. energies above 5 GeV/nucleon [19]. In the latter a central region opens up between the target and projectile fragmentation regions (Figure 1.3*b*). The baryon number from the target and projectile nuclei flows strongly into the backward and forward directions rather than getting stopped in the c.m. frame [10] and consequently, the central region contains nearly no net baryon number, consisting mainly of mesons with equal amounts of quarks and antiquarks.

1.4 Thermal Models

In [20] Schukraft notes that in order to reach the QGP, or even to use macroscopic concepts (such as 'phase' transition) and the language and variables of thermodynamics (such as 'temperature' or 'density'), the system has to be *extended*, *i.e.*, its dimensions ought to be much larger than the typical scale of strong interactions - it has to be in (or near) *equilibrium*, *i.e.*, its lifetime has to be larger than the relevant relaxation times - and the *energy density*, ε, has to exceed the critical threshold for QGP formation. Size, lifetime and density thus being important parameters.

Statistical or thermal modelling of particle production assumes that the particles produced in the fireball have interacted sufficiently so that a common temperature may be used to describe all species in the gas. Comparison of measured particle transverse energy (E_t) distributions with calculations using different event generators, one including scattering (the VENUS code [21]) and one without scattering (the FRITIOF code [22]) for the 158 GeV per nucleon lead beam at CERN's Super Proton Synchrotron (SPS), clearly indicates that a considerable amount of rescattering does take place.

Two-particle correlations (or, HBT - Hanbury-Brown and Twiss correlation), which can tell us about the lifetime and size of the particle source, also support this conclusion [23].

One of the most important phenomenological indications of the 'thermal behaviour' of strong interactions and the thermal-like multihadron production in hadron-hadron collisions, is the 'universal' 'soft'-p_t (transverse momentum) distribution plotted as a function of transverse mass, $m_t = \sqrt{p_t^2 + m^2}$, which, in a purely thermal system, will be independent of the particle mass and, with a common slope for all particles which is inversely proportional to the temperature, T, *i.e.*,

$$1/m_t dN/dm_t = m_t e^{-m_t/T}. \tag{1.1}$$

With the momentum distribution thus plotted, all particles from a thermalized emitter would show the same universal exponential behaviour ("m_t scaling"). Although the systematic deviation from a purely exponential m_t at low values of p_t ("low p_t anomaly") can be quantitatively explained by the steeper m_t spectra of resonance decays, hard scattering phenomena - characterized by a power-like tail in the transverse momenta at higher energies and, by an increase

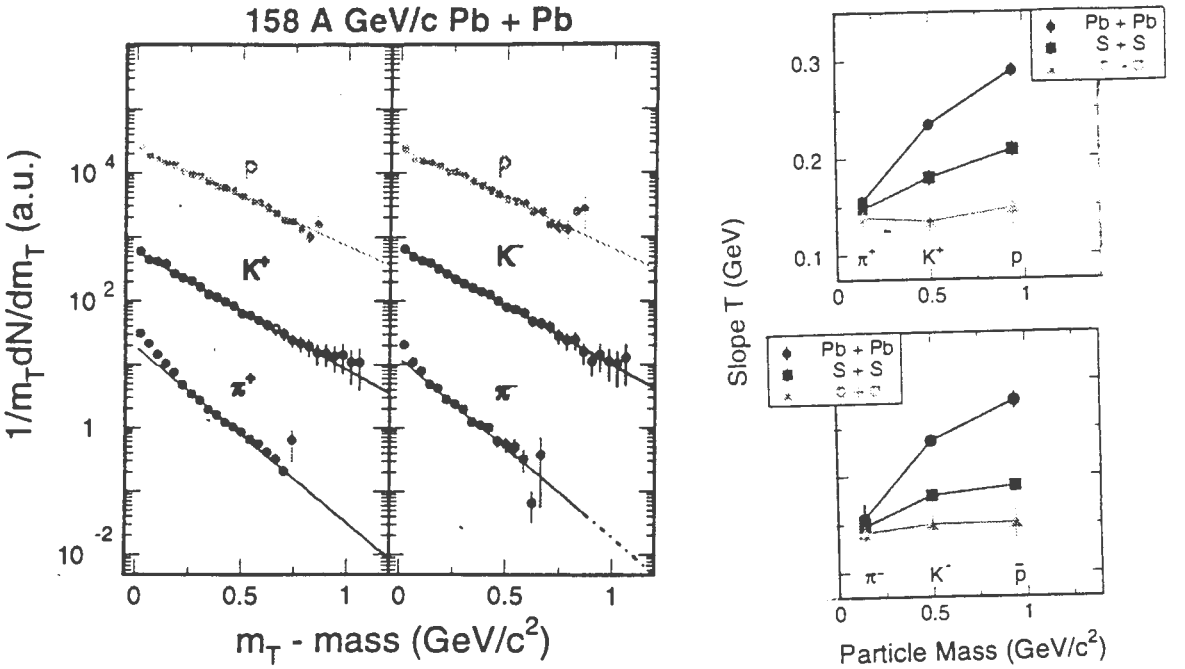

Figure 1.5: *Transverse mass spectra (left) and inverse slope parameters (right) of pions, kaons and protons near midrapidity from NA44 [20].*

in $\langle p_t \rangle$ for higher multiplicity events - cannot, however, be explained within the *Statistical Bootstrap Model* (SBM) phenomenological framework promulgated by Hagedorn in 1964 which contains an exponentially increasing mass spectrum as its most prominent feature.

The right plot of Figure 1.5 shows the inverse m_t-slopes for $p-p$, $S-S$ and $Pb-Pb$ colliding systems at comparable energies ($\sqrt{s} \approx 20$ GeV). We see the slope parameter increasing with the particle mass of the colliding system or, with system size for the heavier reacting systems. In these cases the freeze-out temperature exceeds the Hagedorn limiting temperature, the maximum temperature of a thermalized hadron gas [24]. This picture becomes consistent if, in the expanding system, there is a collective radial flow, mass dependent component in addition to the thermal contribution to the m_t distribution. The sum of these two components can account for the higher than expected freeze-out temperatures obtained. The collective flow component blue-shifts the momentum spectra with a common transverse velocity, β_t, with $\beta_t \approx 0.4c$ describing the data well with freeze-out temperatures of 160 MeV for the NA44 $S-S$ and $Pb-Pb$ data, and, 140 MeV for the AGS $Si-Au$ data [20, 25].

The abundance of particle species in equilibrium hadronic matter can be fully described by only two independent parameters, namely; the temperature, T, and the barochemical potential, μ_B, (as it is usually shown on a phase diagram) which, together with β_t, can fully determine a

hadron gas in thermal (momentum) and chemical (particle abundance) equlibrium.

Production rates of the different hadronic species in the fireball provide a good probe of locally thermalized sources in hadronic collisions since, being a Lorentz invariant quantity, it is not affected by collective motions of the gas [26]. All the thermal manifestations in nuclei-nuclei collisions can be thought of as the outcome of a single fundamental property of strong interactions, namely, that they have an exponential mass spectrum $\rho(m) \sim \exp(m/T_0)$ where T_0 is the singular phase transition temperature [14]. It is now understood that this is a consequence of quark confinement and that T_0 is related to QCD string tension. However, it is not clear what the physical mechanisms are that underlie the assumption of local thermodynamical equilibrium.

A statistical description of particle production provides us with several formulisms which can be used to describe events following a collision. The most often used ones are the:-

- Canonical
- Grand Canonical and,
- Mixed Canonical

descriptions. At relativistic energies particles can be created from kinetic energy, therefore, the canonical description for fixed particle number, N, cannot be used. Thus, with respect to particle number, we are forced in the relativistic scenario to use the grand canonical description. However, with respect to conservation laws which *do* impose constraints on particle number production, a choice between the different formulisms above becomes evident. Hagedorn pointed out in 1968 that the canonical formulism would be more appropriate to use in high energy proton-proton collisions because of small particle numbers and small interaction volumes, and, showed that the production of anti-He^3 is wrong by seven orders of magnitude when the grand canonical formulism is applied in its standard form [13]. This theme has since been considerably developed and expanded in the literature [27]-[32]. It is also found (Reference [33]) that for large interaction volumes a description using the grand canonical ensemble can be justified but, for smaller systems such as in a $p-p$ collision, corrections arising solely from exact strangeness

and baryon number conservation cannot be neglected. This is shown in Appendix A (also [34]) where the effect of imposing exact baryon number conservation in the statistical description of hadronic gas models is investigated for a free point-like proton-antiproton gas and the results compared to the grand canonical ensemble where baryon number holds only as an average over many ensembles.

In the Boltzmann approximation the number of particles of type i, ($i = \pi^+$, K...etc.), N_i, is given by

$$N_i = g_i V \int \frac{d^3p}{(2\pi)^3} e^{\frac{-E}{T}+\frac{\mu_i}{T}} \tag{1.2}$$

where g_i is the spin degeneracy factor, p the momentum, E the total energy, and V is the volume of the system.

The corresponding particle density will be given by

$$n_i = N_i/V. \tag{1.3}$$

Since the model uses statistical weight factors very few parameters are needed to describe the freeze-out stage of the produced system.

At freeze-out all the hadronic resonances decay into the known branching ratios, *e.g.*, for π^+ we have

$$N_{\pi^+} = \sum N_i^0 Br\left(i \rightarrow \pi^+\right). \tag{1.4}$$

The expression for the particle numbers and densities applies to inside a fireball at rest having a temperature, T, and, particle i having a chemical potential, μ_i.

For a system in chemical equilibrium, the possible values of μ_i are determined by the overall chemical potentials for:

$$\begin{aligned} \textit{baryon number} &= \mu_B \\ \textit{strangeness} &= \mu_S \\ \textit{charge} &= \mu_Q. \end{aligned} \tag{1.5}$$

1.5 Equilibrium Stages in the Evolution of the Fireball

We sketch a brief overview in the QGP scenario of the transition from "cold" nuclear matter to a quark-gluon plasma and its eventual condensation into hadrons.

Time scales involved are the equilibration time, τ_0, the delay due to a possible first order phase transition, the conversion rate from one phase to the other, the expansion rate and, the freeze-out time [35]. The total time for the "little bang", as mentioned before, is of the order of a fermi.

Temperature scales that should be noted are the the initial temperature at which local thermal equilibrium occurs, the transition temperature, possible values of superheating/supercooling effects and, the decoupling (freeze-out) temperature [35].

Thermal freeze-out occurs when elastic collisions between hadrons cease.

After the initial interpenetration of the projectile and target lasting $\sim$ 1.5 fm/c and, probably also corresponding to the time required to reach chemical equilibrium of gluons and light non-strange quarks [36], a time period ($\cong$ 5 fm/c) during which the production and equilibration of strange quarks takes place, follows. The fireball expands at constant specific entropy per baryon.

A region between the phase transition and chemical freeze-out, namely; an interacting thermalized hadron gas in which reactions between hadrons are in chemical equlibrium, forms an intermediate phase between the break-up, or hadronization, of the expanding QGP fireball and, the temperature at which chemical interactions cease and particle abundances are fixed.

1.6 Experimental Observables

Experimental observables from collisions can be divided into two categories. These are:

- global hadronic observables (*e.g.,* particle multiplicity, transverse energy, E_T, charged particle distributions, p_T distributions, particle production cross-sections and two-particle correlations).

  They provide information about the system at freeze-out such as energy density and size.

- signature observables, *i.e.,* observables which could serve as possible signals for the phase transition to a QGP (*e.g.,* dileptons, direct photons, J/ψ suppression, strangeness enhancement).

  Signals can be classed into two groups, namely; those providing information about the early stages of the system directly after the collision such as direct photons, and, those pertaining to the late stages in the evolution of the system such as strangeness enhancement.

  A brief description of a few proposed signatures for the QGP follows.

1.7 Signatures of the QGP

Direct Photons

A photon produced in the QGP will leave the plasma with a probability much smaller than that of hadrons to interact and, would retain the memory of the plasma temperature. This makes it a good signature of the QGP provided it can be distinguished from photons produced by hadronic decays, *e.g.,* $\pi^0 \rightarrow 2\gamma$ and $\eta \rightarrow 3\pi^0 \rightarrow 6\gamma$. Since the pions are mainly radiated off the surface and photons are produced throughout the fireball, very heavy-ion collisions may result in a fairly large n_γ/n_π ratio ($\simeq 0.2$ for, *e.g.,* uranium). Also, since photon production through the interaction of quarks and gluons resembles Compton scattering of a photon off a charged particle, the photon production rate and the photon momentum distribution depend on the momentum distribution of the quarks and gluons at the time of the photon production, which means that the photon spectrum tells us about the thermodynamic state of the system at a very early stage [38].

Charmonium Suppression

Charmonium particles (J/ψ, χ, Ψ') consist of the heavy charm quark and antiquark (c and $\bar{c}$) bound together. Since the charm quarks are about ten times heavier than the strange quarks, $c\bar{c}$ pairs can only be formed during the very early stages of the collision when the nuclei penetrate each other. However, if a QGP is formed the gluons in the plasma will interact with the charm quarks in such a way that hinders their binding [9].

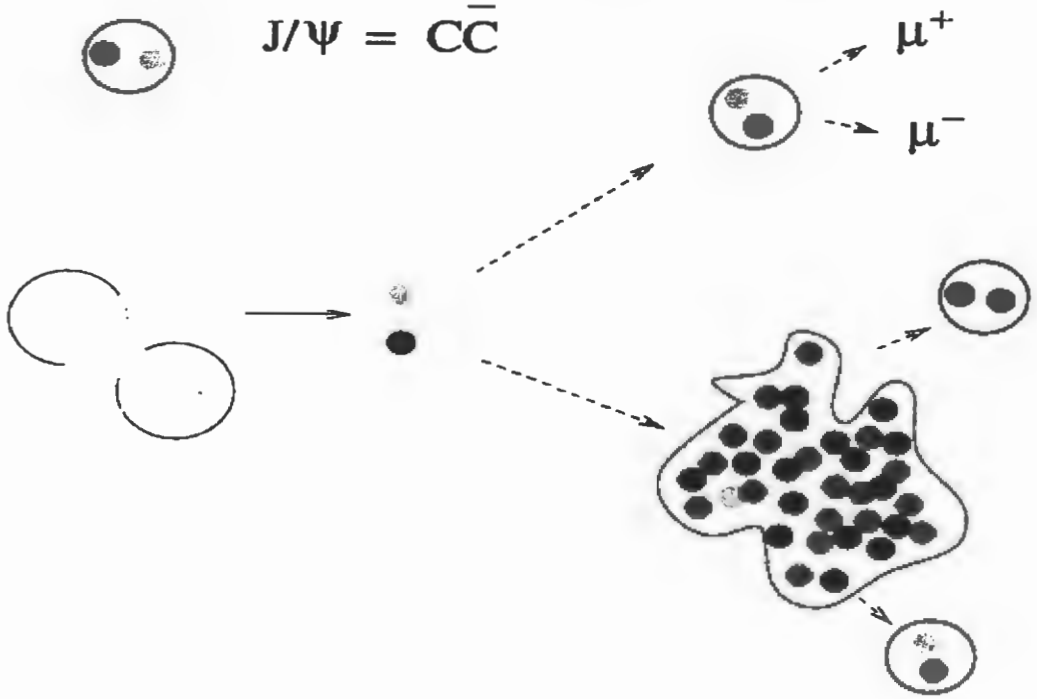

Figure 1.6: *A schematic representation of the J/ψ suppression mechanism [37].*

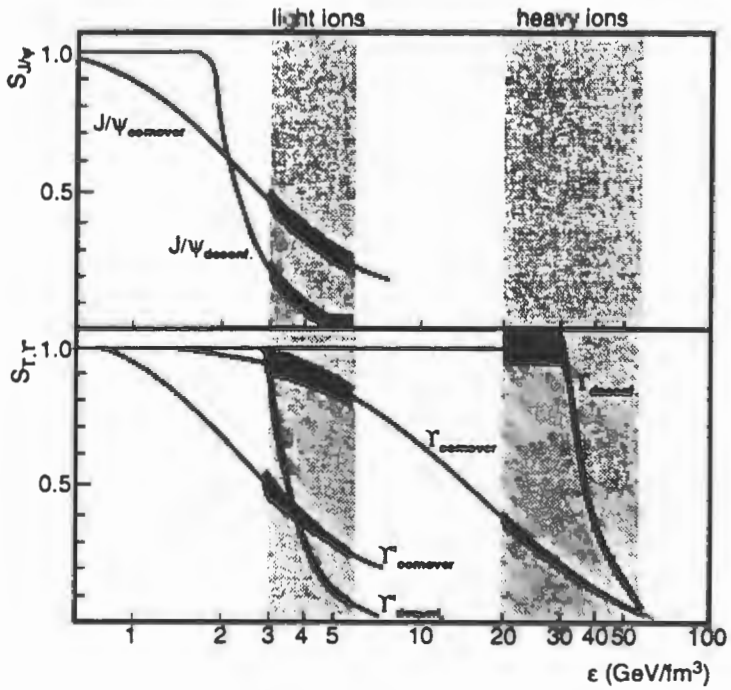

Figure 1.7: *Energy density dependency of charmonium and bottonium survival probabilities as expected from melting in a deconfined medium and from the comover model. The precision of the measurement with the muon spectrometer after one month of operationat the densities expected with light and heavy ions is shown as 1σ error bands (taken from [38]).*

J/ψ production in the plasma can be detected *via* its decay into muon pairs, *i.e.*, $J/\psi \rightarrow \mu^+ + \mu^-$. Muons, like photons, have no strong interactions and, thus, if they are produced in the QGP, leave without interacting. The muons will also carry with them the memory of conditions in the plasma such as temperature.

The suppression of J/ψ production had been predicted by Matsui and Satz [39] prior to any experimental data and relies on a Debye screening mechanism which renders colour interactions short range in a dense medium [20]. The formation of a QGP would have a strong colour field thereby inhibiting the attractive potential necessary for c and $\bar{c}$ quarks to bind.

Experimental results from the NA38 and NA50 experiments at CERN confirmed this prediction but alternative interpretations have been forwarded. Interpretations broadly fall into two categories, namely; those which assume a QGP has been formed, and, those which attribute the suppression to inelastic collisions of the J/ψ with extremely dense hadronic matter created in the collision.

In order to distinguish between suppression as a result of QGP formation and other models, a sufficiently large energy-density region will be covered by the ALICE detector's dimuon arm under construction for the Large Hadron Collider (LHC) at CERN by taking measurements using light- and heavy-ion collisions.

Studying the energy dependence of the survival probability, threshold behaviour for melting would show whether or not the the suppression is due to the formation of a QGP [38].

Strangeness Enhancement

The amount of strange particles produced in collisions is a promising signal for deconfinement - an increase in the number of strange particles produced in heavy-ion collisions compared to their production in hadon-hadron or hadron-nucleus collisions, such as proton-proton or proton-nucleus collisions, was one of the first proposed signatures for QGP formation [40]. As pointed out in [35] however, it is not necessary to have a theorertical explanation in terms of a short-lived QGP since rescattering processes in hot hadronic matter can also change the ratios in the same direction. Enhancement has been observed in nucleus-nucleus collisions relative to $p-p$ collisions at beam energies in which the temperature is too low to form a QGP, for example, the number of kaons per pion produced in $Au-Au$ collisons at Brookhaven's AGS

accelerator is much higher when compared with $p-p$ collisions at the same energy. This can be explained in terms of the fact that kaons are singly strange and easily produced in the final stage expanding hadron gas in which the hadrons react with one another [41].

Therefore, of great interest in resolving the question of strangeness enhancement as a signature for the QGP is the focus on the amount of multistrange particles, that is, particles having two or three strange quarks, produced in a heavy-ion collision, since the enhancement effect is expected to be more pronounced. These particles are less likely to be produced in reactions in the hot hadron gas for key reasons outlined below.

The enhancement of strange particles, particularly strange antibaryon production, in a QGP phase as opposed to in a hadron gas phase, hinges on the fact that the rate of strange pair ($s\bar{s}$) production in the QGP *via* gluon fusion is faster than by hadronic processes in the hadron gas (a few fm/c as opposed to a few 10 to 100 fm/c) since the mass of the strange quark is of the order of the phase transition temperature. Strange phase space saturation thus proceeds much faster in the QGP.

Another distinguishing feature between a QGP and a hadron gas as far as strangeness neutrality goes is that strangeness conservation in a QGP requires a vanishing strange quark chemical potential, *i.e.*, $\mu_s = 0$, independent of temperature or baryon chemical potential, μ_B, while in a hadron gas strangeness neutrality depends on a variety of strange mesons and baryons all of whose abundances depend on μ_B [42].

1.8 Relativistic Nuclear Beams and the making of the QGP

Today, the main experimental programmes dedicated to the study of matter under extreme conditions of temperature and energy density in relativistic heavy-ion collisions happen at the following facilities:

- the AGS (Alternating Gradient Synchrotron) at Brookhaven - accelerating silicon and gold nuclei at beam energies of 14.6 and $2.0-11.6$ GeV per nucleon respectively and centre-of-mass energies per nucleon-nucleon collision ($\sqrt{s_{NN}}$) of 5.4 and $2.2-4.8$ GeV respectively.

- the SIS accelerator at GSI - accelerating nickel and gold at a beam energy of $0.8 - 1.9$ GeV per nucleon and $\sqrt{s_{NN}}$ of $1.5 - 2.1$ GeV.

- the SPS accelerator at CERN - fixed target experiment accelerating sulphur and oxygen nuclei, beam energy of 200 GeV and $\sqrt{s_{NN}}$ of 19 GeV, and lead nuclei, beam energy of 158 GeV and $\sqrt{s_{NN}}$ of 17 GeV.

- RHIC (Relativistic Heavy Ion Collider) at Brookhaven - colliding beam experiment where gold nuclei are made to collide with beam energies of $30 - 100$ GeV, about 100 times their rest mass, and $\sqrt{s_{NN}}$ of $60 - 200$ GeV.
  The first results from RHIC show a greater symmetry between matter and antimatter with a collision energy 7.5 times the SPS energy and the energy density 60% greater.

Beyond RHIC we look forward to the completion of ALICE (A Large Ion Collider Experiment), a colliding beam experiment and dedicated heavy-ion experiment at the Large Hadron Collider (LHC) at CERN, due for completion by 2006. ALICE will operate with a beam energy of 3500 GeV per nucleon and$\sqrt{s_{NN}}$ of 3000 GeV, that is, about 30 times more than at RHIC and with 400 times more energy available than at the SPS.

ALICE represents the future of ultrarelativistic heavy-ion experiments and will bring us closer than ever before in successfully answering crucial questions in our search for the quark-gluon plasma.

Chapter 2

Perspectives on Strangeness Enhancement (?)

We extend our overview with a review of strangeness enhancement, including strange antibaryon to baryon ratios.

2.1 Theoretical Perspectives

Following arguments that, in the case of QGP formation, the dominant process for $s\bar{s}$ pair formation is *via* the interaction of two gluons because of the high gluon density and lower formation energy threshold than in a hadron gas, the enhancement of strange and multistrange mesons and (anti)baryons has long been predicted in the prescence of a QGP compared to a hadron gas at the same temperature, and, thus, suggested as a possible signal for quark deconfinement in heavy-ion collisions [40, 43, 44, 45]. Strangeness equilibration times will also be much faster in a QGP but, as noted by Bass *et al.*, not necessarily sufficiently rapid to cause a saturation in the production of strange hadrons before QGP freeze-out [46]. It has also been shown by Greiner that multimesonic reactions could produce antihyperons on very short time scales [47] while Brown has proposed another mechanism for strangeness equilibration at lower energies involving in-medium modifications of hadron properties [48, 49].
In Reference [50] Redlich discusses what, in experimental terms, based on QGP characteristics, are commonly quoted as signals for deconfinement.

We briefly outline these following his discussion:

1) *global strangeness enhancement* where the strangeness enhancement of secondaries should increase from $p-p$ to $p-A$ through to $A-A$ collisions,

2) *enhancement of multistrange baryons* relative to proton induced reactions should follow deconfinement and,

3) *chemical equilibration of secondaries* where hadronic constituents produced from a hadronizing QGP near chemical equilibrium should in general be driven towards chemical equilibrium after the phase transition.

2.2 Experimental Status and Implications

A synopsis of some relevant experimental results and their implications follows:

- Heavy-ion collisions at CERN's SPS reports a global strangeness enhancement from $p-p$ and $p-A$ through to $A-A$ collisions [51] - for instance, full phase data for $(K+\overline{K})/<\pi>$ from NA35 and NA49 show an increase by about a factor of two when going from $p-p$ to $A-A$ collisions.

- An enhancement of the K/π ratio has been measured at both the AGS and SPS [52]. In Figure 2.2*a* experimental 4π yields of the K^+/π^+ ratio increases as a function of $\sqrt{s}$ from SIS to AGS energies, reaching a maximum at $\sqrt{s}\sim 6-8$ GeV, and dropping at SPS [53]. For midrapidity results (Figure 2.2*b*) the drop at SPS disappears. The suppression of the K^+/π^+ ratio seen for the 4π data has been pedicted by Gazdzicki *et al.* as a possible signal for deconfinement [50, 54].

- K^+/K^-, $\overline{\Lambda}/\Lambda$ and $\overline{p}/p$ production have also been measured at the AGS [55].

- Enhanced production of (anti)hyperon yields have been measured at the SPS [56]-[63].

- The WA94 collaboration, for instance, finds a smooth increase in $\overline{\Xi}/\overline{\Lambda}$ in going from $p-p$ through $p-A$ to $A-A$ collisions [64].

- A hierarchy in the enhancement of multistrange baryons is obtained for $Pb-Pb$ relative to $p-Pb$ collisions in measurements by the WA97 and NA57 collaborations [65, 66].

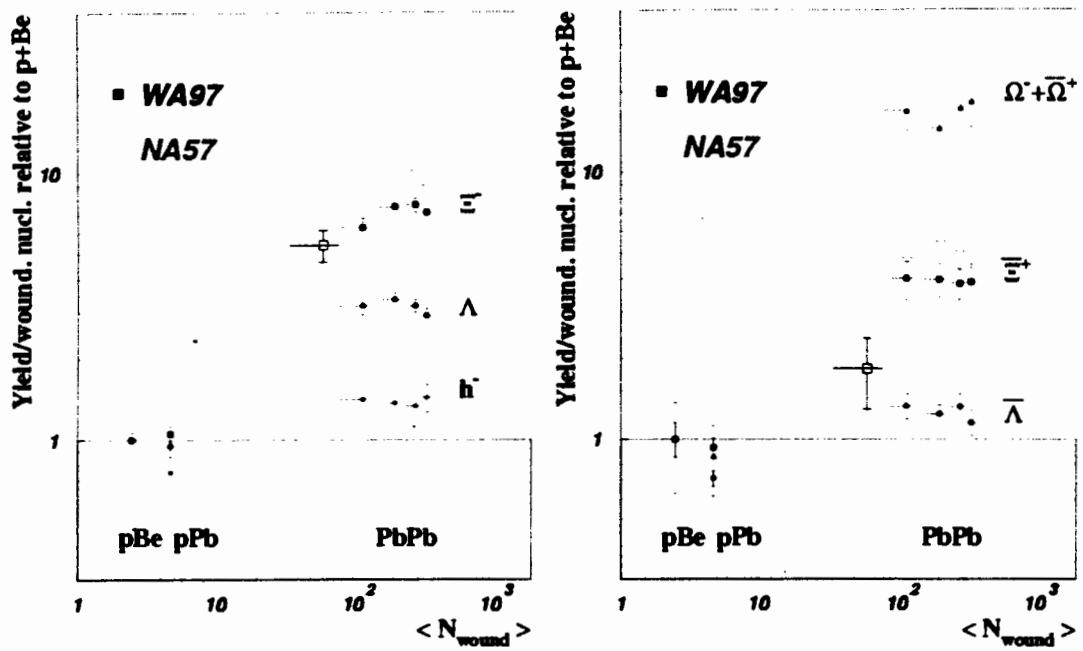

Figure 2.1: *Particle yields per participant in Pb-Pb relative to p-Be and p-Pb collisions centrality dependence. The data are from the WA97 [65] and NA57 collaborations [66].*

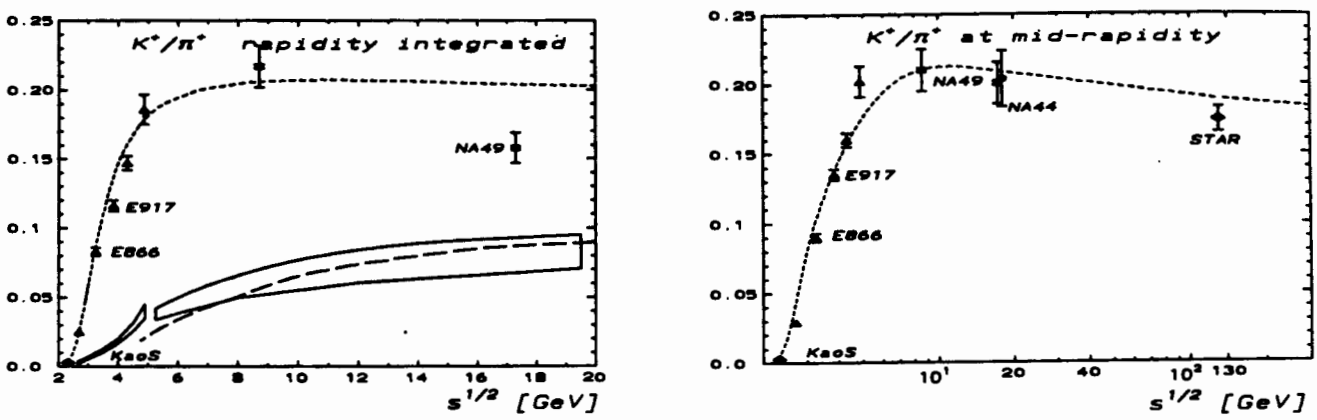

Figure 2.2: *The K^+/π^+ ratio versus the c.m. energy for a) 4π data, b) midrapidity results[53]. Short dashed and dashed lines are for thermal model results [50] and solid lines represent a parameterization of p-p data [67].*

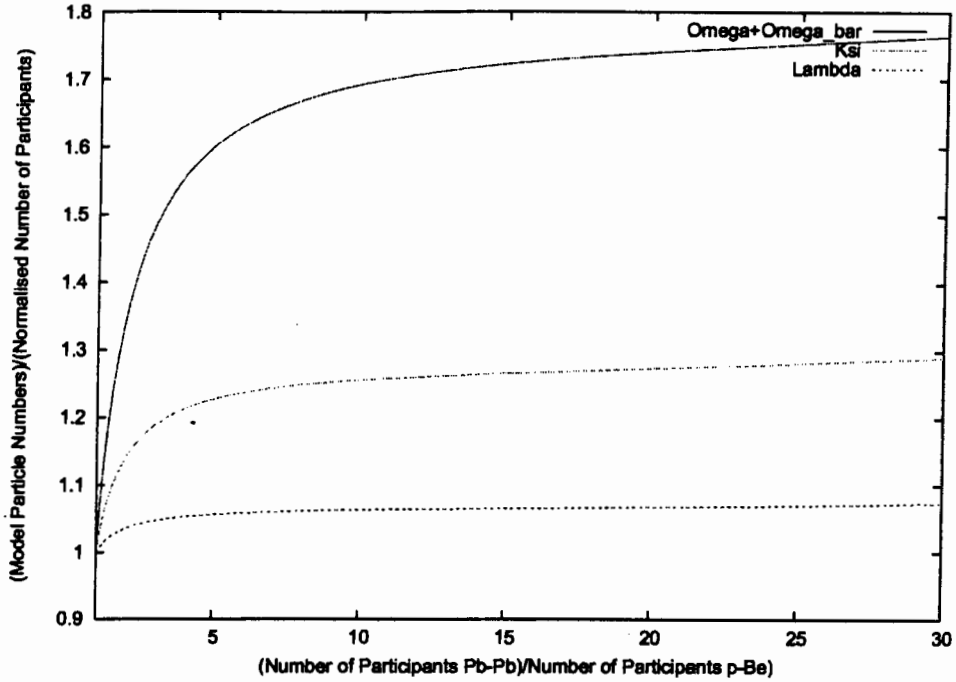

Figure 2.3: *Particle multiplicities per participant as a function of $A_{part.}$ in the statistical model using the canonical ensemble and normalized to its value in p-Be collisions(WA97).*

- $\Omega > \Xi > \Lambda$ as seen in Figure 2.1, which shows the yield per participant. The enhancement pattern of the (anti)hyperons increases with strangeness content of the particle until saturation at about $N_{wounded} > 100$.

- Results for NA57 and NA52, however, show an abrupt change in the anticascade enhancement and the K^+ yield respectively for lower centrality [50].

  In the case of WA97 the statistical model with exact conservation of strangeness reproduces the basic enhancement and saturation patterns consistent with the data - assuming that thermal parameters are independent of $A_{participant}$ in Figure 2.3.

- The appearance of a maximum in the relative *strange/non-strange* particle ratios as a function of $\sqrt{s}$, already seen in the K^+/π^+ ratio, is found to be more pronounced for *strange baryon/meson* ratios which are more sensitive to the baryon chemical potential as seen for Λ/π^+ and Ξ^-/π^+ in Figure 2.4. This is related to the sharper decrease of μ_B compared to only moderate changes in T with increasing incident energies above AGS. There is a shift of the maximum to higher energies with increasing strangeness - the higher strangeness content suppressing the dependence of the ratio on μ_B [68, 69].

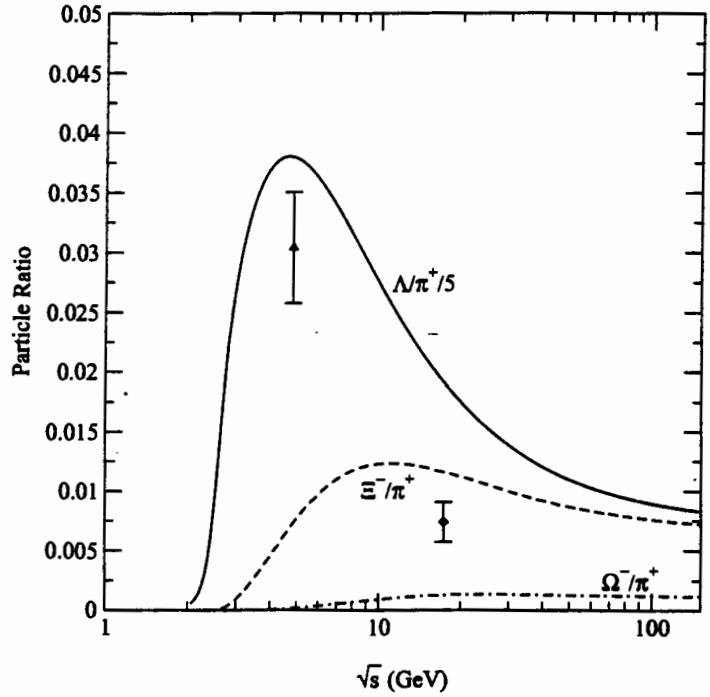

Figure 2.4: *Prediction for the Λ/π^+ ratio (note the factior of 5), Ξ^-/π^+ and the Ω^-/π^+ ratios as a function of $\sqrt{s}$ [68]. Theoretical curves correspond to $\gamma_s = 1$. For a compilation of the data see [70].*

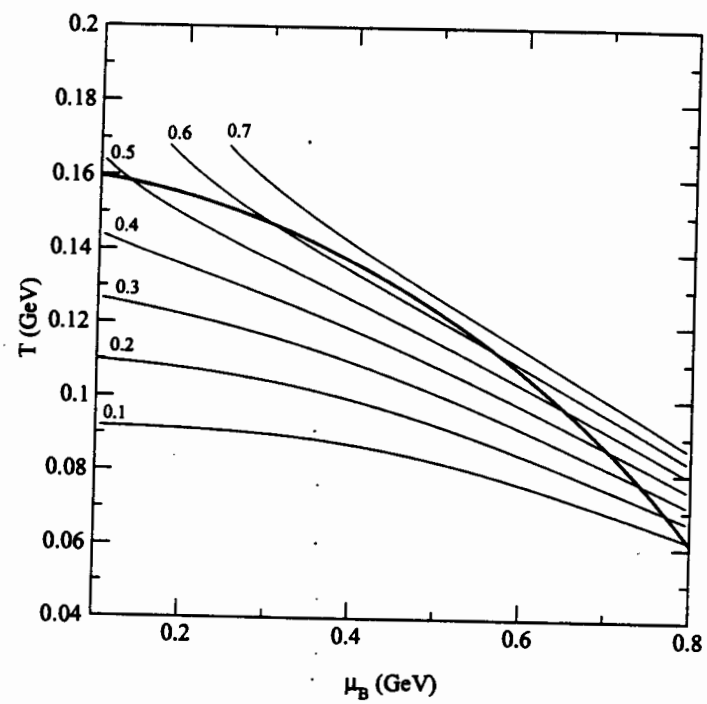

Figure 2.5: *Lines of constant λ_s (thin lines) in the $T-\mu_B$ plane together with the freeze-outcurve (thick solid line) [68].*

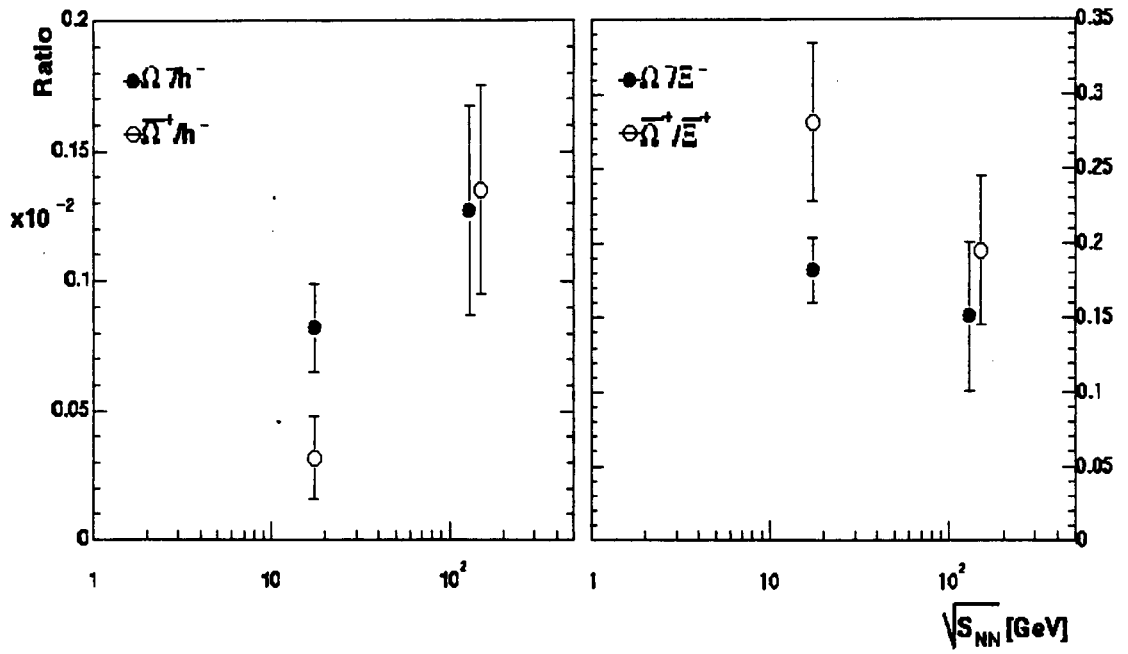

Figure 2.6: Ω/h^- *and* Ω/Ξ *ratios as a function* $\sqrt{s}$ *of at the SPS and RHIC [71].*

- The appearance of the maximum is also reflected in the Wroblewski factor (λ_s, discussed in Chapter 4) as seen in Figure 2.5 where lines of constant λ_s are plotted in the $T - \mu_B$ plane together with the chemical freeze-out curve. λ_s rises with increasing T for a fixed μ_B from SIS to GSI, signalling an increase in the *strange/nonstrange* particle ratios reaching a maximum then, decreasing, signalling a decrease in the ratios with the strange baryons being affected more than the strange mesons as μ_B decreases [68, 69].

- Preliminary results for the Ω/h^- and Ω/Ξ ratios are shown in Figure 2.6 (*a* and *b*). The errors shown are statistical only and, although there are hints at systematic trends toward a multistrange excitation function, for instance, an increase of the Ω/h^- ratio with temperature, more statistics are needed for the study of these ratios as emphasized by J-P Coffin [71].

2.2.1 Quo vadit Strangeness?

The observed strangeness enhancement from $p - p$ through $p - A$ to $A - A$ collisions as an appropriate signal for deconfinement has come under review [50]. Enhancement already appears in some form in $p - A$ collisions [72]; in $p - Pb$ collisions by NA49 measuring $\langle K^+ \rangle$ / $\langle \pi^+ \rangle$ in the forward hemisphere, the ratio shows an increase with the number of collisions due to secondary

production. Also, more than 50% of the the enhancement of the $\left\langle \overline{K} + K \right\rangle / \langle \pi \rangle$ ratio is already accounted for in going from $p - p$ to $p - A$ [50, 73]. Redlich proposes that in order to search for QGP formation through the strangeness composition of secondaries, we should rather be looking for non-monotonic behaviour of strange particle yields versus centrality or collision energy [50].

Blaizot reminds us that statistical models which are so well able to describe freeze-out transitions and which involve constraints on the volume over which matter can be equlibrated, together with the need to conserve quantum numbers exactly in small systems, leads to a change in perspective: "*what is usually regarded as strangeness enhancement in nucleus-nucleus collisions should perhaps better be viewed as strangeness suppression in proton-proton collisions*" [48].

The abrupt enhancement of strange particles reported by the NA57 collaboration [66] as well as inconsistencies between the NA52 and WA97 data may well signal the onset of new dynamics and, as pointed out by Redlich [50], more study experimentally and theoretically is still required here, for instance, it is not clear what the role of centrality dependence is, for example, regarding Ξ and $\overline{\Xi}$.

Chapter 3

Exact Strangeness Conservation in Heavy Ion Collisions

"In relativistic theory chemical potentials regulate not particle numbers but the value of conserved charges...strangeness is conserved as we neglect "slow" weak interactions." [74]

Relativistic heavy-ion collisions analysed in the framework of a grand-canonical formulism with respect to quantum number conservation, is justified on the basis of the high energies obtained in these collisions and the large number of hadrons present in the final state hadron gas [75].

It is also expected that some of the protons and neutrons in the colliding system will not participate in the thermalized hadron gas giving rise to a heat bath of baryons which can thus be treated grand-canonically [76].

In the volume of hot hadronic matter created in a nucleus-nucleus collision, matter is created consisting of a central region containing few baryons, and, two highly excited baryon-rich fragmentation regions so that baryon density varies strongly with respect to rapidity region. A *baryochemical potential*, μ_B, is thus introduced to regulate the conserved baryon quantum number, B, which holds only as an average over many ensembles.

The number of charged particles in the final state is always large thus, charge is also treated grand-canonically. A *charge chemical potential*, μ_Q, is introduced to regulate the conserved charge quantum number, Q, regulating charge conservation on average. The value of μ_Q is fixed by giving the neutron surplus, $B/2Q$, and forcing this to be equal in the hadron gas and the colliding system of protons and neutrons.

Since

$$p \propto e^{+\frac{\mu_B}{T}+\frac{\mu_Q}{T}} \tag{3.1}$$

and

$$n \propto e^{+\frac{\mu_B}{T}}, \tag{3.2}$$

where p and n are the number of protons and neutrons respectively, it follows that

$$\frac{n}{p} = \exp(-\frac{\mu_Q}{T}). \tag{3.3}$$

When the number of initial state protons and neutrons are equal, $\mu_Q = 0$.

This is the case for $S - S$. For $Pb - Pb$, $n > p$ therefore μ_Q is small and negative.

The exact conservation of strangeness (that is, the canonical approach to strangeness conservation) within this framework must, however, be considered [77]-[79] (also, [27]) in cases where the number of strange particles in the final state of the hadron gas is very small, for example, data from GSI SIS, where the temperature is very low [75] or, if a relatively small system size is considered as with the AGS $Si - Au$ data [70].

In heavy-ion collisions we also require the overall strangeness of the system (strange and antistrange particles) to be zero since the strangeness quantum number, S, is conserved with respect to strong interactions [80]. That is,

$$|S| = |n_s - n_{\bar{s}}| = 0, \tag{3.4}$$

where n_s and $n_{\bar{s}}$ are the number of strange and antistrange particles respectively.

In the first section which follows, we develop the formulism for the partition function with exact strangeness conservation for a hadron gas composed of all particles and resonances at chemical freeze-out for the three cases, namely; a gas containing particles of strangeness 0 and $\pm 1; \pm 2; \pm 3$.

The effect of different mass cut-offs is examined in the next chapter in which we use the model to analyse data from Brookhaven's RHIC and AGS, CERN's SPS and the GSI SIS experiments.

Expressions for particle number production are obtained from the partition functions in the second section.

In the third section the model parameters on which the overall multiplicities of hadrons in the final state of the hadron gas depends, are discussed.

In the final section of this chapter we briefly look at the method of fit to the experimental data which is used to find the model parameters at freeze-out.

3.1 The Hadron Gas Partition Function

3.1.1 Case 1: Strangeness $= 0, \pm 1$

This case includes the hyperons, $Y(qqs)$ and $\overline{Y}(\overline{qqs})$, comprising the isosinglet lambda $\Lambda(uds)$ and the isotriplet sigma $\Sigma(i.e., \Sigma^0, \Sigma^{\pm})$ particles. The valence quark content is indicated in parenthesis. For a survey of the strange particle properties, decays and prototype detection methods, see reference [36].

Starting with the following projection [81], *i.e.*,

$$Z_n = \frac{1}{2\pi}\int_0^{2\pi} d\phi e^{-in\phi} Z(\phi), \tag{3.5}$$

we apply this to restrict the ensemble summation to a fixed value of the strangeness, S,

$$Z_S = \frac{1}{2\pi}\int_0^{2\pi} d\phi e^{-iS\phi} Z(T, \lambda_B, \lambda_s, \lambda_Q), \tag{3.6}$$

where the fugacity λ_S has been replaced by

$$\lambda_s = e^{i\phi} \tag{3.7}$$

and $Z(\phi)$ is the generating function for all restricted partition functions:

$$Z(\phi) = Z\left(\lambda_s = e^{i\phi}\right) = Tr\left[e^{-\beta\widehat{H}+i\phi\widehat{N}}\right]. \tag{3.8}$$

The partition function for a gas containing particles of strangeness 0 and ± 1 can be thus be written in the following way [31], [32]:

$$Z_S^1 = \frac{1}{2\pi}\int_0^{2\pi} d\phi e^{-iS\phi} \exp\left(K_0 + K_{+1}e^{i\phi} + K_{-1}e^{-i\phi}\right), \tag{3.9}$$

here K_{+1} stands for the sum of all single-particle partition functions with strangeness plus one:

$$K_{+1} = Z_K + Z_{\overline{\Lambda}} + Z_{K^*} + \cdots, \tag{3.10}$$

and K_{-1} stands for the sum of all single-particle functions with strangeness minus one:

$$K_{-1} = Z_{\overline{K}} + Z_\Lambda + Z_{\overline{K^*}} + \cdots. \tag{3.11}$$

K_0 stands for all non-strange particles.

For vanishing overall strangeness, $S = 0$, Equation 3.9 becomes

$$Z^1_{S=0} = \frac{1}{2\pi}\int_0^{2\pi} d\phi \exp\left(K_0 + K_{+1}e^{i\phi} + K_{-1}e^{-i\phi}\right). \tag{3.12}$$

We can clearly see that baryon number is being treated grand-canonically by looking at the explicit form of, say, Z_Λ, assuming Boltzmann statistics,

$$Z_\Lambda = \frac{2V}{(2\pi)^3}\int_0^{2\pi} d^3p \exp\left(\left(-E_\Lambda + \mu_B\right)/T\right). \tag{3.13}$$

The above form of Equation 3.12 is not convenient for numerical analysis as the integrand is a strongly oscillating function. The ϕ integration can, however, be done exactly as we show below.

Equation 3.12 can be rewritten as

$$Z^1_{S=0} = \frac{1}{2\pi}\exp K_0 \int_0^{2\pi} d\phi \exp\left(\sqrt{K_{+1}K_{-1}}\left[\sqrt{\frac{K_{+1}}{K_{-1}}}e^{i\phi} + \sqrt{\frac{K_{-1}}{K_{+1}}}e^{-i\phi}\right]\right). \tag{3.14}$$

Using the following Bessel function representation,

$$\exp\{\frac{\rho}{2}\left(t + \frac{1}{t}\right)\} = \sum_{-\infty}^{\infty} I_m(\rho)\, t^m, \tag{3.15}$$

where I_m is the modified Bessel function, Equation 3.14 becomes

$$Z^1_{S=0} = \frac{1}{2\pi}\exp K_0 \int_0^{2\pi} d\phi e^{im\phi} \sum_{m=-\infty}^{\infty} I_m(x_1)\, y_1^m, \tag{3.16}$$

with

$$\begin{aligned} \frac{\rho}{2} &= \sqrt{K_{+1}K_{-1}} \\ \rho &= 2\sqrt{K_{+1}K_{-1}} \\ t &= \sqrt{\frac{K_{+1}}{K_{-1}}}e^{i\phi} \\ x_1 &= \rho \\ y_1 &= \sqrt{\frac{K_{+1}}{K_{-1}}}. \end{aligned} \tag{3.17}$$

Performing the integration over ϕ imposes the condition that $e^{im\phi} = 1$, implying that $m = 0$, and, one obtains in closed form free of oscillating terms,

$$Z^1_{S=0} = \exp K_0 I_0(x_1). \tag{3.18}$$

3.1.2 Case 2: Strangeness $= 0, \pm 1, \pm 2$

In this case one includes the doubly strange cascade baryons and antibaryons, the $\Xi^0(ssu)$ and $\overline{\Xi}(\overline{ss}d)$ particles, which have strangeness ∓ 2 respectively.

The partition function can thus be extended in the following way:

$$Z^2_{S=0} = \frac{1}{2\pi}\int_0^{2\pi} d\phi \exp\left(K_0 + K_{+1}e^{i\phi} + K_{-1}e^{-i\phi} + K_{+2}e^{2i\phi} + K_{-2}e^{-i2\phi}\right), \tag{3.19}$$

here K_{+2} stands for the sum of all single-particle partition functions with strangeness plus two:

$$K_{+2} = Z_{\Xi} + Z_{\Xi^*} + \cdots, \tag{3.20}$$

and K_{-2} stands for the sum of all single-particle functions with strangeness minus two:

$$K_{-2} = Z_{\overline{\Xi}} + Z_{\overline{\Xi}^*} + \cdots. \tag{3.21}$$

Equation 3.19 can be rewritten as

$$\begin{aligned} Z^2_{S=0} &= \frac{1}{2\pi}\exp K_0 \int_0^{2\pi} d\phi \exp\left(\sqrt{K_{+1}K_{-1}}\left[\sqrt{\frac{K_{+1}}{K_{-1}}}e^{i\phi} + \sqrt{\frac{K_{-1}}{K_{+1}}}e^{-i\phi}\right]\right. \\ &\left. + \sqrt{K_{+2}K_{-2}}\left[\sqrt{\frac{K_{+2}}{K_{-2}}}e^{2i\phi} + \sqrt{\frac{K_{-2}}{K_{+2}}}e^{-2i\phi}\right]\right). \end{aligned} \tag{3.22}$$

Using the Bessel function representation in Equation 3.15, with

$$\begin{aligned} x_2 &= 2\sqrt{K_{+2}K_{-2}} \\ y_2 &= \sqrt{\frac{K_{+2}}{K_{-2}}} \end{aligned}. \tag{3.23}$$

and x_1 and y_1 as before, Equation 3.22 can be written as

$$Z^2_{S=0} = \frac{1}{2\pi}\exp K_0 \int_0^{2\pi} d\phi e^{im\phi}e^{2in\phi} \sum_{m=-\infty}^{\infty}\sum_{n=-\infty}^{\infty} I_m(x_1)\, y_1^m I_n(x_2)\, y_2^n. \tag{3.24}$$

Therefore, after integrating over ϕ, which imposes the condition that $m+2n=0$, so $m=-2n$, Equation 3.24 can be written in closed form as

$$Z^2_{S=0} = \exp K_0 \sum_{n=-\infty}^{\infty} I_n(x_2)\, y_2^n I_{-2n}(x_1)\, y_1^{-2n} \tag{3.25}$$

or,

$$Z^2_{S=0} = \exp K_0 \sum_{n=-\infty}^{\infty} I_n(x_2)\, I_{2n}(x_1)\, y_2^n y_1^{-2n}, \tag{3.26}$$

since

$$I_n(x) = I_{-n}(x). \tag{3.27}$$

3.1.3 Case 3: Strangeness $= 0, \pm 1, \pm 2, \pm 3$

In the final case we include the omegas, $\Omega^-\,(sss)$ and $\overline{\Omega}\,(\overline{sss})$, which have strangeness ± 3 respectively.

Extending the partition function to include the omegas, we obtain:

$$Z^3_{S=0} = \frac{1}{2\pi}\int_0^{2\pi} d\phi \exp\left(K_0 + K_{+1}e^{i\phi} + K_{-1}e^{-i\phi} + K_{+2}e^{2i\phi} + K_{-2}e^{-i2\phi} + K_{+3}e^{3i\phi} + K_{-3}e^{-3i\phi}\right), \tag{3.28}$$

here K_{+3} stands for:

$$K_{+3} = Z_{\Omega^-}, \tag{3.29}$$

and K_{-3} stands for:

$$K_{-3} = Z_{\overline{\Omega}}. \tag{3.30}$$

Equation 3.28 can be written as

$$\begin{aligned} Z^3_{S=0} \;=\; & \frac{1}{2\pi}\exp K_0 \int_0^{2\pi} d\phi \exp\left(\sqrt{K_{+1}K_{-1}}\left[\sqrt{\frac{K_{+1}}{K_{-1}}}e^{i\phi} + \sqrt{\frac{K_{-1}}{K_{+1}}}e^{-i\phi}\right]\right. \\ & + \sqrt{K_{+2}K_{-2}}\left[\sqrt{\frac{K_{+2}}{K_{-2}}}e^{2i\phi} + \sqrt{\frac{K_{-2}}{K_{+2}}}e^{-2i\phi}\right] \\ & \left. + \sqrt{K_{+3}K_{-3}}\left[\sqrt{\frac{K_{+3}}{K_{-3}}}e^{3i\phi} + \sqrt{\frac{K_{-3}}{K_{+3}}}e^{-3i\phi}\right]\right). \end{aligned} \tag{3.31}$$

Proceeding as before with

$$\begin{aligned} x_3 &= 2\sqrt{K_{+3}K_{-3}} \\ y_3 &= \sqrt{\frac{K_{+3}}{K_{-3}}}, \end{aligned} \tag{3.32}$$

Equation 3.31 can be written as

$$Z^3_{S=0} = \frac{1}{2\pi}\exp K_0 \int_0^{2\pi} d\phi e^{im\phi}e^{2in\phi}e^{3ip\phi} \sum_{m=-\infty}^{\infty}\sum_{n=-\infty}^{\infty}\sum_{p=-\infty}^{\infty} I_m(x_1)\, y_1^m I_n(x_2)\, y_2^n I_p(x_3)\, y_3^p, \tag{3.33}$$

so, by imposing the condition that $m + 2n + 3p = 0 \Rightarrow m = -2n - 3p$,

$$Z^3_{S=0} = \exp K_0 \sum_{n=-\infty}^{\infty}\sum_{p=-\infty}^{\infty} I_n(x_2)\, I_p(x_3)\, I_{2n+3p}(x_1)\, y_2^n y_3^p y_1^{-2n-3p}. \tag{3.34}$$

Relatively rapid convergence is shown in Figure 3.1, the sums converging within ~ 7 terms.

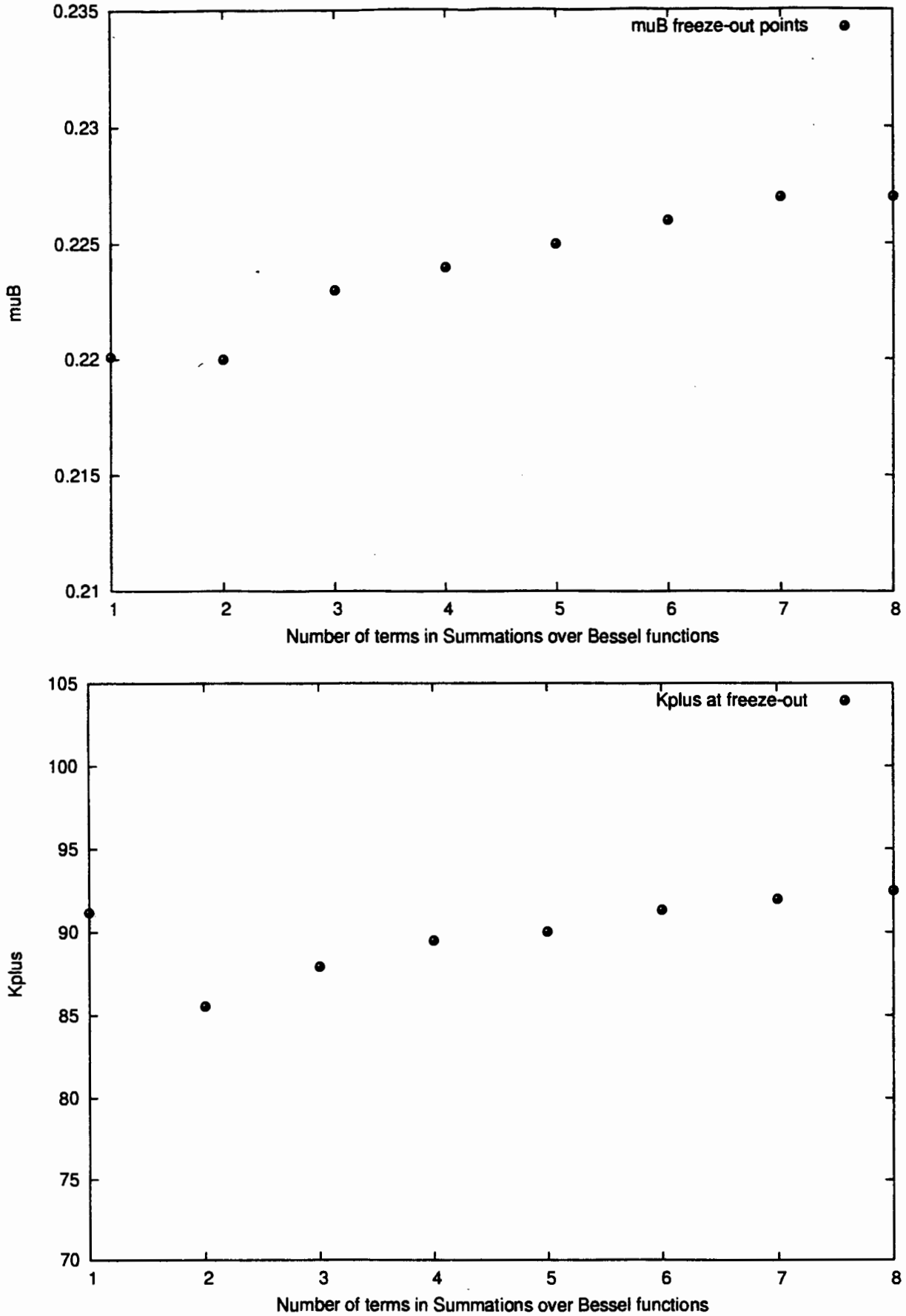

Figure 3.1: *Convergence shown by μ_B (top) and K^+ (bottom) as a function of the number of terms taken in the bessel function sums (CERNS's NA49 Pb-Pb experiment).*

3.2 Particle Numbers

Particle multiplicities can be calculated from the expressions for the partition functions in the usual way of introducing an additional (fictitious) chemical potential for the conserved quantity (in our case strangeness) and projecting out the particle numbers using the standard grand canonical method, namely;

$$\langle N_i \rangle = \frac{T}{Z}\frac{\partial Z}{\partial \mu_i}\bigg|_{\mu_i=0} \tag{3.35}$$

or,

$$\langle N_i \rangle = \frac{\lambda_i}{Z}\frac{\partial Z}{\partial \lambda_i}\bigg|_{\lambda_i=1} \tag{3.36}$$

where $\lambda = e^{\mu/T}$.

The $\mu_i's$ are set to zero afterwards to keep within the canonical formulism for the conserved quantity.

The differentiation of the partition functions leads to an increase or decrease of the index of $I_{index}(x_1)$, and, a corresponding decrease or increase of the exponent of y_1 by $1, 2$ or 3 for $|strangeness| = 1, 2, 3$ respectively, for the expressions in closed form.

This is shown below where the results of carrying out this procedure follows.

3.2.1 Case 1: Strangeness $= 0, \pm 1$

Differentiating Equation 3.18 for particles of $strangeness = \pm 1$, we proceed as follows:

$$\begin{aligned}
\left\langle N^1_{i\pm} \right\rangle &= \frac{Z^1_{i\pm}}{Z^1_{S=0}} \cdot \frac{\partial Z^1_{S=0}}{\partial K_{\pm 1}} \\
&= \frac{Z^1_{i\pm}}{I_0(x_1)} \cdot \frac{\partial I_0(x_1)}{\partial x_1} \cdot \frac{\partial x_1}{\partial K_{\pm 1}} \\
&= \frac{Z^1_{i\pm}}{I_0(x_1)} \cdot I_1(x) y_1^{\mp 1}.
\end{aligned}$$

$\left\langle N^j_{i\pm} \right\rangle$ and $Z^j_{i\pm}$ are the particle abundance and single particle partition function respectively, of species $\pm i$ with $|strangeness| = j$.

3.2.2 Case 2: Strangeness $= 0, \pm 1, \pm 2$

$$\left\langle N^1_{i\pm} \right\rangle = \frac{Z^1_{i\pm} \exp K_0}{Z^2_{S=0}} \sum_{n=-\infty}^{\infty} I_n(x_2)\, I_{2n\pm 1}(x_1)\, y_2^n y_1^{-2n\mp 1}.$$

$$\left\langle N_{i\pm}^{2}\right\rangle = \frac{Z_{i\pm}^{2}\exp K_0}{Z_{S=0}^{2}} \sum_{n=-\infty}^{\infty} I_n\left(x_2\right) I_{2n\pm 2}\left(x_1\right) y_2^n y_1^{-2n\mp 2}. \tag{3.37}$$

3.2.3 Case 3: Strangeness $= 0, \pm 1, \pm 2, \pm 3$

$$\left\langle N_{i\pm}^{1}\right\rangle = \frac{Z_{i\pm}^{1}\exp K_0}{Z_{S=0}^{3}} \sum_{n=-\infty}^{\infty}\sum_{p=-\infty}^{\infty} I_n\left(x_2\right) I_p\left(x_3\right) I_{2n+3p\pm 1}\left(x_1\right) y_2^n y_3^p y_1^{-2n-3p\mp 1}.$$

$$\left\langle N_{i\pm}^{2}\right\rangle = \frac{Z_{i\pm}^{2}\exp K_0}{Z_{S=0}^{3}} \sum_{n=-\infty}^{\infty}\sum_{p=-\infty}^{\infty} I_n\left(x_2\right) I_p\left(x_3\right) I_{2n+3p\pm 2}\left(x_1\right) y_2^n y_3^p y_1^{-2n-3p\mp 2}.$$

$$\left\langle N_{i\pm}^{3}\right\rangle = \frac{Z_{i\pm}^{3}\exp K_0}{Z_{S=0}^{3}} \sum_{n=-\infty}^{\infty}\sum_{p=-\infty}^{\infty} I_n\left(x_2\right) I_p\left(x_3\right) I_{2n+3p\pm 3}\left(x_1\right) y_2^n y_3^p y_1^{-2n-3p\mp 3}. \tag{3.38}$$

Since the above expressions can be shown to strongly suppress (multi)strange particles relative to its grand-canonical value in the limit of small x_i and, to coincide with the grand-canonical result in the limit of large x_i, they are applicable both where a small number of strange particles are produced per event (such as at SIS energies where the number of strange particles is as small as 10^{-2}) and, at the higher energies of SPS or RHIC where over a hundred strange particles are produced on average in each event [69].

3.3 Model Parameters

Relatively few parameters are required in the hadron gas model, which makes use of statistical weight factors, to describe the freeze-out stage in the produced system in ultrarelativistic heavy-ion collisions [82].

The free parameters in our model, which are determined by a fit to the data, are: temperature, T, baryon chemical potential μ_B, radius, R, and an additional strange quark (suppression) factor, γ_s, to account for the fact that the system at freeze-out may not be in perfect strangeness equilibrium ($\gamma_s = 1$).

The volume, V, is taken to be $4\pi R^3/3$, and, since strangeness is conserved exactly, multiplicities or ratios involving strange particles are not independent of V which should be seen as the volume in which we find vanishing strangeness [70].

The multiplicities of neutral hadrons with a fraction f of $s\bar{s}$ content will be modified by the multiplicative factor γ_s^{2f}. All other (strange) hadron multiplicities will be modified according to their strangeness by $\gamma_s^{|Strangeness|}$.

We also investigate a light quark pair (abundance) factor, γ_q, to parameterize the deviation of light quarks from perfect chemical equilibrium [44, 83, 84] where the deviation will be more pronounced if hadronization is a sudden process on the scale of chemical quark equilibration. This scenario involves the sudden break-up of a quark-gluon plasma fireball [85].
In the investigation of the factor γ_q, the multiplicities of hadrons with n_q light quarks will be modified by the multiplicative factor $\gamma_q^{n_q}$.

3.4 Fit to the Experimental Data

In our model we have parameters for which the values are not known for the event in question. We thus need some way of determining the parameter values for the best fit of model generated multiplicities/ratios to the experimental data. The chisquare (χ^2) function utilized by a *minimization* routine (in our case the CERN function minimization and error analysis routine, *Minuit*) fulfills this criteria by allowing us to find parameter values for the best fit to the data or, lowest chisquare.
Minuit computes the best values of the set of parameters (and their uncertainties) where "best" is defined as those values which minimize a given function, in our case a chisquare function which is given by

$$\chi^2 = \sum_{i=1}^{n} \frac{(Model\ value - Experimental\ value)^2}{(Experimental\ Uncertainty)^2} \ . \tag{3.39}$$

For example,

$$\chi^2 = \frac{\left(N^{\pi}_{model} - N^{\pi}_{experimental}\right)^2}{(\sigma_{pions})^2} + \frac{\left(N^{K}_{model} - N^{K}_{experimental}\right)^2}{(\sigma_{kaons})^2} + \cdots . \tag{3.40}$$

The measurement errors are intrinsic is this procedure and is required by *Minuit* to yield meaningful parameter errors which will be proportional to the uncertainty in the data [86]. A variable-metric method with inexact line search relying heavily on first derivatives is used by *Minuit* to carry out the minimization procedure. The χ^2 value is quoted as χ^2 *per degrees of freedom* where the number of degrees of freedom is given by

$$d.o.f. = number\ of\ input\ values - number\ of\ parameters. \tag{3.41}$$

The above technique will be utilized in the chapter which follows to analyse data from heavy-ion collisions done at RHIC, SPS, AGS and SIS.

Chapter 4

Results obtained using Model Calculations

We analyse data from Brookhaven, CERN and GSI in terms of our model in which strangeness is conserved exactly. Comparisons with analysis done by other authors are also made.

A purely statistical-thermal model analysis of experimental particle yields without any consideration of dynamical effects may, as stated in [70] (see also [75]), apply only to data obtained from fully integrated phase space (or 4π) multiplicity measurements. Conservation laws that apply to the collisions are only valid for global measurements, not locally [87].

The requirement of vanishing overall strangeness therefore necessitates full phase space measurements as strangeness need not be conserved in a limited rapidity window.

A major consideration when choosing and discussing data will thus be, whether it was measured over full phase space or, in the absence of this, whether spectra measured in a limited rapidity window have been extrapolated to full phase space.

In the first section we consider and describe the data set to be used.

The effect of different mass cut-offs is discussed in the second section as this becomes a major consideration in thermal models especially at higher temperatures ($\succeq$ 200 MeV).

In the third section strangeness equilibration in terms of the strangeness equilibration factor, γ_s, and its effect on the fit to the data in terms of χ^2, is discussed.

In the final section we present the best-fit results obtained from our model calculations with special emphasis on the plot obtained in the $T-\mu_B$ plane at freeze-out for the various collisions.

4.1 The Data Set

The general rule that we follow in using recently available data is to concentrate on fully integrated particle yields.

A synopsis of the collisions in the data set from which the particle multiplicities and ratios are obtained, is given below.

Pb – Pb Collisions at CERN's SPS - NA49 Collaboration

Central $Pb - Pb$ collisions (5% centrality) with beam momentum of 158 GeV/c per nucleon on a fixed target (see [88] for example) are considered here. The following 4π experimentally measured/extrapolated particle multiplicities are used: $(\pi^+ + \pi^-)/2$, K^+, K^-, K^0_s, p, $\bar{p}$, ϕ, Ξ^-, $\overline{\Xi^-}$ and, the $\overline{\Lambda}/\Lambda$ ratio. It has been found in two independent thermal model analysis in [70] that the temperature is significantly affected by the multiplicity of the heaviest particles namely, ϕ and Ξ, as they are almost entirely directly produced thus providing a major lever arm on the slope of the production versus mass function. However, it is found in the same reference that the exclusion of these particles does not significantly affect γ_s.

Au – Au Collisions at GSI's SIS

In central $Au - Au$ collisions with beam momentum of $1.7A$ GeV/c (see [89] for example), the following (4π) particle ratios are used in the fit: π^+/p, K^+/π^+, π^-/π^+, η/π^0. Because of the small number of available data points the radius will be fixed at 35.5 GeV^{-1} or, 7 fm (assuming a volume given by $4\pi r^3/3$). γ_s will be fixed at one, the value for full strangeness equilibration in a hadron gas.

Si–Au Collisions at Brookhaven's AGS

With $Si - Au$ collisions, beam momentum of $14.6A$ GeV/c (see [55, 90] for example), we make an exception to the rule of having only 4π particle yields or particle ratios by using the $\overline{\Lambda}/\Lambda$ and $\bar{p}/\overline{K}$ ratios [90, 91] which are not available in full phase space. The reason for the exception is that the above ratios are the only recent measurements available involving antibaryons for $Si - Au$; antibaryons playing an effective role in fixing μ_B. The other (4π) particle multiplicities and ratios used in the fit are: π^+, π^-/π^+, K^+/π^+, K^-/π^- and ϕ. The total number of parti-

Table 4.1: Table showing beam energies, centre-of-mass energies per nucleon-nucleon collision, $\sqrt{s_{NN}}$, B and Q for the various colliding systems.

Colliding System	Accelerator	Beam Energy (GeV)	$\sqrt{s_{NN}}$ (GeV)	B	Q
$Au - Au$	SIS	1.7	2.2	197.0	79
Si $- Au$	AGS	14.6	5.4	102.7	44
$Pb - Pb$	SPS (NA49)	158	17	207.2	82
$Pb - Pb$	SPS (WA97)	158	17	207.2	82
$Au - Au$	RHIC	8992	130	197.0	79

cipating baryons are also included.

$B/2Q$ (for $Si - Au$) has been calculated by calculating B and Q using a geometrical model (see Appendix B).

Au – Au Collisions at Brookhaven's RHIC

RHIC data is only available in a very limited kinematical window; pseudo-rapidity coverage limited to the central region, $-0.5 < \eta < 0.5$ ([92]). However, if the energy is sufficiently high such that the data exhibits boost-invariant rapidity plateaus, an analysis in a limited region around midrapidity using particle ratios may still be possible within a statistical-thermal approach which relies on full phase space measurements since, the influence of dynamical effects (*e.g.*, hydrodynamical flow) should have a smaller influence [92, 93]. The average multiplicity per rapidity interval, dN/dy, is approximately flat over a large enough interval on either side of midrapidity. The current energy at RHIC seems close to this regime [92]. The experimentally obtained ratios used in the fit are: π^-/π^+, $\overline{p}/\pi^-$, K^-/K^+, K^-/π^-, K_0^*/h^-, $\overline{K_0^*}/h^-$, $\overline{p}/p$, $\overline{\Lambda}/\Lambda$ and $\overline{\Xi}/\Xi$ from the STAR [94]-[97], PHENIX [98], PHOBOS [99] and BRAHMS [100, 101] collaborations.

Pb – Pb Collisions at CERN's SPS - WA97 Collaboration

The WA97 experiment, using the same beam and fixed target as in NA49, has been designed for the systematic study of the production of the multistrange hadrons, Λ, $\overline{\Lambda}$, Ξ, $\overline{\Xi}$, Ω and $\overline{\Omega}$ in $Pb - Pb$ interactions at SPS energy [102, 103]. Only a limited kinematical region is available, about one unit of rapidity centred at midrapidity.

The strange particles decay *via* weak decays, *e.g.*:

$$\begin{aligned} \Lambda &\rightarrow p + \pi^- + c.c. \\ \Xi^- &\rightarrow \Lambda + \pi^- \\ &\quad \llcorner\, p + \pi^- + c.c. \\ \Omega^- &\rightarrow \Lambda + K^- \\ &\quad \llcorner\, p + \pi^- + c.c. \end{aligned}$$

Residual feeding from Ξ decays into Λ and $\overline{\Lambda}$ are estimated to be $< 5\%$ and $< 10\%$ respectively [102, 104]. The following experimentally obtained particle multiplicities are used in the fit: h^- $(\pi^- + K^- + \bar{p} + \Xi^- + ...)$, K^0_s, Λ, $\overline{\Lambda}$, Ξ^-, $\overline{\Xi^+}$, $\Omega^- + \overline{\Omega^+}$.

Mainly 4π data will be considered for the plot in the $T - \mu_B$ plane with the only exception being the $Au - Au$ RHIC data because of the considerations discussed earlier.

The data set in the foregoing discussion forms the main focus of analysis to follow.
Additional data, used primarily as a supplement to the main focus points for the plot in the $T - \mu_B$ plane, are given below.

<u>**Ni – Ni Collisions at GSI's SIS**</u>

$Ni - Ni$ collisions are analysed analogously to the $Au - Au$ SIS data discussed earlier because of the small number of experimentally obtained ratios available, *i.e.*, by fixing γ_s to one and the radius, in this case, to 20 GeV^{-1}.

- $Ni - Ni$ (0.8 A GeV) - Ratios from central collisions: π^+/p and K^+/π^+ [105].
- $Ni - Ni$ (1.0 A GeV) - Ratios from central collisions: π^+/p, K^+/π^+, d/p [105].
- $Ni - Ni$ (1.8 A GeV) - Ratios from central collisions: π^+/p, K^+/π^+, d/p, K^+/K^- [105].
- $Ni - Ni$ (1.93 A GeV) - In this case we left γ_s as a free parameter in the system. The following experimentally obtained ratios are: K^+/K^-, K^+/π^+, ϕ/K^-, π^+/π^-, π^+/p, π^0/B, d/p [106].

Pb – Pb (40A GeV) Collisions at CERN's SPS

Preliminary NA49 data with beam momentum of 40 A GeV corresponding to a nucleon-nucleon centre-of-mass energy of 8.7 GeV, is analysed using the following particle abundances: π^+, π^-, K^+, K^-, Λ, $\overline{\Lambda}$, N_p [107].

4.2 Effect of Mass Cut-offs

A major problem inherent in thermal models is where to stop the summation over hadronic resonances when determining the overall abundances of hadrons of any type, i, by using $n_i = n_i^{primary} + \sum Br(j \rightarrow i) n_i$, when taking into account the contribution from decays of heavier resonances. With increasing mass our knowledge of the hadronic spectrum becomes less accurate as masses and widths are not well determined. The contribution from possible missing states (starting from about 1.7 GeV) are expected to play an important role for temperatures $\geq$ 200 MeV (see [70] in which two independent analysis using different mass cut-offs of 1.8 and 2.4 GeV have been performed).

In this section we investigate the sensitivity of our model to mass cut-offs as this would influence the reliability of results if the dependence was too strong.

By introducing a low mass cut-off, heavier resonances as well as their decay products from decays into lighter, more stable particles, such as pions and kaons, are eliminated. One thus expects fewer pions and kaons in the final state hadron gas for example.

In order to keep the same (experimental) number for the lighter particles and thus, to compensate for the low mass cut-off, the temperature would have to increase.

Figure 4.1 shows how the (freeze-out) temperature varies as a function of mass cut-off.

From the graph we see a sharp decrease until a cut-off mass of $\sim$ 1.7 GeV. Beyond this the temperature begins to level out. The temperature stabilizes around 2.0 GeV reaching a constant value of 157.1 MeV (at $\sim$ 2.6 GeV). The values of μ_B, γ_s and the volume, V, also stabilize around 2.0 GeV and remain stable from $\sim$ 2.6 GeV onwards

This stabilisation occurs even though a fictitious ('Δ') particle with mass 2.5 GeV and degeneracy, g=100, has been introduced in the table for this plot.

The masses, widths and branching ratios, $Br(j \rightarrow i)$, have been taken mainly from the 1998 issue of the Particle Data Table [108]. Modifications to the single-particle partition function

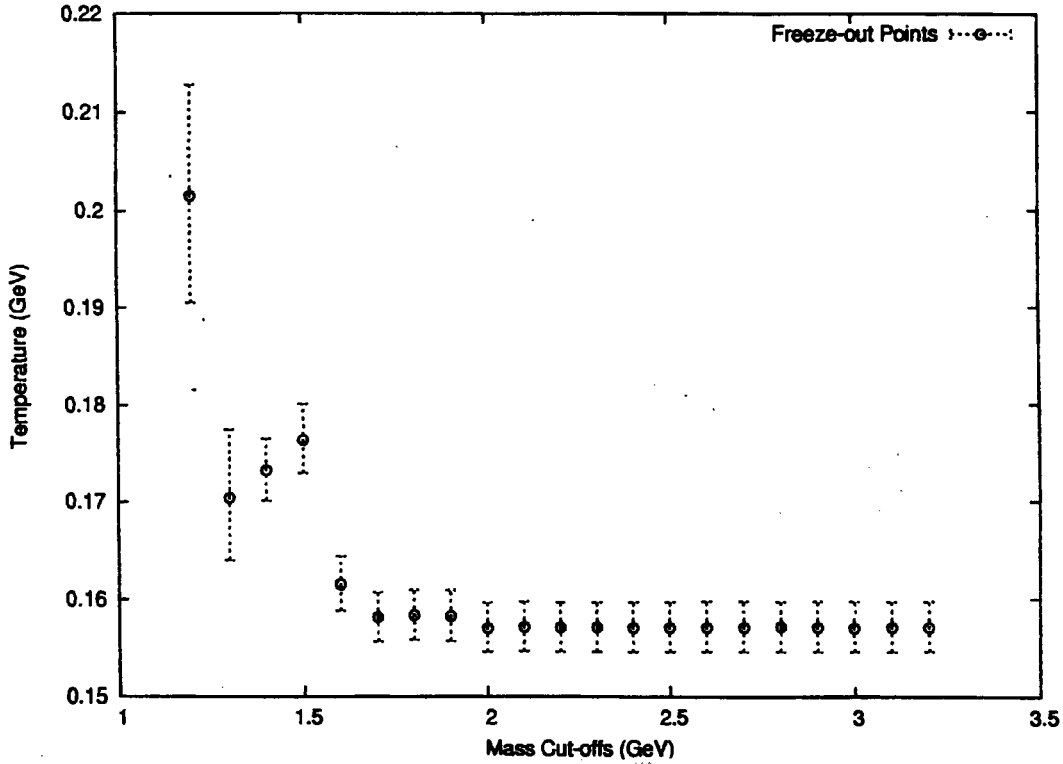

Figure 4.1: *Temperature dependence on Mass Cut-off in the thermal model (NA49).*

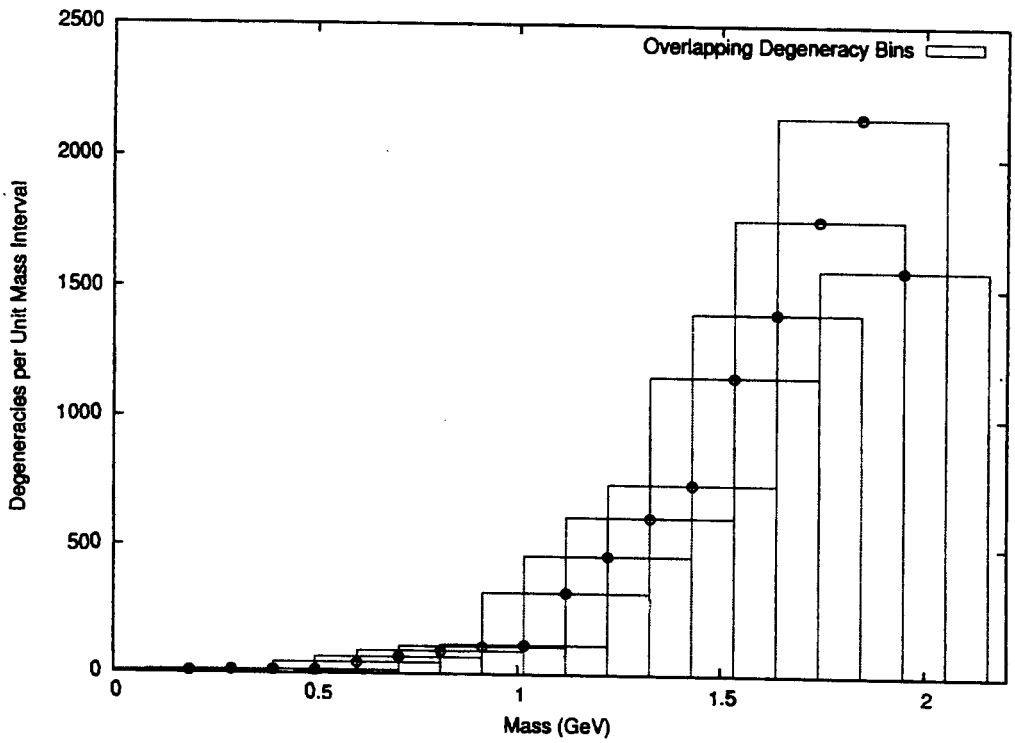

Figure 4.2: *Degeneracy per unit Mass as a function of Mass for the known particle spectrum.*

taking into acount the width of resonance masses is given in Appendix C.

4.3 The χ^2 Contour Surface and γ_s

The three dimensional plots shown in Figure 4.3 of $T - \mu_B - \chi^2$ for the $Pb - Pb$ NA49 data, show the effect on χ^2 of fixing γ_s, the factor measuring the deviation from perfect strangeness equilibrium in the hadron gas, at different values (0.700, 0.799, 0.850, 0.900). We notice an increasing sharpness and depth in the χ^2 minimum of the contour surface as γ_s nears the optimal value of 0.799 (the optimal values for the parameters are discussed in the next section) and greater flattening as it moves away. The flatter the descent and the shallower the χ^2 minimum of the surface, the more difficult the convergence. The shape of the contour around the minimum gives information about the uncertainty in the best parameter values (of T and μ_B in the case of Figure 4.3). A decrease in temperature is observed as γ_s is increased towards one. The degree of strangeness equilibration in percentage in terms of γ_s is given by

$$S_{Equlibration} = \gamma_s \times 100. \tag{4.1}$$

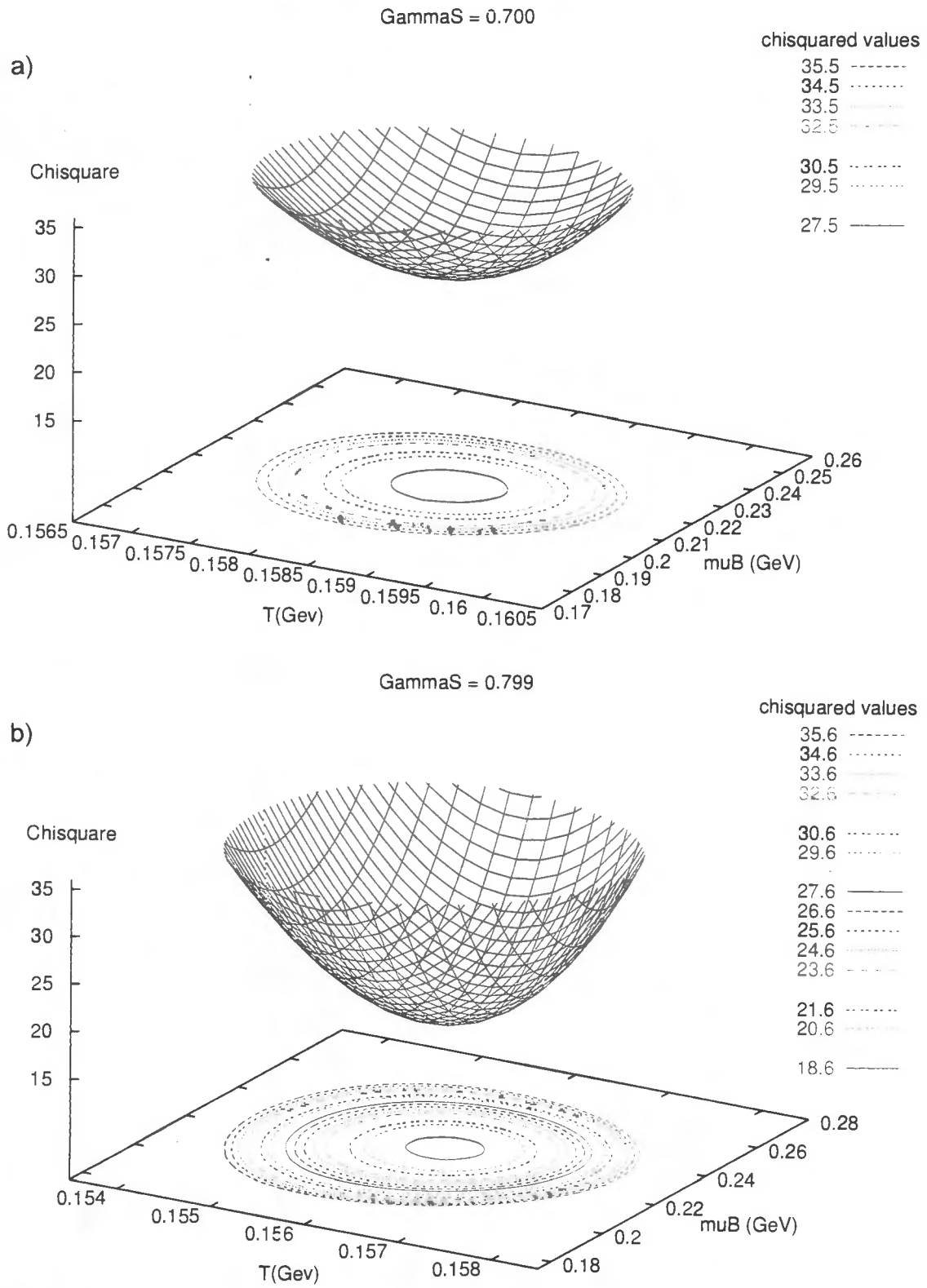

Figure 4.3: *The variation of the χ^2 contour surface for different values of γ_s in $Pb - Pb$ collisions (NA49): a) $\gamma_s = 0.700$, b) $\gamma_s = 0.799$ and overleaf, c) $\gamma_s = 0.850$ and, d) $\gamma_s = 0.900$.*

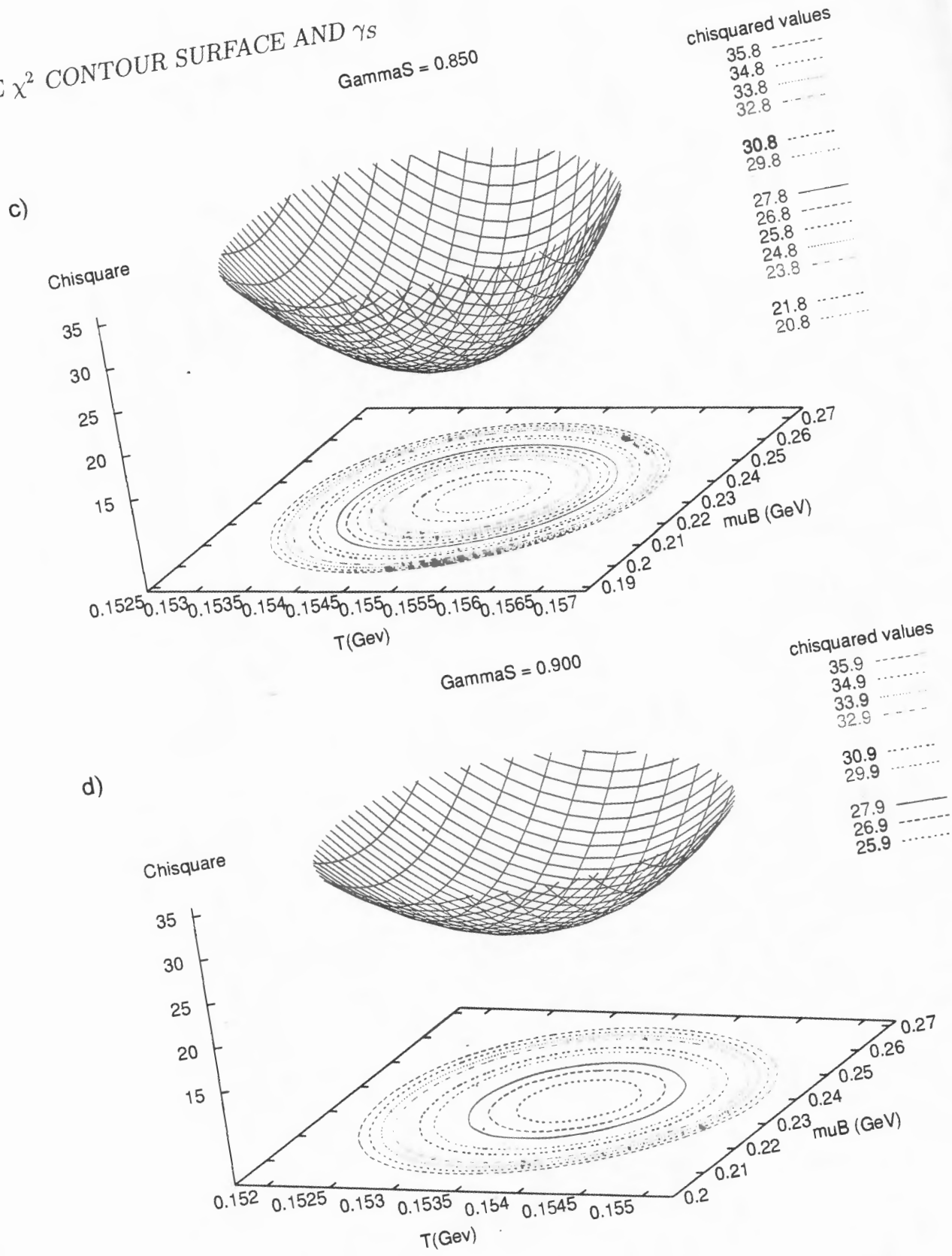
c)
GammaS = 0.850
chisquared values
35.8
34.8
33.8
32.8
30.8
29.8
27.8
26.8
25.8
24.8
23.8
21.8
20.8
Chisquare
35
30
25
20
15
0.1525
0.153
0.1535
0.154
0.1545
0.155
0.1555
0.156
0.1565
0.157
T(Gev)
0.19
0.2
0.21
0.22
0.23
0.24
0.25
0.26
0.27
muB (GeV)
d)
GammaS = 0.900
chisquared values
35.9
34.9
33.9
32.9
30.9
29.9
27.9
26.9
25.9
Chisquare
35
30
25
20
15
0.152
0.1525
0.153
0.1535
0.154
0.1545
0.155
T(Gev)
0.2
0.21
0.22
0.23
0.24
0.25
0.26
0.27
muB (GeV)

Table 4.2: Summary of fit results. The free-fit parameters as well as the minimum χ^2's are given.

Parameters at freeze-out	Values obtained from model	Average values from [70]
$Au - Au1.7A$ GeV/c		
T (MeV)	$49.6^{+1.0}_{-1.2}$	49.6±2.5
μ_B (MeV)	821^{+24}_{-17}	813±23
γ_s	1 (fixed)	1 (fixed)
V (fm^3)	1437(fixed)	1437 (fixed)
χ^2/dof	6.1/2	14.9/2 and 15.1/2
Si $-Au$ 14.6A GeV		
T (MeV)	$141.5^{+7.0}_{-5.9}$	135.4±4.3
μ_B (MeV)	571^{+40}_{-31}	581±32
γ_s	$0.759^{+0.082}_{-0.071}$	0.845±0.101
Radius (GeV^{-1})	$19.2^{+2.9}_{-3.0}$	
$VT^3\exp(-0.7GeV/T)$		0.534±0.130
χ^2/dof	12.9/4	14.3/4 and 11.6/4
$Pb - Pb$ 158A GeV		
T (MeV)	$156.1^{+2.5}_{-2.4}$	158±3.2
μ_B (MeV)	228^{+12}_{-12}	238±13
γ_s	$0.799^{+0.038}_{-0.036}$	0.789±0.052
Radius (GeV^{-1})	$49.5^{+2.1}_{-2.1}$	
$VT^3\exp(-0.7GeV/T)$		21.7±2.6
χ^2/dof	17.9/6	14.4/6 and 22.6/6

4.4 Fit Results and Discussion

4.4.1 Main Fit Results

Table 4.2 summarizes fit results obtained by applying our model to the data set discussed in the first section. The results are compared with (average) results obtained in [70]. While [70] uses a grand-canonical approach for the SPS $Pb-Pb$ data, we have used exact strangeness conservation throughout.

Table 4.3 summarizes the fit results for $Au-Au$ collisions at RHIC and compares it with recent analysis in [87], [92], and [109].

Table 4.3: Summary of fit results for RHIC $Au-Au$ collisions.

	From model	From [92]	From [109]	From [87]
T (MeV)	$178.3^{+12.2}_{-8.4}$	175±7	165±7	190±20
μ_B (MeV)	47^{+8}_{-6}	51±6	41±5	45±15
γ_s	$1.0373^{+0.149}_{-0.131}$			
Radius (GeV^{-1})	$27.0^{+14.0}_{-19.5}$			
χ^2/dof	12.8/5	5.7/7		

A fit using only the most recently available STAR results will also be done in the following section.

The temperature and the baryon chemical potential vary considerably between the lowest colliding energy at SIS for $Au-Au$, $\sqrt{s}=2.3$ GeV, and the highest colliding energy at RHIC for $Au-Au$, $\sqrt{s}=130$ GeV. The variation in T and μ_B is opposite, that is, as T increases μ_B decreases. The values of μ_B and T at different collision energies are shown in Figure 4.4. The energy dependence has been parametrized phenomenologically in [110] as

$$\mu_B(s) = \frac{a}{(1+\sqrt{s}/b)} \quad , \tag{4.2}$$

where $a \simeq 1.27$ GeV and $b \simeq 4.3$ GeV, together with the freeze-out condition of a fixed energy per hadron [111] of

$$\langle E \rangle / \langle N \rangle \simeq 1 \text{ GeV}. \tag{4.3}$$

At higher beam energies greater transparency is expected as the two colliding nuclei, now much more Lorentz contracted, essentially pass through each other giving rise to a central region

which contains a low net baryon number content, *i.e.*, it is more symmetrical in quarks and antiquarks. The baryon number from the target and projectile nuclei flows strongly into the forward and backward directions [10]. The decrease in μ_B is thus expected as we move to higher colliding energies and higher freeze-out temperatures. For $Au-Au$ collisions at RHIC we see a much lower $\mu_B(= 47$ MeV) when compared with $\mu_B(= 228$ MeV) for $Pb-Pb$ collisions at the SPS. This is a strong indication that at RHIC, with $\sqrt{s_{NN}} = 130$ GeV, a medium is created with a lower net baryon density. This is also shown by a dramatic increase in the $\overline{p}/p$ ratio (~ 10 times) going from SPS ($\overline{p}/p = 0.062$) to RHIC ($\overline{p}/p = 0.617$) (see Table 4.4).
With the change in T and μ_B being opposite, we find that the energy per particle is approximately constant (~ 1.0 GeV) across the various colliding systems (Table 4.5).
γ_s is around $0.7 - 0.8$ in cases for the main fit results where it has been kept as a free-fit parameter except for $Au-Au$ at RHIC ($\gamma_s = 1.0373^{+0.149}_{-0.131}$) where the system comes the closest to perfect strangeness equilibrium.

Table 4.4 compares the measured and fitted particle multiplicities and ratios. It shows the contribution of the individual values in the fit to the chisquare value. The individual contributions are calculated using:

$$Contribution = \frac{(Model\ value - Experimental\ value)^2}{(Experimental\ Uncertainty)^2} \quad . \tag{4.4}$$

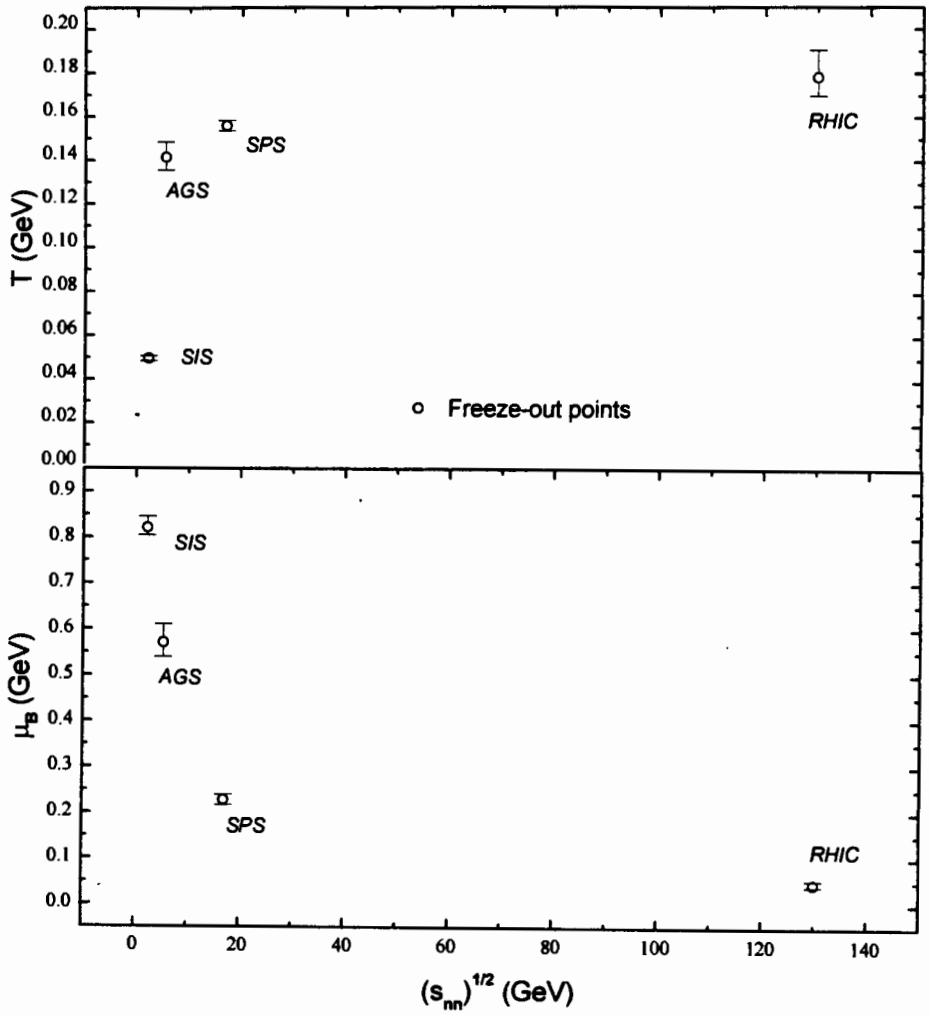

Figure 4.4: *Behaviour of the freeze-out baryon chemical potential, μ_B, (upper curve) and temperature, T, (lower curve) as a function of the c.m. energy, $\sqrt{s}$.*

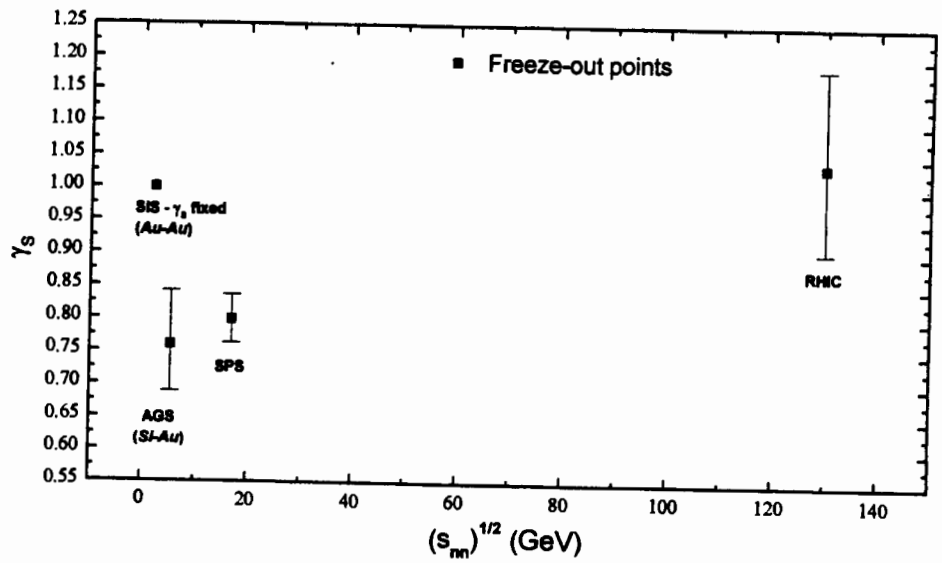

Figure 4.5: *Behaviour of γ_s as a function of the c.m. energy, $\sqrt{s}$.*

Table 4.4: Measured and model particle and ratio values along with their contribution to χ^2.

Multiplicities and ratios	Reference	Measured	Model Values	Contribution to χ^2
		Au – *Au* 1.7*A* GeV/c		
π^+/p	[70, 105]	0.052±0.013	0.0527	0.003
K^+/π^+	[70, 105]	0.003±0.00075	0.00301	0.0003
π^-/π^+	[70, 105]	2.05±0.51	2.004	0.008
η/π^0	[70, 105]	0.018±0.007	0.00072	6.096
χ^2				6.1
		Si – *Au* 14.6*A* GeV		
Participants	[55]	115±10	96.16	3.551
π^+	[55]	33±3	35.54	0.714
π^-/π^+	[55]	1.09±0.13	1.160	0.251
K^+/π^+	[90]	0.18±0.02	0.1558	1.462
K^-/π^-	[90]	0.034±0.004	0.0277	2.482
$\overline{p}/K^-$	[91]	0.018±0.0034	0.0158	0.409
$\overline{\Lambda}/\Lambda$	[90]	0.003±0.0015	0.00313	0.007
ϕ	[90]	0.09±0.04	0.1699	3.991
χ^2				12.9
		Pb – *Pb* 158*A* GeV		
$(\pi^+ + \pi^-)/2$	[72]	600±30	555.1	2.241
K^+	[72]	95±10	95.60	0.004
K^-	[72]	50±5	59.49	3.604
K^0_S	[72]	60±12	77.26	2.069
p	[72]	140±12	151.7	0.961
$\overline{p}$	[72]	10±1.7	9.422	0.116
ϕ	[112]	7.6±1.1	7.460	0.016
Ξ^-	[112]	4.42±0.31	3.860	3.278
$\overline{\Xi^-}$	[112]	0.74±0.04	0.7580	0.203
$\overline{\Lambda}/\Lambda$	[72]	0.2±0.04	0.1072	5.382
χ^2				17.9
		Au – *Au* 8992*A* GeV		
π^-/π^+	[99, 100, 109]*	0.995±0.014	1.014	1.898
$\overline{p}/\pi^-$	[94]	0.08±0.01	0.0803	0.0008
K^-/K^+	[95, 98, 99, 109]*	0.87±0.04	0.8996	0.549
K^-/π^-	[95, 109]*	0.15±0.02	0.1730	1.323
$K^*/hmin$	[95, 96]*	0.060±0.012	0.0384	3.239
$\overline{K^*}/hmin$	[95, 96]*	0.058±0.012	0.0329	4.382
$\overline{p}/p$	[94, 98, 99, 100, 109]*	0.59±0.04	0.6172	0.463
$\overline{\Lambda}/\Lambda$	[95]	0.73±0.03	0.7049	0.698
$\overline{\Xi}/\Xi$	[95]	0.82±0.08	0.8559	0.201
χ^2	* = average taken			12.8

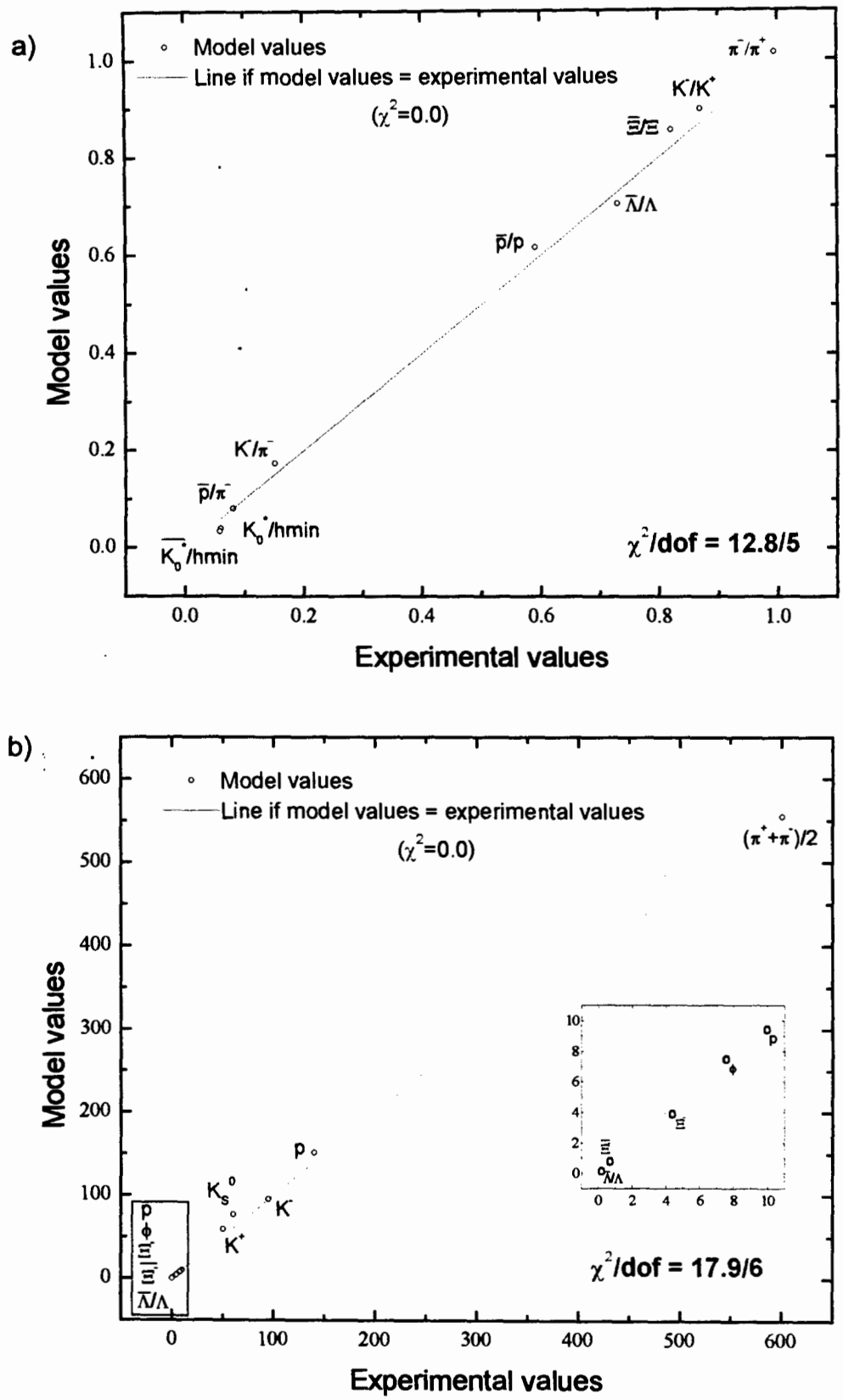

Figure 4.6: *The deviation of the model values from the experimental values i.e. from* $\chi^2 = 0.0$ *for a) RHIC (Au-Au) and b) NA49 (Pb-Pb).*

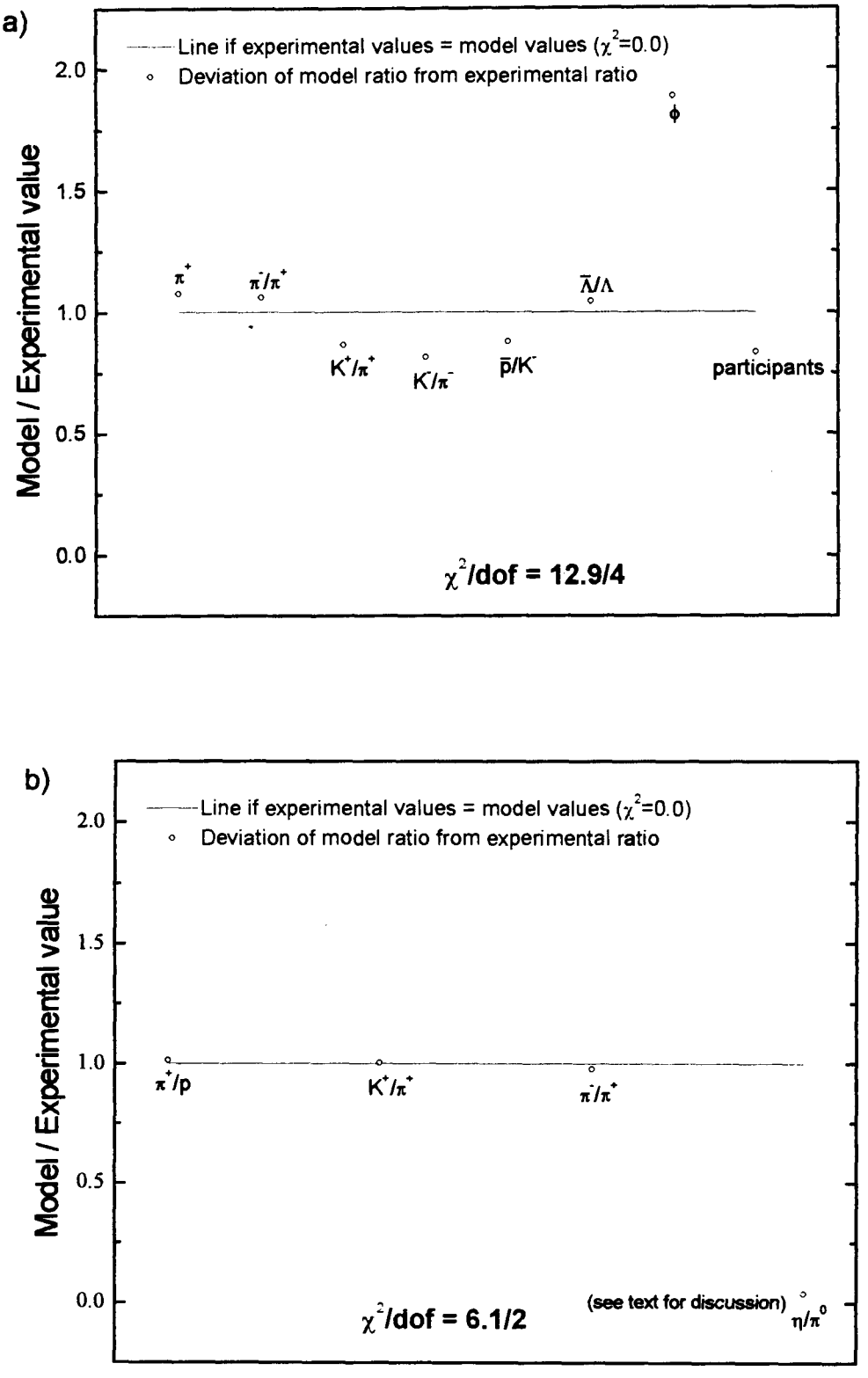

Figure 4.7: *The deviation of the model values from the experimental values i.e. from* $\chi^2 = 0.0$ *for a) AGS (Si-Au) and b) SIS (Au-Au).*

For $Au - Au$ collisions at SIS we see that the dominant contribution to χ^2 is from the η/π^0 ratio (99.8%) due to an underestimation of this value.

The discrepency of the thermal model on the level of η production still remains an unsolved problem. Discussions surrounding this include the possibility of a sequential freeze-out of different particle species where η's are produced at an earlier time and with higher temperature but, this line of argument applied to the other particle ratios presents a problem when one considers how well they are described by the model without invoking a sequential freeze-out scenario [105].

The hidden strangeness content of η mesons could possibly be a crucial factor in how it is considered in a thermal model; being treated as a non-strange particle means that the η yield is not subject to corrections due to canonical strangeness suppression, which, conceivably, it should be. However, as pointed out in [105], it is not clear as to how this could be included in a consistent way. Also, the η yield is possibly of dynamical origin and *a priori* not in the scope of explanation of a thermal model. It is noteworthy to mention that transport-model calculations reproduce the measured η and π^0 spectra [113].

For $Si - Au$ at AGS we find the highest contribution coming from an overestimation of ϕ (contributing 31.0%) using the main fit results in Table 4.2.

The dominant contribution to χ^2 for $Pb - Pb$ collisions at the SPS comes from an underestimation of the $\overline{\Lambda}/\Lambda$ ratio, contributing 30.1%, followed by an overestimation of K^- which contributes 20.2%.

At RHIC, for $Au - Au$, the highest contribution comes from an underestimation of $\overline{K_0^*}/h\,\mathrm{min}$ (contributing 34.4%) followed by $\overline{K_0^*}/h\,\mathrm{min}$ with a contribution of 25.4%.

Investigation of the χ^2 contour surface in the region of the optimum values for the thermal parameters at RHIC, obtained by fitting the data using the minimization routine, *Minuit*, reveals interesting features and marked differences with those obtained for $Pb - Pb$ collisions at the SPS's NA49 experiment. The most notable feature in Figure 4.9 is the asymmetry in the surface and contour plots along the T and μ_B axes compared to NA49.

From the shape of the contours for RHIC we can see that there is more freedom for variation

in terms of T. This is also evident from the error bars in Table 4.3 and Figure 4.20.

μ_B is more constrained as we see from the narrower χ^2 surface along this axis.

With the $\gamma_s - Radius$ plane in Figure 4.10, the question of whether there is a slight volume dependence and whether the grand canonical limit is reached, comes to the fore. There is less than a 7% difference in χ^2 between the lowest and highest contour plot *i.e.*, not a strong variation in χ^2 at all. The difference in a pure proton-proton gas between the exact and grand canonical cases at a radius of 10 fm is $\approx 1\%$. In the full system this difference is amplified to $\sim 7\%$ for a radius $\succeq 10$ GeV^{-1}. Thus one can see that the canonical formulation approaches the grand canonical limit.

A problem highlighted by the almost feartureless "wall" at a radius ≈ 41 GeV^{-1}, constraining the upper limit on the radius, is the numerically computable contraints on the bessel functions. In the limit of $x >> n$,

$$I_n(x) \rightarrow \frac{exp(x)}{\sqrt{2\pi x}} . \tag{4.5}$$

Clearly, if x is large, then the $exp(x)$ will be very large and cause an "overflow" - a number larger than the largest representable number on the computer will arise. For example:

$$\begin{aligned} if\ R &= 40\ \text{GeV}^{-1}\ then\ x = 554, \\ if\ R &= 45\ \text{GeV}^{-1}\ then\ x = 788. \end{aligned} \tag{4.6}$$

We find that reliable results are obtained up till about $x = 700$. Larger than this one gets infinity for the result.

From Figure 4.8 we see that at large x the result is approaching the asymptotic limit to within 2 parts in 10^4.

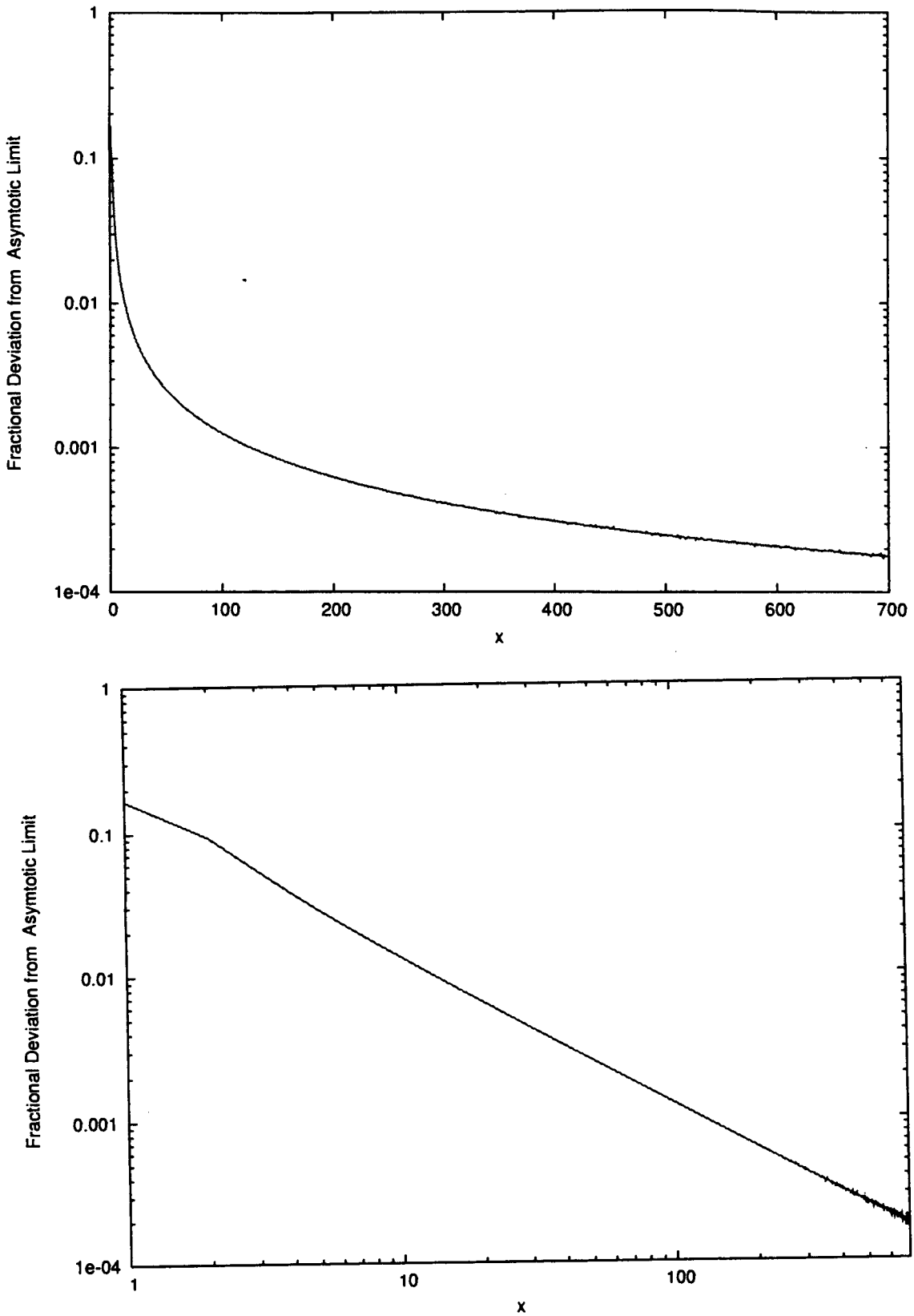

Figure 4.8: *To test the large limit of the bessel functions, $I_n(x)$, we can plot the fractional deviation from the analytic large x limit.*

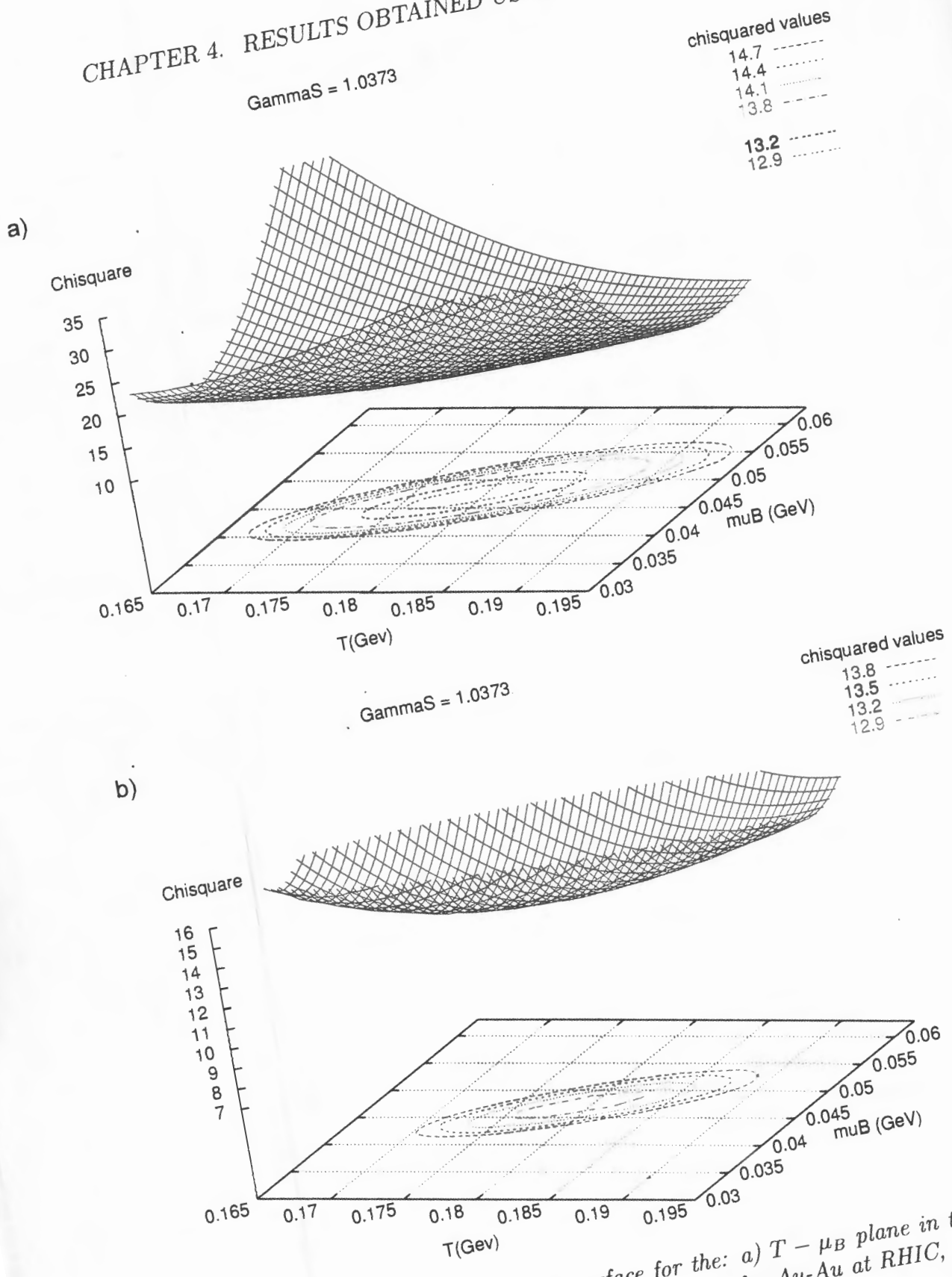

Figure 4.8: *The variation of the χ^2 contour surface for the: a) $T - \mu_B$ plane in the region of the optimum values for the parameters obtained for Au-Au at RHIC, b) Magnified view of plot in a) over a smaller range of T.*

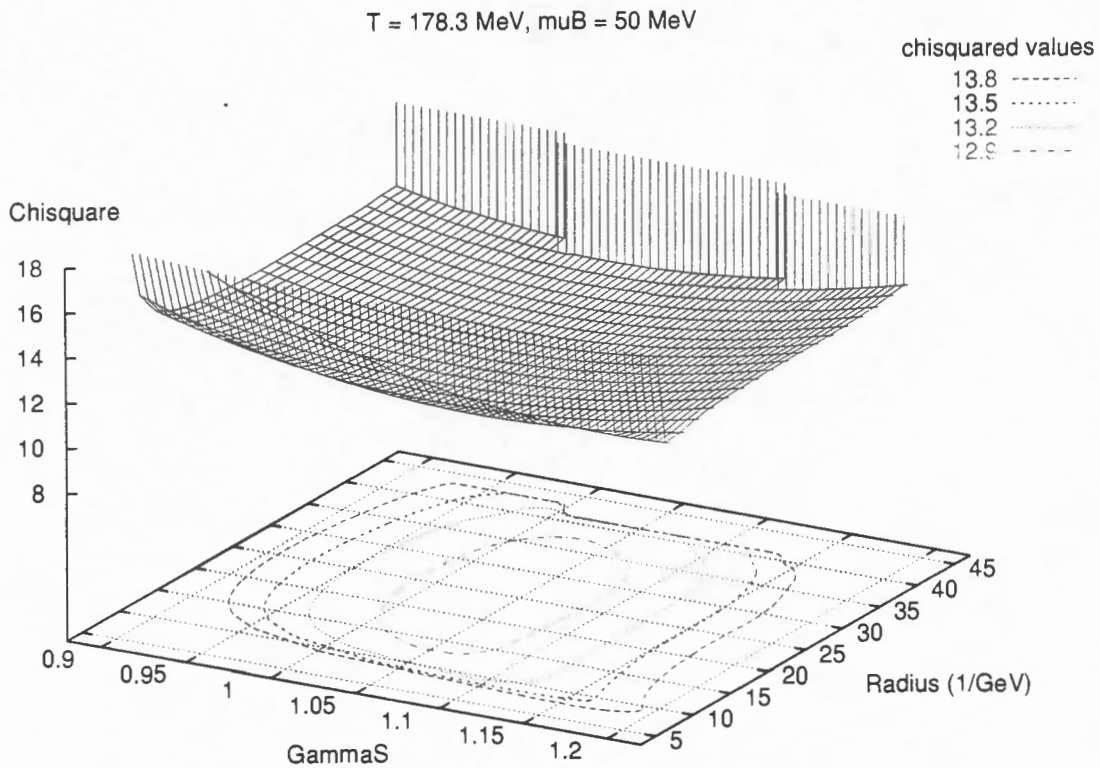

Figure 4.9: *The variation of the χ^2 contour surface for the γ_s – Radius plane in the region of the optimum values for the parameters obtained for Au-Au at RHIC.*

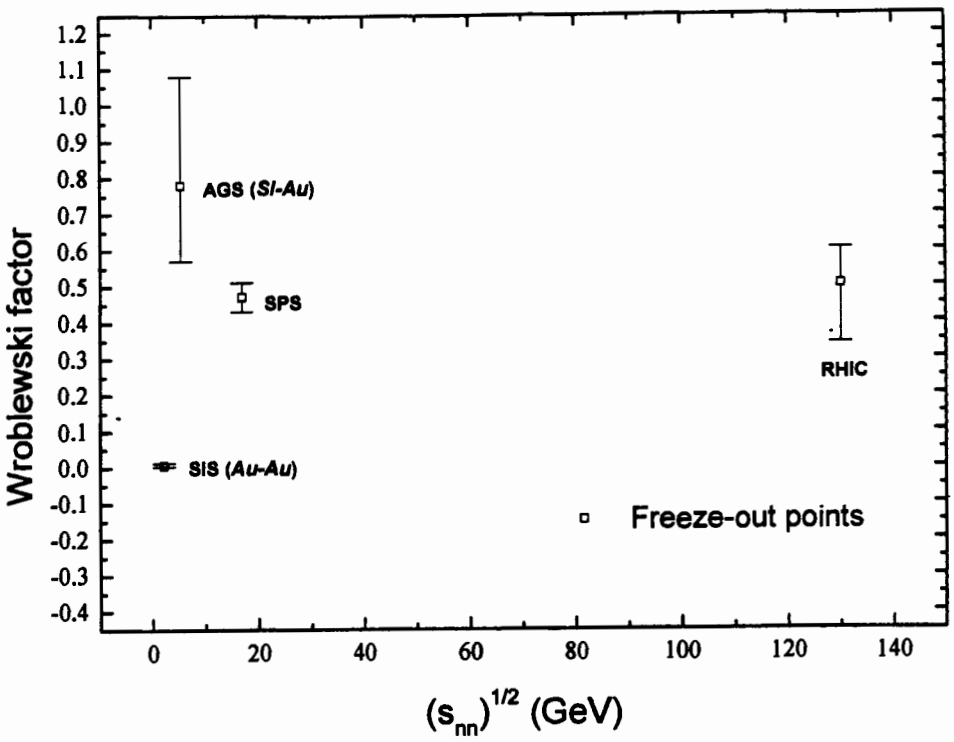

Figure 4.13: *Behaviour of λ_S as function of the c.m. energy, $\sqrt{s}$.*

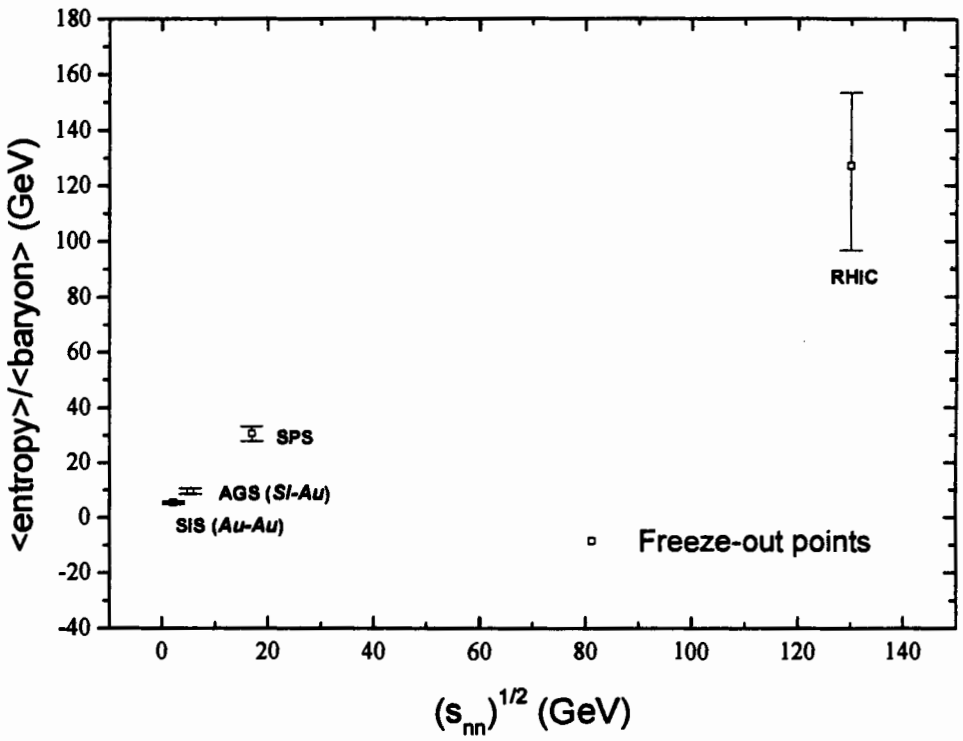

Figure 4.14: *Behaviour of $\frac{\langle entropy \rangle}{\langle baryon \rangle}$ as function of the c.m. energy, $\sqrt{s}$.*

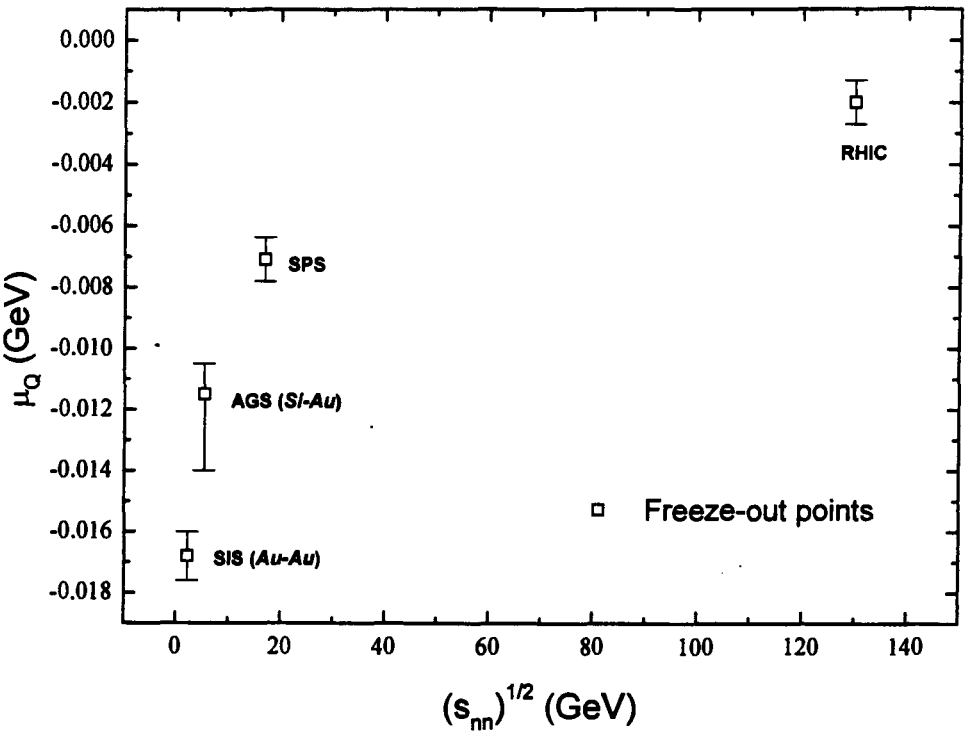

Figure 4.12: *Behaviour of μ_Q as a function of the c.m. energy, $\sqrt{s}$.*

Also listed in Table 4.5 we see the Wrobelowski factor, λ_s, measuring the number of newly created primary valence $s\bar{s}$ pairs compared to the newly created non-strange primary valence quark pairs - quark pairs being found before particle decays take place, *i.e.*, we take the *primary* multiplicities of all hadron species and exclude all quarks that were present in the target and projectile;

$$\lambda_s = \frac{2\langle s\bar{s}\rangle}{\langle u\bar{u}\rangle + \langle d\bar{d}\rangle} \,. \tag{4.9}$$

The behaviour of μ_Q, λ_s, and $\frac{\langle entropy\rangle}{\langle baryon\rangle}$ as a function of $\sqrt{s}$ is shown in figures 4.12 to 4.14. The average energy per particle for the various colliding systems will be discussed in the last section.

4.4.3 μ_Q, μ_s, λ_s, $\frac{\langle entropy \rangle}{\langle baryon \rangle}$ and $\frac{\langle energy \rangle}{\langle particle \rangle}$

Table 4.5: Table showing the chemical potentials, μ_Q and μ_S, the Wroblewski factor (λ_s), the entropy per baryon and, the energy per particle for each colliding system.

	Au-Au (SIS)	*Si-Au* (AGS)	*Pb-Pb* (SPS)	*Au-Au* (RHIC)
$\sqrt{s_{nn}}$ (GeV)	2.2	5.4	17	130
μ_Q (GeV)	$-0.0168^{+0.0008}_{-0.0008}$	$-0.0115^{+0.0010}_{-0.0025}$	$-0.0071^{+0.0007}_{-0.0007}$	$-0.0020^{+0.0007}_{-0.0007}$
μ_S (GeV)	$0.022^{+0.032}_{-0.027}$	$0.152^{+0.029}_{-0.028}$	$0.050^{+0.005}_{-0.005}$	$0.013^{+0.004}_{-0.051}$
λ_s	$0.006^{+0.007}_{-0.003}$	$0.78^{+0.30}_{-0.21}$	$0.47^{+0.04}_{-0.04}$	$0.50^{+0.10}_{-0.16}$
$\frac{\langle entropy \rangle}{\langle baryon \rangle}$ (GeV)	$5.4^{+0.5}_{-0.6}$	$9.5^{+1.1}_{-1.0}$	$30.5^{+2.6}_{-2.7}$	$127.1^{+26.3}_{-30.3}$
$\frac{\langle energy \rangle}{\langle particle \rangle}$ (GeV)	$0.960^{+0.014}_{-0.014}$	$1.154^{+0.085}_{-0.049}$	$1.042^{+0.044}_{-0.046}$	$1.100^{+0.098}_{-0.129}$

In Table 4.5 the strangeness chemical potential, μ_s, although not a parameter in our model in which strangeness is conserved exactly, is calculated following the method used in [128]. We first define the strangeness chemical factor, C_s, where

$$C_s = \frac{Z_{S-1}(T,V)}{Z_{S=0}(T,V)} \,. \tag{4.5}$$

$Z_{S-1}(T,V)$ is the factor taken from the first of the expressions labelled 3.38 (in the previous chapter) for particle number obtained by differentiating the total partition function, $Z_{S=0}(T,V)$,

$$\left\langle N^1_{i+} \right\rangle = \frac{Z^1_{i+} K_0}{Z_{S=0}} \underbrace{\sum_{n=-\infty}^{\infty} \sum_{p=-\infty}^{\infty} I_n(x_2)\, I_p(x_3)\, I_{2n+3p+1}(x_1)\, y_2^n y_3^p y_1^{-2n-3p-1}}_{Z_{S-1}(T,V)} \,. \tag{4.6}$$

$\left\langle N^1_{i+} \right\rangle$ and Z^1_{i+} are the particle abundance and single particle partition function respectively, of species $+i$ with $strangeness = 1$.

In the grand-canonical limit one gets

$$\lim_{V\to\infty} C_s = strangeness\ fugacity = \exp(\frac{\mu_s}{T}), \tag{4.7}$$

from which μ_s can be calculated, *i.e.*,

$$\mu_s = T \ln\left(\frac{Z_{S-1}(T,V)}{Z_{S=0}}\right). \tag{4.8}$$

The value of μ_Q, as we discussed in the previous chapter, is fixed by giving the neutron surplus, $B/2Q$, and forcing this to be equal in the hadron gas and the colliding system of protons and neutrons.

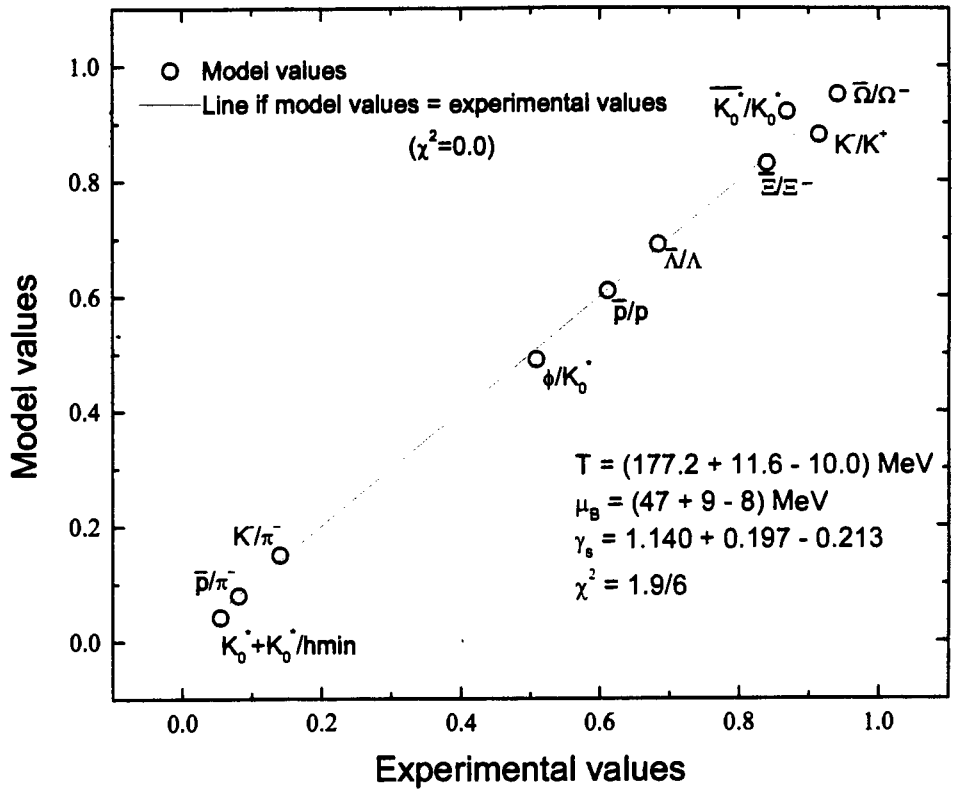

Figure 4.10: *The deviation of the model values from the experimental values i.e. from $\chi^2 = 0.0$ for RHIC (Au-Au) for our STAR fit.*

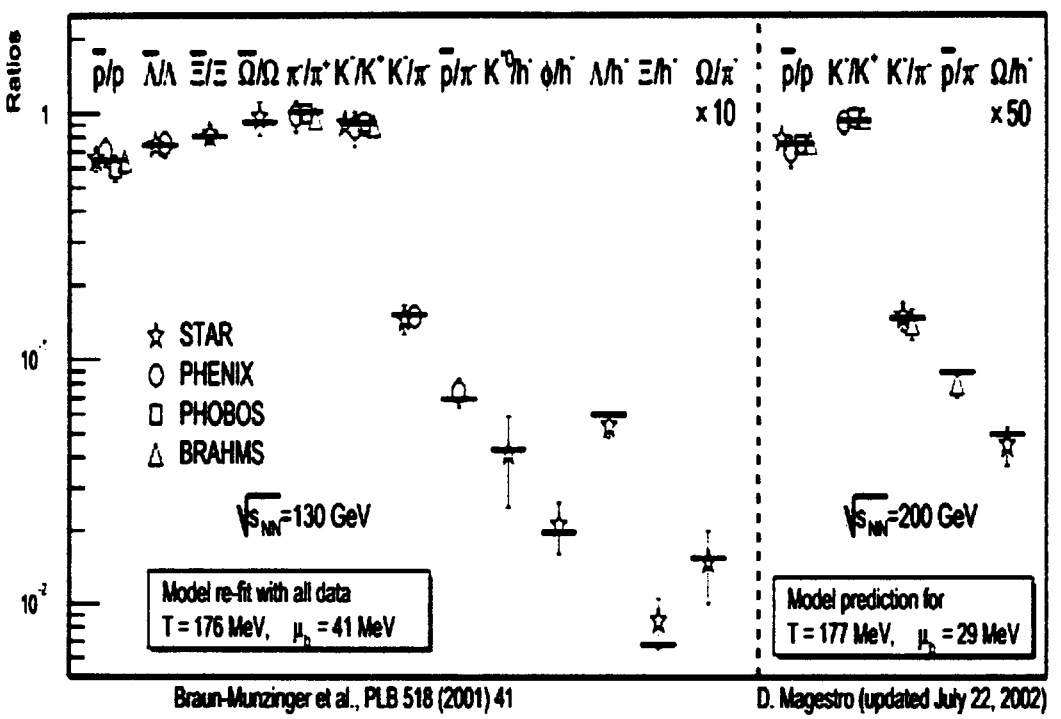

Figure 4.12: *Comparison of Statistical Model results with RHIC data [92].*

- $\overline{K_0^\star}/K_0^\star = 0.92 \pm 0.14(stat.)$ - obtained from central events, the ratio is consistent with other particle to antiparticle ratios measured at RHIC [121]-[123].
- $K_0^\star/h^- = 0.042 \pm 0.004(stat.) \pm 0.01(syst.)$ - for the top 14% most central collisions.
- $\phi/K_0^\star = 0.49 \pm 0.059(stat.) \pm 0.12(syst.)$ - for the 14% most central collisions. This ratio is greater than in elementary collisions and, as stated in [114], may be indicative of strangeness enhancement and/or additional effects such as rescattering or coalescence [119].

Antibaryon to baryon ratios used are:

- $\overline{\Lambda}/\Lambda = 0.69 \pm 0.01(stat.) \pm 0.03(syst.)$ [71] - 11% most central, feed-down corrected.
- $\overline{\Xi}/\Xi^- = 0.83 \pm 0.03(stat.) \pm 0.05(syst.)$ [124, 71] - 11% most central, feed-down corrected.
- $\overline{\Omega}/\Omega^- = 0.95 \pm 0.15(stat.) \pm 0.05(syst.)$ [71]- 11% most central, feed-down corrected.

Ratios used in the first analysis and that are used again without any change are:

- $\overline{p}/\pi^- = 0.08 \pm 0.01$ [94].
- $K^-/\pi^- = 0.15 \pm 0.02$ [95].
- $K^-/K^+ = 0.88 \pm 0.05$ [95].
- $\overline{p}/p = 0.61 \pm 0.07$ [94].

4.4.2 Fit of Recent STAR Results

An updated analysis of $Au - Au$ collisions at RHIC, based on most recently available STAR results, follows. We first make a few brief remarks about the latest particle ratios, different to those for STAR used in our analysis presented earlier.

The results of our STAR fit follows in Figure 4.12.

$\mathbf{K_0^\star(892)}$ [114]

The first measurements of $K_0^\star(892)$ and $\overline{K_0^\star}(892)$ for relativistic heavy-ion collisions from STAR are discussed. $K_0^\star$ and $\overline{K_0^\star}$ are strongly decaying resonant states and the dominant resonances in the $K\pi$ system [114].

These resonances have relatively short lifetimes, comparable with the time-scale for the evolution of the dense matter created in a collision.

Thus expected, is that characteristic properties of the resonances such as width, branching ratios, yield, and transverse momentum spectra, will be sensitive to the dynamics and chiral properties of the produced high energy-density medium [115, 116]. It is found at STAR that the measured yield for $K_0^\star$, $dN/dy = 10.0 \pm 0.9(stat.) + 2.5(syst.)$, is relatively high compared to elementary collisions and thermal model predictions especially considering the short lifetime and expected losses due to rescattering of the daughter particles in the dense medium [114]. Two possible scenarios for which this would be consistent are put forward in [114], namely; (1) a sudden freeze-out scenario where there is a short time duration between chemical and kinetic freeze-out (hence a shorter time for the rescattering phase between these two freeze-out stages) or, (2) a relatively long period of expansion ($\succeq$ 20 fm/c) characterized by high hadron density and significant $K_0^\star$ regeneration *via* elastic processes like $\pi K \rightarrow K_0^\star \rightarrow \pi K$ [114].

Together with ϕ measurements, a novel avenue becomes available to distinguish between different hadronic expansion and freeze-out scenarios [117, 118, 119].

The strange quark content of the $K_0^\star$ also makes it interesting in terms of strangeness enhancement as a signature for the QGP.

The $K_0^\star$ yields from STAR represent the average value from the combined spectra of $K_0^\star$ and $\overline{K_0^\star}$. The ratios from STAR involving $K_0^\star(892)$ that we use are: $\overline{K_0^\star}/K_0^\star$, $K_0^\star/h^-$ and $\phi/K_0^\star$. The latest results follows [114, 120]:

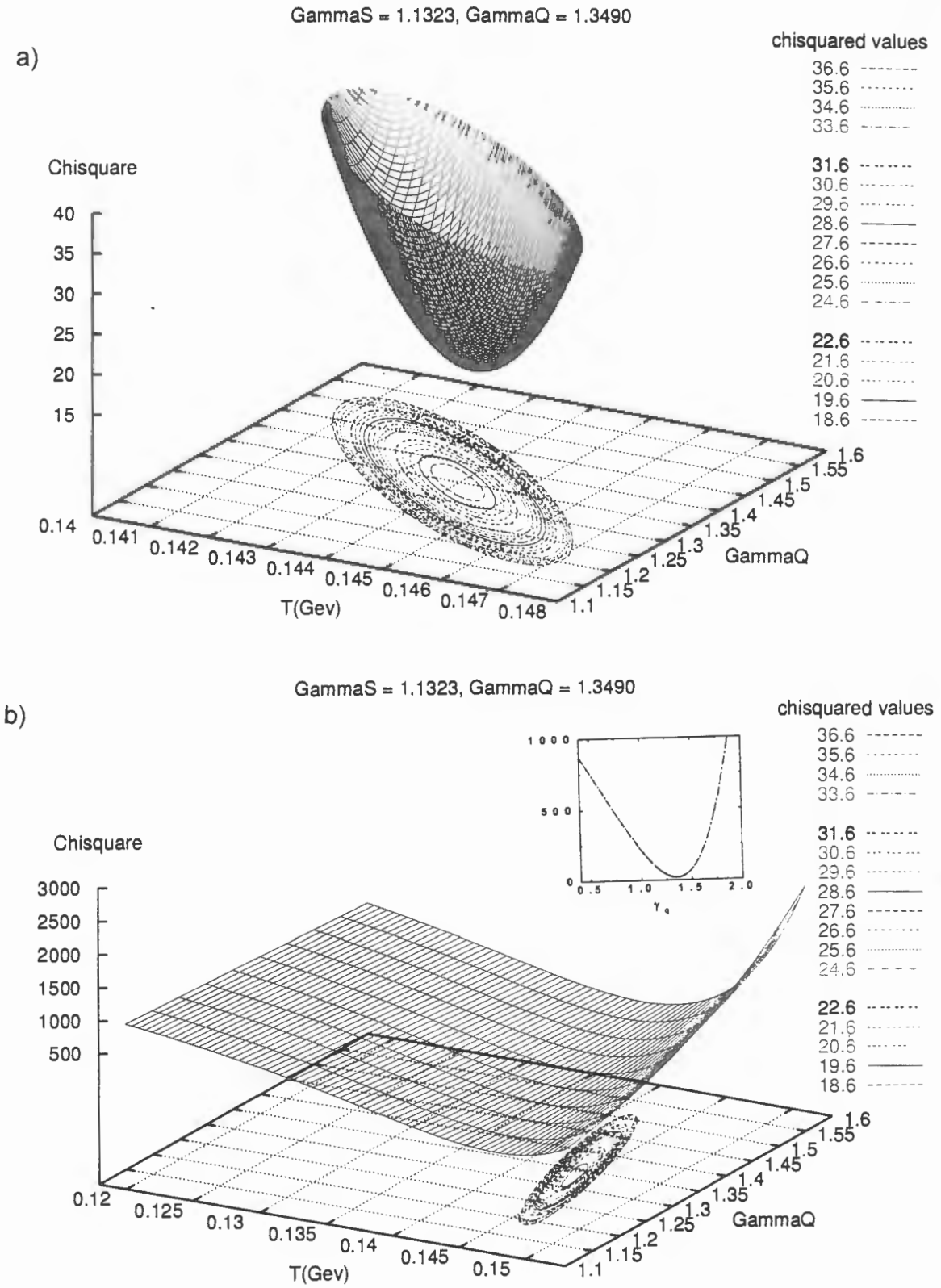

Figure 4.15: *The variation of the χ^2 contour surface for the: a) $T - \mu_B$ plane in the region of the optimum values for the parameters obtained for Pb-Pb at the SPS with γ_q as a parameter, b) Extended view of plot in a) over a larger range of χ^2. Insert: χ^2 as a function of γ_q in the region of the minimum.*

4.4.4 Introducing a Light Quark Pair Abundance Factor, γ_q

The effect of introducing a light quark pair (abundance) factor, γ_q, as a free-fit parameter to parameterize the deviation of light quarks from perfect chemical equilibrium (see Chapter 2), is seen in Table 4.6. The results for the freeze-out parameters of $Pb - Pb$ collisions at SPS (NA49) with γ_q fixed and, γ_q free, are shown.

Table 4.6: Summary of fit results for $Pb - Pb$ (NA49) with γ_q fixed to one and, as a free parameter.

Parameters at freeze-out	Wth γ_q fixed	With γ_q free
T (MeV)	$156.1^{+2.5}_{-2.4}$	$144.0^{+0.7}_{-0.8}$
μ_B (MeV)	228^{+12}_{-12}	207^{+45}_{-33}
γ_s	$0.799^{+0.038}_{-0.036}$	$1.132^{+1.324}_{-0.534}$
γ_q	1	$1.349^{+0.044}_{-0.038}$
Radius (GeV^{-1})	$49.5^{+2.1}_{-2.1}$	$48.0^{+3.3}_{-6.7}$
χ^2/dof	17.9/6	17.6/5

According to the model presented in [83] and [84] this scenario involves the sudden break-up of a quark-gluon plasma fireball - the non-equilibrium of light non-strange quarks being more pronounced if hadronization is a sudden process on the time-scale of chemical quark equlibration.

In Figure 4.16*b*, taken over a larger chisquare range than Figure 4.16*a*, we see that the convergence to a minimum is very sharp, as would be expected for a sudden process. This is also shown in the insert plot in Figure 4.16*b* in which the chisquared value is plotted as a function of γ_q.

From the table we see a significant lowering of the freeze-out temperature from the main fit result in Table 4.2 although, with much larger error bars.

Comparing the ratio $\frac{\gamma_s}{\gamma_q}$ for both fits we find; $\frac{\gamma_s}{\gamma_q} = 0.592$ with γ_q free and, $\frac{\gamma_s}{\gamma_q} = 0.799$ with γ_q fixed to one.

The overabundance of the light phase space occupancy, $\gamma_q > 1$, could arise due to the effect of gluon fragmentation and early chemical equilibration in a QGP phase. According to [84], this is expected from a high entropy phase and high value for $\frac{\langle entropy \rangle}{\langle baryon \rangle}$ (= 16.1 GeV for our analysis).

4.4.5 Comparing Multiplicities from a Hadron Gas containing Strange Particles up to $\pm 1, \pm 2, \pm 3$ respectively

Table 4.7 compares the fit results for SPS $Pb - Pb$ collisions for a hadron gas containing $|strangeness| = 1, 2, 3$ respectively. Table 4.8 compares the fitted multiplicities for the three cases.

Table 4.7: Summary of fit results for $Pb - Pb$ (NA49) for $|strangeness| = 0, 1, 2, 3$.

Parameters at freeze-out	With S up to ± 1	With S up to ± 2	With S up to ± 3
T (MeV)	$157.3^{+5.6}_{-5.0}$	$156.3^{+2.5}_{-2.4}$	$156.1^{+2.5}_{-2.4}$
μ_B (MeV)	209^{+14}_{-13}	228^{+12}_{-12}	228^{+12}_{-12}
γ_s	$0.702^{+0.056}_{-0.054}$	$0.801^{+0.037}_{-0.036}$	$0.799^{+0.038}_{-0.036}$
Radius (GeV^{-1})	$49.7^{+4.5}_{-4.5}$	$49.4^{+2.1}_{-2.1}$	$49.5^{+2.1}_{-2.1}$
χ^2/dof	11.3/3	17.8/6	17.9/6
$\frac{\langle entropy \rangle}{\langle baryon \rangle}$ GeV	34.4	30.5	30.5
$\frac{\langle energy \rangle}{\langle particle \rangle}$ GeV	1.1	1.0	1.0

Table 4.8: Particle multiplicities for $Pb - Pb$ (NA49) for $|strangeness| = 0, 1, 2, 3$.

Multiplicities	With S up to ± 1	With S up to ± 2	With S up to ± 3
$(\pi^+ + \pi^-)/2$	569.4	555.3	555.1
K^+	85.96	95.21	95.60
K^-	57.42	59.40	59.49
K^0_S	71.30	77.18	77.26
p	144.1	151.7	151.8
$\overline{p}$	11.63	9.518	9.422
ϕ	6.232	7.523	7.460
Ξ^-		3.863	3.859
$\overline{\Xi^-}$		0.7573	0.7580
$\overline{\Lambda}/\Lambda$	0.1225	0.1058	0.1072

While there is very little difference in the best-fit parameters and the χ^2 value between $S = \pm 2$ and $S = \pm 3$, differences with $S = \pm 1$ are more pronounced. In particular we note the higher freeze-out temperature and the lower μ_B for $S = \pm 1$. Practically consistent across all three cases are the values for $\langle energy \rangle$ / $\langle particle \rangle \simeq 1.0$ GeV and $\langle entropy \rangle$ / $\langle baryon \rangle \simeq 30.1$ GeV (average value).

Notable observations in Table 4.8 are:

- the lower kaon and ϕ values and,
- the higher $\bar{p}$ and $\overline{\Lambda}/\Lambda$ values obtained for $S = \pm 1$,
- a slight increase in the K^+/π^+ ratio going from left to right across the table.

4.4.6 Parameters at Freeze-out for WA97 Pb-Pb

Table 4.9 shows the fitted results obtained by model calculations for the WA97 collaboration for $Pb - Pb$ collisions. As mentioned, the WA97 experiment uses the same beam and fixed target as in NA49. However, only a limited kinematical region is available, about one unit of rapidity centred at midrapidity. The results are compared with those obtained in [70].

By fixing T and μ_B to the values obtained for $Pb - Pb$ (NA49) in Table 4.2 and, adjusting γ_s and V, we are essentially using γ_s and V as an overall normalizing combination keeping in mind that γ_s is the factor measuring the deviation from complete strangeness equilibrium in a volume, V, in which strangeness is conserved. A $\chi^2/dof = 27.8/5$ is obtained. This compares well with the result in [70] in which T, μ_B, and γ_s have been fixed to the values obtained for their NA49 fit while only V has been adjusted (*i.e.*, an overall normalizing volume). The χ^2 result obtained for the latter is $\chi^2/dof = 28.9/6$.

The greatest contributions (29.7% and 26.4%) to the χ^2 value in our fit comes from $\overline{\Lambda}$ and Λ respectively.

The high value of the χ^2 strengthens the contention that a statistical-thermal analysis is not able to reproduce data in a limited kinematical window and in full phase space at the same time without resorting to a more detailed dynamical model (see [70]).

Table 4.9: Comparison between measured particle multiplicities in central $Pb - Pb$ collisions, WA97, and model calculations. The particle contributions to χ^2 are also shown.

Multiplicities	Measured [126]	Calculated	Contribution to χ^2	Calculated in [70]
h^-	178±22	197.5	0.86	207.9
K^0_S	21.9±2.4	27.87	4.74	23.66
Λ	13.7±0.9	11.11	6.38	15.58
$\overline{\Lambda}$	1.8±0.2	1.259	8.08	1.543
Ξ^-	1.5±0.1	1.645	2.22	1.251
$\overline{\Xi^+}$	0.37±0.06	0.3449	0.17	0.2354
$\Omega^- + \overline{\Omega^+}$	0.41±0.08	0.2731	2.76	0.1662
χ^2/dof			27.8/5	28.9/6
$\frac{\langle entropy \rangle}{\langle baryon \rangle}$ GeV			29.1	
$\frac{\langle energy \rangle}{\langle particle \rangle}$ GeV			0.98	

4.4.7 $\overline{p}$ to p Ratio at the SPS and RHIC

Antibaryon to baryon ratios provide a very sensitive measurement of the net baryon density at midrapidity. The reaction mechanism between heavy ions at high energies as a function of $\sqrt{s}$ is expected to evolve in the following way: 1) complete stopping for lower $\sqrt{s}$ - baryons from the colliding nuclei are shifted from beam to midrapidity where a significant baryon density is found - through to the other extreme, namely; 2) full transparency, the Bjorken limit, at higher $\sqrt{s}$ - baryons from the colliding nuclei are shifted from beam rapidity but midrapidity is devoid of primordial baryons [100]. A central region consisting of almost zero net baryon density but high energy density opens between the colliding fragments.

For central $Au - Au$ collisions at RHIC it is estimated that about 2/3 of midrapidity protons come from baryon creation *via* string fragmentation, and about 1/3 come from baryon transport processes whereby the initial baryons from the colliding nuclei are transported over 5 units of rapidity to the midrapidity region [97]. A dramatic increase in the $\overline{p}/p$ ratio is observed in going from SPS ($\sqrt{s} = 17$ Gev) to RHIC ($\sqrt{s} = 130$ GeV). Our model calculations yield the following results for $\overline{p}/p$:

$$\begin{aligned} \overline{p}/p\ (SPS) &= 0.062 \\ \overline{p}/p\ (RHIC) &= 0.617. \end{aligned} \tag{4.12}$$

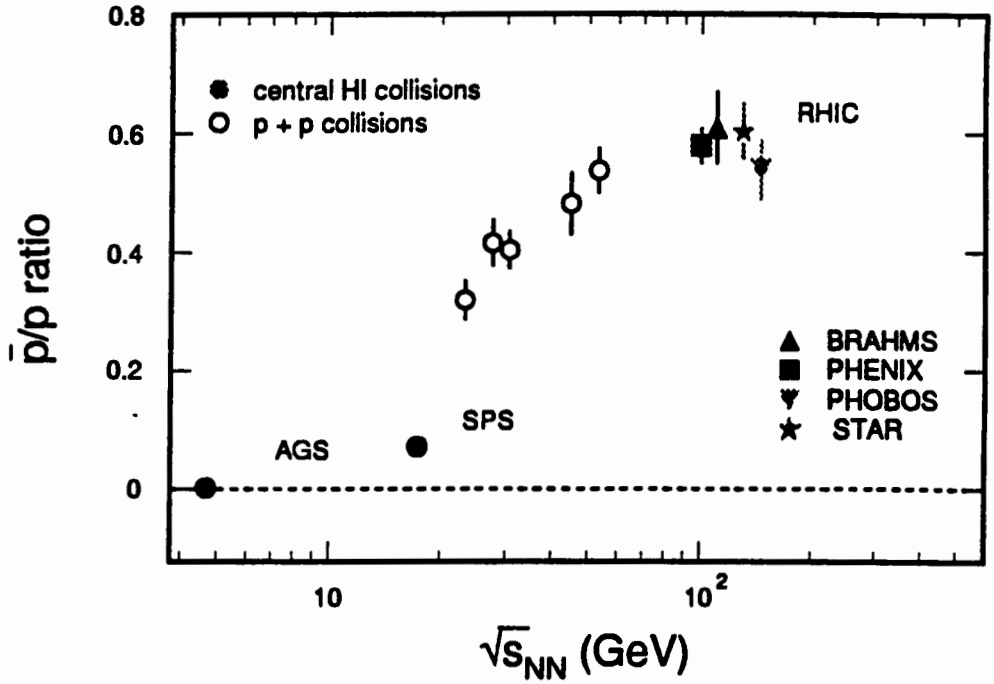

Figure 4.16: *Midrapidity $\overline{p}/p$ ratios measured in central heavy-ion collisions (filled symbols) and $p+p$ collisions (open symbols) [90].*

The dependence of the $\overline{p}/p$ ratio as a function of $\sqrt{s}$ is shown in Figure 4.17. The limiting value for a baryon free region is $\overline{p}/p = 1$.

Although significantly below unity, the ratio at RHIC is much higher than the ratio at the SPS or the AGS. This indicates that, at RHIC, a system with a much lower net baryon density is created at midrapidity. Gluon dynamics are expected to dominate particle production for central rapidity at RHIC [97].

The rapidity dependence of the $\overline{p}/p$ ratio for $Au-Au$ collisions at RHIC - indicating the balance between baryon number transport to the central region and antibaryon pair production - has been shown in the BRAHMS collaboration where it decreases from mid to forward rapidity, suggesting that there is still a significant contribution from participant baryons over the entire rapidity range and the full transparency of the Bjorken model has not yet been achieved [100].

Also reported by the BRAHMS collaboration is the π^-/π^+ ratio which is found to be close to unity over the same rapidity range as the $\overline{p}/p$ ratio [100].

It is shown in [97, 100] that there is no significant dependence of antibaryon to baryon ratios on transverse momentum or centrality for $Au-Au$ collisions at RHIC.

4.4.8 Improved $\overline{\Lambda}/\Lambda$ Ratio for NA49

We present an improved estimate for the $\overline{\Lambda}/\Lambda$ ratio based on recent results in [127, 128] from the NA49 experiment at CERN's SPS for $Pb - Pb$ collisions of 158 GeV/c per nucleon.
The $\overline{\Lambda}$ multiplicity has been calculated by finding the area under the Gaussian in Figure 4.18.
The Λ multiplicity has been found from Figure 4.19.

$$\begin{aligned} \overline{\Lambda}/\Lambda \ (\textit{previous estimate}\ [72]) &= 0.2 \pm 0.040. \\ \overline{\Lambda}/\Lambda \ (\textit{new estimate}) &= 0.130 \pm 0.016. \end{aligned} \tag{4.13}$$

A fit using our new estimate yields the freeze-out parameters given in Table 4.10.

Table 4.10: Fit results at the SPS for $Pb - Pb$ collisions using previous and new estimate of $\overline{\Lambda}/\Lambda$.

Parameters at freeze-out	Previous fit	New fit
T (MeV)	$156.1^{+2.5}_{-2.4}$	$156.2^{+2.5}_{-2.4}$
μ_B (MeV)	228^{+12}_{-12}	226^{+11}_{-10}
γ_s	$0.799^{+0.038}_{-0.036}$	$0.794^{+0.036}_{-0.035}$
Radius (GeV^{-1})	$49.5^{+2.1}_{-2.1}$	$49.5^{+2.1}_{-2.1}$
$\frac{\langle energy \rangle}{\langle particle \rangle}$ (GeV)	1.04	1.04
χ^2/dof	17.9/6	14.4/6

From the table we see a significant lowering of the chisquared value but, very small or no changes to the parameters from our previous fit.
The increase in $\overline{\Lambda}/\Lambda$ from SPS to RHIC, as with $\overline{p}/p$, reinforces what has been stated earlier, namely; at RHIC ($\overline{\Lambda}/\Lambda = 0.73 \pm 0.03$) we have a region of lower net baryon number than at the SPS.
It is also found that the $\overline{\Lambda}/\Lambda$ ratio is higher than the $\overline{p}/p$ ratio by about 8% in central collisions and by about 20% in very peripheral collisions at RHIC [97].

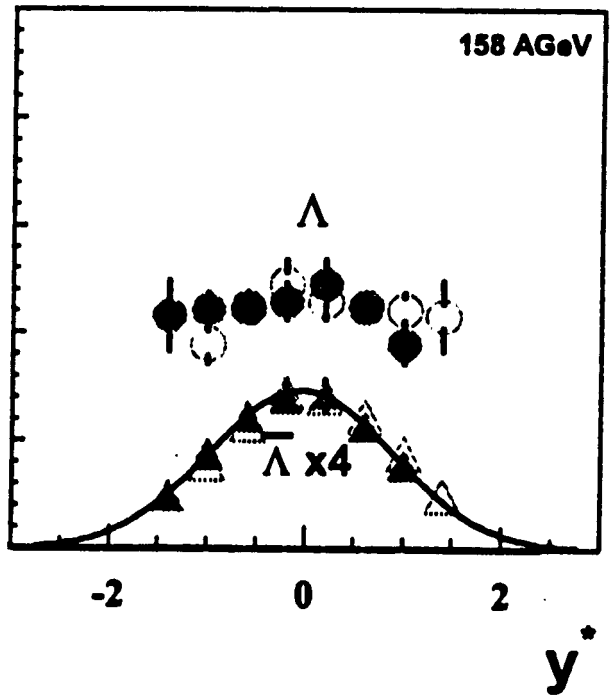

Figure 4.18: *Rapidity distribution of Λ and $\bar{\Lambda}$ produced in central Pb-Pb collisions at 158 A GeV. The open symbols are the reflected points and the filled symbols are the measured points [127].*

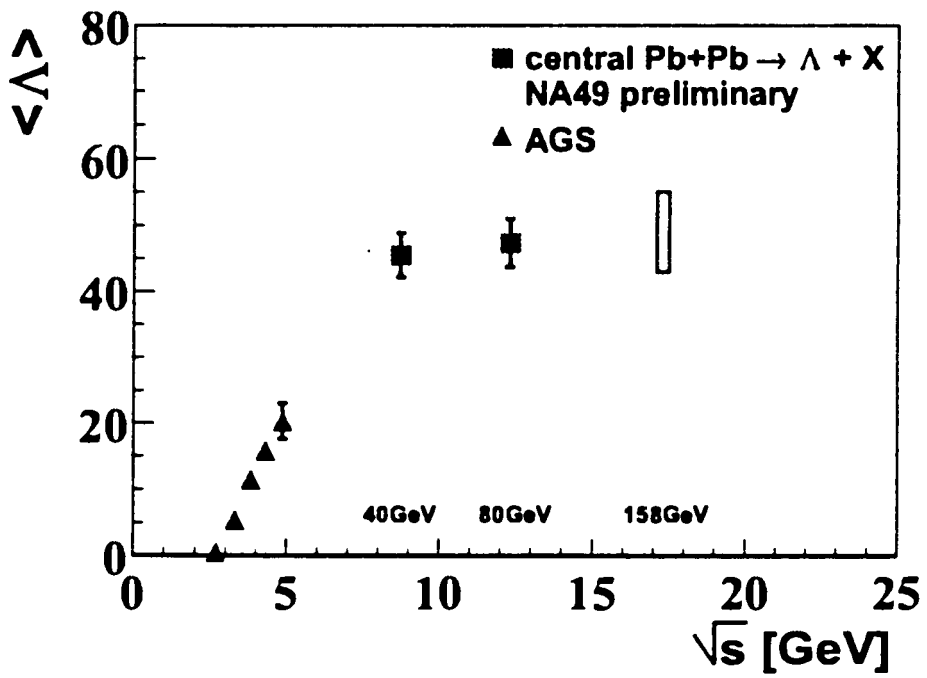

Figure 4.19: *The total Λ multiplicity as function of the c.m. energy, $\sqrt{s}$, for central Pb-Pb collisions [128].*

4.4.9 Chemical Freeze-out in the $T - \mu_B$ plane

The points in Figure 4.20 are the chemical freeze-out points plotted in the $T - \mu_B$ plane, *i.e.*, when the number-changing inelastic collisions cease and the particle abundancies are frozen in. The strangeness neutrality condition, $\langle S \rangle = 0$, shown to be appropriate in heavy-ion collisions, has been used to eliminate the dependence of the thermodynamical observables on the strangeness chemical potential. A lower μ_B indicates a lower net baryon number (the central region consisting mainly of mesons) hence a greater symmetry between quarks and antiquarks. From the figure we that a lower μ_B is accompanied by a higher temperature, *i.e.*, a lower baryon number in the central region corresponds to greater energy.

Results for SIS $Ni - Ni$ and SPS $Pb - Pb$ 40A GeV are given below.

Table 4.11: Summary of fit results for SIS $Ni - Ni$ collisions.

$Ni - Ni$ (SIS)				
A GeV	0.8	1.0	1.8	1.93
T (MeV)	$47.6^{+1.0}_{-1.1}$	$53.0^{+1.2}_{-1.4}$	$66.5^{+1.4}_{-1.6}$	$71.2^{+6.0}_{-6.1}$
μ_B (MeV)	821^{+24}_{-16}	800^{+26}_{-18}	735^{+5}_{-4}	733^{+17}_{-10}
γ_s	1	1	1	0.645
Radius (GeV^{-1})	20	20	20	20
χ^2	1.3E^{-7}	2.2E^{-10}	1.6	3.5

Table 4.12: Summary of fit results for SPS $Pb - Pb$ 40A GeV.

$Pb - Pb$ 40A GeV Preliminary (SPS)			
	This Analysis	without Λ	From [107]
T (MeV)	$156.3^{+2.6}_{-2.6}$	$156.3^{+2.6}_{-2.7}$	149.3±2.4
μ_B (MeV)	379^{+11}_{-10}	$361^{+9.4}_{-8.8}$	$\mu_B/T = 2.637 \pm 0.068$
γ_s	$0.872^{+0.076}_{-0.068}$	$0.722^{+0.060}_{-0.057}$	0.822±0.058
Radius (GeV^{-1})	$35.3^{+1.8}_{-1.8}$	$37.0^{+1.8}_{-1.7}$	
χ^2/dof	65.1/3	22.3/3	13.5/3

For $Pb - Pb$ 40A GeV we see that the χ^2/dof is higher than that obtained in [107] and drops substantially with the exclusion of Λ without a great change in the parameter values. The data is preliminary and more stable parameter values with a lower χ^2 and greater consistency across different thermal model analyses is expected later.

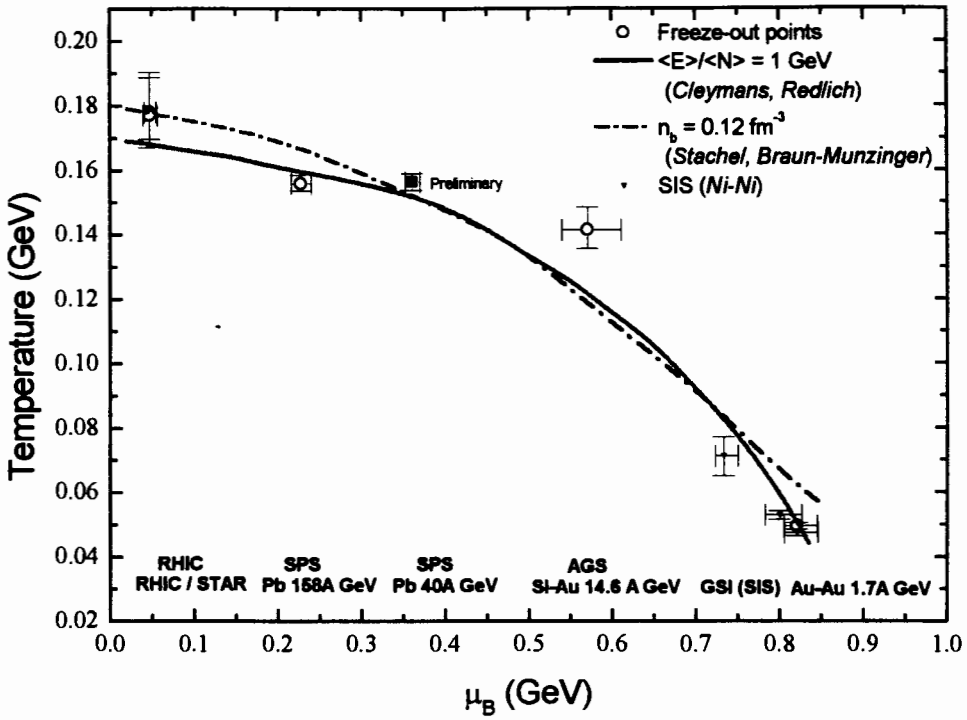

Figure 4.20: *Fitted temperatures and baryon chemical potentials plotted together with a curve of constant energy per hadron and of constant total baryon density.*

4.4.10 Universal freeze-out conditions

Two independent suggestions for a unified description or interpretation of the chemical freeze-out trajectory in the $T - \mu_B$ plane proposed in recent times, are discussed here.

The first (reference [129]) suggests that the particle freeze-out occurs at a fixed energy per particle, $\langle E \rangle / \langle N \rangle \approx 1$ GeV, while the other (reference [130]) differs significantly in its interpretation by suggesting that the total baryon plus antibaryon density $n_b = 0.12/\text{fm}^3$.

Energy per Particle at Freeze-out

We see from the phenomenological $\langle E \rangle / \langle N \rangle$ curve in Figure 4.20 that the energy per particle at chemical freeze-out remains practically constant which strengthens the conjecture that hadrons freeze out with an energy of approximately 1.0 GeV. This is also seen in Table 4.5. The ratio $\langle E \rangle / \langle N \rangle$ depends on only two thermal parameters; the temperature, T, and the baryon chemical potential, μ_B.

At low T ($T \sim 50$ MeV), too low for the prescence of pions, and with the system consisting

only of nucleons, a theoretical prediction can be made for SIS energies. We find in what is essentially a non-relativistic regime that

$$\begin{aligned}
\lim_{T\to 0} \frac{\langle E\rangle}{\langle N\rangle} &= \underbrace{m_N}_{\textit{mass of nucleon}} + \underbrace{KE}_{\textit{kinetic energy of an ideal gas}} \\
&= m_N + \frac{3}{2}T \\
&= 940 \text{ MeV} + \left(\frac{3}{2}\times 50\right) \text{ MeV} \\
&= 1015 \text{ MeV} \\
&= 1.015 \text{ GeV} \qquad (4.14)
\end{aligned}$$

From the model we obtain $\langle E\rangle / \langle N\rangle = 0.960^{+0.014}_{-0.014}$ at a freeze-out temperature of $49.6^{+1.0}_{-1.2}$ MeV for $Au - Au$ $1.7A$ GeV collisions at SIS.
$\langle E\rangle / \langle N\rangle \approx 1$ is found to be a fairly robust and model independent condition.

Constant Total Baryon Density

The interpretation of the freeze-out trajectory taking place at constant total baryon density implies the following physical picture: chemical freeze-out takes place at a critical baryon density through baryon-baryon and baryon-meson interactions.
The actual value of $n_b = 0.12/\text{fm}^3$ depends on the fact that in [131] excluded volume corrections are introduced based on repulsive hadron-hadron interactions.

In the next chapter we compare the chemical freeze-out trajectory obtained *via* our model calculations to a phase boundary curve obtained from calculations using a bag model.

Chapter 5

The Phase Transition and Chemical Freeze-Out

"The central assumption of the quark-bag approach is that inside a hadron where quarks are found, the true vacuum is displaced or destroyed and coloured particles propagate easily. One can turn this point around: quarks can only propagate in domains of space in which the true vacuum structure is absent." [132]

"Bag" models offer a schematic yet attractive way of incorporating quark confinement, whereby quarks (and more generally, all coloured particles) are confined to small regions of space, into hadronic structure calculations since QCD is too complicated from which to obtain simple analytical solutions [133].

A variety of bag models have been developed and discussed in the literature (for example, see [134]).

In this chapter we apply ideas based on the M.I.T.-bag model [135], [136] to compare the phase transition from a quark-gluon plasma to a hadron gas in heavy-ion collisions, to a chemical freeze-out curve obtained by using a model which conserves strangeness exactly for results in central $Au - Au$, $Pb - Pb$ and $Si - Au$ collisions presented in the preceding chapter. We look at both the phase boundary and chemical freeze-out in the $T - \mu_B$ plane.

The M.I.T.-bag model is based in a simple way on two fundamental features of QCD namely; aymptotic freedom and, confinement. In the model, hadrons are bubbles in the vacuum in

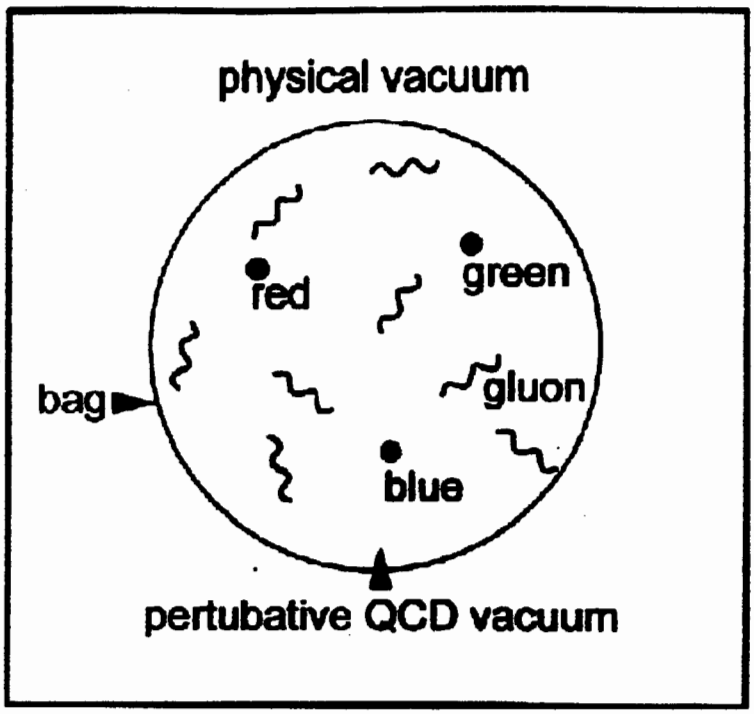

Figure 5.1: *Schematic presentation of the (M.I.T.) Bag Model.*

which freely moving quarks are confined and interactions are neglected or treated to lowest order perturbation theory. Outside the bag, quarks or gluons (single colour charges) cannot exist as free particles [137].

The motion of the quarks in the bag gives rise to a *Fermi pressure* [138] which would cause the bag to expand. To counteract this, the vacuum would have to exert an external pressure on the bag. A constant *vacuum* (or *"bag") pressure*, B, with units of energy density is introduced to parametrize confinement effects. That is, B guarantees confinement. Limits on the value of B have been estimated phenomenologically usually from fits to the hadronic mass spectrum such as in [139]-[141] or, from sum rule considerations [142].

To find the phase boundary between the hadron gas and the quark-gluon plasma, we first need to consider conditions necessary to maintain a state of equilibrium between the phases.

5.1 Criteria for Phase Equilibrium

Stability of the bag depends on maintaining equilibrium between the pressures inside and, outside the bag. The Gibbs coexistence criteria prescribes the equilibrium conditions for two phases consisting of identical particles. These are; the equalities of pressure and temperature between both phasess [143].

In the case of a quark-gluon-plasma (QGP) and hadron gas (HG) which are in equilibrium:

$$\begin{aligned} P_{QGP} &= P_{HG} \ (\textit{Mechanical Equlibrium}) \\ T_{QGP} &= T_{HG} \ (\textit{Thermal Equilibrium}) \end{aligned} \tag{5.1}$$

We consider the baryon content of the system which consists partly of quarks and partly of nucleons. The number, N^B, of baryons from the quark-gluon component is

$$N^B_{QGP} = \frac{1}{3}\left(N^Q - N^{\overline{Q}}\right), \tag{5.2}$$

where N^Q and $N^{\overline{Q}}$ are the number of quarks and antiquarks respectively.

The number of baryons from the hadron gas component is

$$N^B_{HG} = \sum_i N_i^{Baryons} = \left(N^B - N^{\overline{B}}\right). \tag{5.3}$$

The conservation of total baryon number implies that in the mixed phase

$$d\left(N^B_{QGP} + N^B_{HG}\right) = 0. \tag{5.4}$$

Therefore,

$$dN^B_{QGP} = -dN^B_{HG}\ , \tag{5.5}$$

so that,

$$\frac{1}{3}d\underbrace{\left(N^Q - N^{\overline{Q}}\right)}_{QGP} = -d\underbrace{\left(N^B - N^{\overline{B}}\right)}_{HG} \tag{5.6}$$

or,

$$-\frac{1}{3}dN^B_{QGP} = dN^B_{HG}\ , \tag{5.7}$$

a baryon consisting of three quarks.

To find a relationship between the chemical potentials of the quarks and baryons at phase equilibrium, we start by substituting the first law of thermodynamics,

$$dE = TdS - PdV + \mu dN, \tag{5.8}$$

into the Gibbs free energy,

$$G(T, P, N) = E - TS + PV, \tag{5.9}$$

thus, obtaining:

$$dG = -SdT + VdP + \mu_B dN_B. \tag{5.10}$$

By minimizing the Gibbs free energy at fixed temperature and pressure, we derive the condition that

$$\mu_B^{QGP} dN_{QGP}^B + \mu_B^{HG} dN_{HG}^B = 0 \tag{5.11}$$

which, with equation 5.7 from the condition that baryon number is conserved in the mixed phase, we obtain:

$$-3\mu_B^{QGP} dN_{HG}^B + \mu_B^{HG} dN_{HG}^B = 0. \tag{5.12}$$

Therefore,

$$\mu_B^{QGP} = \frac{1}{3}\mu_B^{HG}\,. \tag{5.13}$$

The condition for mechanical equilibrium can thus be written as

$$P^{QGP}\left(T, \frac{1}{3}\mu_B\right) = P^{HG}(T, \mu_B)\,. \tag{5.14}$$

In plotting the $T - \mu_B$ phase boundary, T will be calculated by fixing μ_B and using the above condition for pressures.

Before this, however, we examine expressions for P^{QGP} and P^{HG} in closer detail, including the addition of the bag constant, B.

5.2 Pressures in the Two Phases

5.2.1 Pressure of the Quark-Gluon Plasma

The pressure of an ideal Fermi or Bose gas is given by

$$P = \frac{T}{V}\ln Z. \tag{5.15}$$

In the bag model an additional term, containing B, is added to describe the ground state shift from the physical vacuum into the perturbative QCD vacuum inside the bag and is written as

$$\ln Z_{vacuum} = -BV/T \tag{5.16}$$

or,

$$\frac{T}{V}\ln Z_{vacuum} = -B. \tag{5.17}$$

Since we are treating quarks and gluons as ultra-relativistic ideal Fermi and Bose gases respectively, the pressure of the quark-gluon plasma is therefore

$$P_{QGP} = \frac{T}{V}\ln Z_{QGP} - B. \tag{5.18}$$

$\frac{T}{V}\ln Z$ can be calculated exactly (see [138]) and written in closed form (restricting ourselves first to non-strange quarks) as

$$\frac{T}{V}\ln Z_{QGP} = \frac{\pi^2}{45}N_g T^4 + \frac{1}{6}N_c N_q\left(\frac{7}{30}\pi^2 T^4 + \mu_q^2 T^2 + \frac{1}{2\pi^2}\mu_q^4\right), \tag{5.19}$$

where

$$\begin{aligned} N_g &= Number\ of\ gluons \\ N_c &= Number\ of\ colours \\ N_q &= Number\ of\ light\ quark\ flavours \\ \mu_q &= \mu_b^{non-strange\ quarks} = \frac{\mu_B}{3} \end{aligned} \tag{5.20}$$

so that,

$$P_{QGP} = \frac{\pi^2}{45}N_g T^4 + \frac{1}{6}N_c N_q\left(\frac{7}{30}\pi^2 T^4 + \mu_q^2 T^2 + \frac{1}{2\pi^2}\mu_q^4\right) - B. \tag{5.21}$$

With

$$\begin{aligned} N_g &= N_{colours}^2 - 1 = 8\ \ (for\ SU(3)) \\ N_c &= 3 \\ N_q &= 2, \end{aligned} \tag{5.22}$$

the pressure can be written as

$$P_{QGP} = \underbrace{\frac{8\pi^2}{45}T^4}_{gluon\ contribution} + \underbrace{\frac{N_q}{15\pi^2}\left[\underbrace{\frac{7}{4}(\pi T)^4}_{pure\ thermal\ contribution} + \underbrace{\frac{15}{2}\left(\mu_q(\pi T)^2 + \frac{1}{2}\mu_q^4\right)}_{finite\ density\ contribution}\right]}_{non-strange\ quark\ contribution} - B. \tag{5.23}$$

Strange quarks may be added in a similar way to yield:

$$\begin{aligned} P_{QGP} &= \frac{8\pi^2}{45}T^4 - B \\ &+\frac{N_q}{15\pi^2}\left[\frac{7}{4}(\pi T)^4 + \frac{15}{2}\left(\mu_q(\pi T)^2 + \frac{1}{2}\mu_q^4\right)\right] \\ &+\frac{N_s}{15\pi^2}\left[\frac{7}{4}(\pi T)^4 + \frac{15}{2}\left(\mu_s(\pi T)^2 + \frac{1}{2}\mu_s^4\right)\right], \end{aligned} \tag{5.24}$$

where $N_s = 1$ for the number of strange quarks flavours and, $\mu_s = 0$ for exact strangeness conservation ($s = \overline{s}$).

Perturbative Corrections to P_{QGP}

In this section we consider α_s order thermal QCD corrections. This can be introduced into equation 5.24 as c_1, c_2 and c_3 in the following way, [144], [145], and following the notation in [146]:

$$\begin{aligned} P_{QGP} &= \frac{8\pi^2}{45}c_1T^4 - B \\ &+\frac{N_q}{15\pi^2}\left[\frac{7}{4}c_2(\pi T)^4 + \frac{15}{2}c_3\left(\mu_q(\pi T)^2 + \frac{1}{2}\mu_q^4\right)\right] \\ &+\frac{N_s}{15\pi^2}\left[\frac{7}{4}c_2(\pi T)^4 + \frac{15}{2}c_3\left(\mu_s(\pi T)^2 + \frac{1}{2}\mu_s^4\right)\right], \end{aligned} \tag{5.25}$$

where

$$\begin{aligned} c_1 &= 1 - \frac{15\alpha_s}{4\pi} + \cdots \\ c_2 &= 1 - \frac{50\alpha_s}{21\pi} + \cdots \\ c_3 &= 1 - \frac{2\alpha_s}{\pi} + \cdots. \end{aligned} \tag{5.26}$$

The QCD coupling constant, $\alpha_s(\mu)$, is given by

$$\alpha_s(\mu) \simeq \frac{2}{b_0\overline{L}}\left[1 - \frac{2b_1}{b_0^2}\frac{\ln\overline{L}}{\overline{L}}\right], \quad \underset{\Lambda=QCD\ Scale\ Parameter}{\overline{L} = \ln\left(M^2/\Lambda^2\right)}, \tag{5.27}$$

for the two-loop approximation and, by

$$\alpha_s \simeq \frac{2}{b_0\overline{L}}, \tag{5.28}$$

for the one-loop approximation,

where

$$\begin{aligned} b_0 &= \frac{11 - 2N_f/3}{2\pi} \\ b_1 &= \frac{51 - 19N_f/3}{4\pi^2} \quad , N_f = number\ of\ flavours. \end{aligned} \tag{5.29}$$

Choosing an energy or momentum scale, since, in QCD with the introduction of loop approximations, the coupling constant becomes scale dependent and the whole idea would be to minimise this or subsume it into the scale parameters, we set the scale (based on the Matsubara frequency), M [145], [146], by

$$M = \sqrt{(\pi T)^2 + \mu_q^2}, \tag{5.30}$$

to relate the QCD scale to the temperature.

Mass Correction due to Strange Quark Mass

Starting with the expression for the pressure of a fermion,

$$P\left(T, \mu; m^2\right) = 2T \int \frac{d^3p}{(2\pi)^3} \left[\ln\left(1 + e^{-(E-\mu)/T}\right) + \ln\left(1 + e^{-(E+\mu)/T}\right)\right], \text{ [145]}, \tag{5.31}$$

where

$$E = \sqrt{p^2 + m^2}\ , \tag{5.32}$$

we differentiate P to obtain,

$$\begin{aligned} P'(T, \mu; 0) &\equiv \frac{\partial}{\partial m^2} P\left(T, \mu; m^2\right)|_{m^2=0} \\ &= 2T \frac{4\pi}{8\pi^3} \int_0^\infty p^2 dp \frac{1}{2p} \frac{\partial}{\partial p} \left[\ln\left(1 + e^{-(E-\mu)/T}\right) + \ln\left(1 + e^{-(E+\mu)/T}\right)\right]_{m^2=0} \\ &= T \frac{1}{2\pi^2} \int_0^\infty dp.p \frac{d}{dp} \left[\ln\left(1 + e^{-(p-\mu)/T}\right) + \ln\left(1 + e^{-(p+\mu)/T}\right)\right] \\ &= -\frac{T}{2\pi^2} \int_0^\infty dp \left[\ln\left(1 + e^{-(p-\mu)/T}\right) + \ln\left(1 + e^{-(p+\mu)/T}\right)\right] \\ &= -\frac{T^2}{2\pi^2} \int_0^\infty dY \left[\ln\left(1 + e^{-Y+\mu/T}\right) + \ln\left(1 + e^{-Y-\mu/T}\right)\right], \end{aligned} \tag{5.33}$$

making,

$$t = 1 + e^{-Y \pm \mu/T} \Rightarrow \ln(t-1) = -Y \pm \mu \Rightarrow dY = -\frac{dt}{t-1}\ . \tag{5.34}$$

Therefore,

$$\begin{aligned} P'(T,\mu;0) &= -\frac{T^2}{2\pi^2}\left[\left\{-\int\limits_{1+e^{\mu/T}}^{1}\frac{dt}{t-1}\ln t-\int\limits_{1+e^{-\mu/T}}^{1}\frac{dt}{t-1}\ln t\right\}\right] \\ &= \frac{T^2}{2\pi^2}\left[f\left(1+e^{\mu/T}\right)+f\left(1+e^{-\mu/T}\right)\right], \end{aligned} \tag{5.35}$$

where $f(x)$ in 5.35 is the Spence Dilogarithm function as defined in [147] *i.e.*,

$$f(x) = -\int\limits_{1}^{x}\frac{\ln t}{t-1}dt. \tag{5.36}$$

with (among other) the following identities:

$$\begin{aligned} f(x)+f(\frac{1}{x}) &= -\frac{1}{2}(\ln x)^2 \qquad (0\le x\le 1) \\ f(x)+f(1-x) &= -\ln x\ln(1-x)+\frac{\pi^2}{6} \qquad (0\le x\le 1), \end{aligned} \tag{5.37}$$

so that,

$$\begin{aligned} P'(T,\mu;0) &= \frac{T^2}{2\pi^2}\left[f\left(1+e^{-\mu/T}\right)-f\left(\frac{1}{1+e^{\mu/T}}\right)-\frac{1}{2}\ln^2\left(\frac{1}{1+e^{\mu/T}}\right)\right] \\ &= \frac{T^2}{2\pi^2}\left[f\left(1+e^{-\mu/T}\right)-\left\{\frac{\pi^2}{6}-\ln\left(\frac{1}{1+e^{\mu/T}}\right)\ln\left(\frac{e^{\mu/T}}{1+e^{\mu/T}}\right)-f\left(\frac{e^{\mu/T}}{1+e^{\mu/T}}\right)\right\}\right. \\ &\quad \left.-\frac{1}{2}\ln^2\left(\frac{1}{1+e^{\mu/T}}\right)\right] \\ &= \frac{T^2}{2\pi^2}\left[f\left(1+e^{-\mu/T}\right)+f\left(\frac{1}{1+e^{-\mu/T}}\right)-\frac{\pi^2}{6}+\ln\left(\frac{1}{1+e^{\mu/T}}\right)\ln\left(\frac{e^{\mu/T}}{1+e^{\mu/T}}\right)\right. \\ &\quad \left.-\frac{1}{2}\ln^2\left(\frac{1}{1+e^{\mu/T}}\right)\right] \\ &= \frac{T^2}{2\pi^2}\left[-\frac{\pi^2}{6}-\frac{1}{2}\ln^2\left(\frac{1}{1+e^{\mu/T}}\right)+\ln\left(\frac{1}{1+e^{-\mu/T}}\right)\ln\left(\frac{e^{-\mu/T}}{1+e^{-\mu/T}}\right)\right. \\ &\quad \left.-\frac{1}{2}\ln^2\left(\frac{e^{-\mu/T}}{1+e^{-\mu/T}}\right)\right] \\ &= \frac{T^2}{2\pi^2}\left[-\frac{\pi^2}{6}-\frac{1}{2}\ln^2\left(e^{-\mu/T}\right)\right] \\ &= -\frac{T^2}{12}-\frac{T^2}{4\pi^2}\left(-\frac{\mu}{T}\right)^2 \\ &= -\frac{T^2}{12}-\frac{\mu^2}{4\pi^2}\,. \end{aligned} \tag{5.38}$$

Therefore,

$$P\left(T,\mu;m^2\right) \simeq P\left(T,\mu;0\right) - \frac{T^2m^2}{12} - \frac{\mu^2m^2}{4\pi^2}\ , \tag{5.39}$$

for one colour, order m^2 corrections.

Energy Density of the Quark-Gluon Plasma

The pressure of the QGP has the form

$$P_Q = aT^4 + bT^2\mu^2 + c\mu^4 - B, \tag{5.40}$$

while the energy density of the QGP has the form

$$\begin{aligned}
\epsilon_Q &= -P_Q + T\frac{\partial}{\partial T}P_Q + \mu\frac{\partial}{\partial \mu}P_Q \\
&= -aT^4 - bT^2\mu^2 - c\mu^4 + B \\
&\quad +4aT^4 + 2bT^2\mu^2 \\
&\quad +2bT^2\mu^2 + 4c\mu^{-1}.
\end{aligned} \tag{5.41}$$

Therefore,

$$\epsilon_Q = 3aT^4 + 3bT^2\mu^2 + 3c\mu^4 + B. \tag{5.42}$$

If $a = a(T,\mu)$, $b = b(T,\mu)$ and $c = c(T,\mu)$, then

$$\begin{aligned}
\epsilon_Q &= \left[3a + \left(T\frac{\partial a}{\partial T} + \mu\frac{\partial a}{\partial \mu}\right)\right]T^4 \\
&\quad + \left[3b + \left(T\frac{\partial b}{\partial T} + \mu\frac{\partial b}{\partial \mu}\right)\right]T^2\mu^2 \\
&\quad + \left[3c + \left(T\frac{\partial c}{\partial T} + \mu\frac{\partial c}{\partial \mu}\right)\right]\mu^4 + B
\end{aligned} \tag{5.43}$$

For comparison with lattice results we set $\mu = 0$. With $a = a(\alpha_s(T,\mu))$

$$\begin{aligned}
\left(T\frac{\partial}{\partial T} + \mu\frac{\partial}{\partial \mu}\right)a &= \frac{\partial a}{\partial \alpha_s}\left(T\frac{\partial}{\partial T} + \mu\frac{\partial}{\partial \mu}\right)\alpha_s(T,\mu) \\
&= \frac{\partial a}{\partial \alpha_s}\left(M\frac{\partial \alpha_s}{\partial M}\right)\left(T\frac{\partial M}{\partial T} + \mu\frac{\partial M}{\partial \mu}\right)/M \\
&= \left(\frac{\partial a}{\partial \alpha_s}\right)\left[-b_0\alpha_s^2 - b_1\alpha_s^3\right] \\
&\quad \cdot\frac{1}{\sqrt{(\pi T)^2 + \mu^2}}\left[\frac{1}{2}\frac{2(\pi T)^2}{\sqrt{(\pi T)^2 + \mu^2}} + \frac{1}{2}\frac{2\mu^2}{\sqrt{(\pi T)^2 + \mu^2}}\right]
\end{aligned}$$

$$= \left(\frac{\partial a}{\partial \alpha_s}\right) \underbrace{\left[-b_0\alpha_s^2 - b_1\alpha_s^3\right]}_{\textit{from renormalization group}} \qquad \text{(for the two-loop case)}$$

$$= \left(\frac{\partial a}{\partial \alpha_s}\right)\left[-b_0\alpha_s^2\right] \qquad \text{(for the one-loop case).} \tag{5.44}$$

From equation 5.24,

$$a = \left[\underbrace{\frac{8}{45\pi^2}c_1}_{Gluons} + \underbrace{\frac{n_q}{15\pi^2}\cdot\frac{7}{4}c_2}_{Non-Strange\ Quarks} + \underbrace{\frac{n_s}{15\pi^2}\cdot\frac{7}{4}c_2}_{Strange\ Quarks}\right]\pi^4$$

$$= \left[\frac{8}{45\pi^2} - \frac{8}{45\pi^2}\frac{15\alpha_s}{4\pi} + \frac{n_q}{15\pi^2}\frac{7}{4} - \frac{n_q}{15\pi^2}\frac{7}{4}\frac{50\alpha_s}{21\pi} + \frac{n_s}{15\pi^2}\frac{7}{4} - \frac{n_s}{15\pi^2}\frac{7}{4}\frac{50\alpha_s}{21\pi}\right]\pi^4 \tag{5.45}$$

Therefore,

$$\frac{\partial a}{\partial \alpha_s} = -\frac{8}{45\pi}\frac{15}{4} - \frac{n_q}{15\pi}\frac{7}{4}\frac{50}{21} - \frac{n_s}{15\pi}\frac{7}{4}\frac{50}{21} \tag{5.46}$$

Comparison with lattice results for both P_Q/T^4 and ϵ_Q/T^4 are shown in Figure 5.2. As can be seen from the plots, the quark side pressure, which is used to establish the equilibrium condition in the construction of the phase boundary, follows the trend of the lattice points well, whereas with the quark side energy density it is well known that perturbation theory does not do a good job near the critical temperature (see for example [150]) and this is the case in the ϵ_Q/T^4 plot. Quasi-Particle Models (for example, [148]) do a better job with ϵ_Q but, are basically restricted to, and not successful in extending it significantly away from $\mu_B = 0$. Consequently, they are not successful in determining the phase boundary.

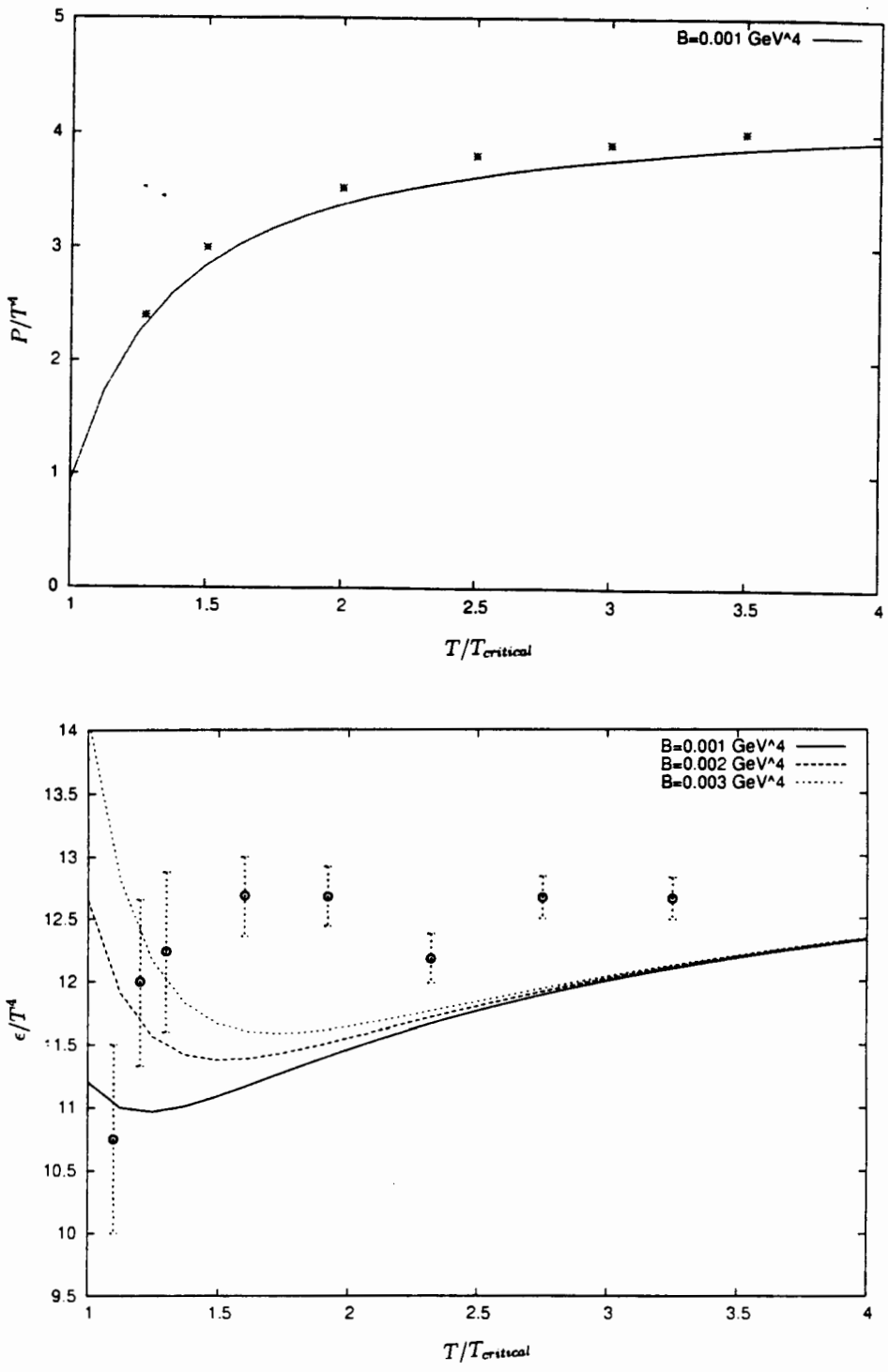

Figure 5.2: *Comparison of model plots with lattice points (from [149] and [150] respectively) for* P/T^4 *and* ϵ/T^4 *(3 flavours).*

5.2.2 Pressure of the Hadron Gas

The hadron gas is considered here as an ideal gas of pions, nucleons and antinucleons, taking into account all resonance decays and particle widths.

The pressure of a species in a weakly interacting gas with g internal degrees of freedom and chemical potential, μ, can be expressed in terms of its phase space distribution (or occupancy) function, $f(\overrightarrow{p})$ [151], as:

$$P = \frac{g}{(2\pi)^3} \int \frac{|\overrightarrow{p}|}{3E} f(\overrightarrow{p}) d^3p, \tag{5.47}$$

where $E^2 = |\overrightarrow{p}| + m^2$ and $f(\overrightarrow{p})$ is given by

$$f(\overrightarrow{p}) = \left[\exp\left((E-\mu)/T\right) \pm 1\right]^{-1}, \tag{5.48}$$

that is, by the Fermi-Dirac $(+1)$ or Bose-Einstein (-1) distributions for the species in thermal equilibrium.

The total pressure of all species in equilibrium in a hadron gas can be expressed in terms of the temperature, T, at chemical freeze-out as

$$P = \sum_i \frac{g_i}{(2\pi)^3} \int \frac{|\overrightarrow{p_i}|^2}{3E_i} \frac{d^3p}{e^{\frac{E_i-\mu_i}{T}} \pm 1} \quad , \; i = all \; species. \tag{5.49}$$

Inclusion of Interactions in the Hadron Gas

In Figure 5.3 we see the results of balancing the pressures for the hadron gas and the quark gluon plasma in the $T - \mu_B$ plane for different values of the bag constant. For higher temperatures we see the contours curling up, contrary to expectation. This clearly shows that what we have in terms of the (hadron) pressure is not sufficient to construct a phase boundary curve, and that our initial assumptions will have to be re-examined.

To unravel the issues concerning the hadron gas pressure we first assume:

(i) non-relativistic kinematics,

(ii) statistics in the limit of Maxwell-Boltzmann,

(iii) the baryons and mesons can in some average sense be represented by a particle of mass (M for baryons and m for mesons in the equations which follow) with degeneracy (G for baryons and g for mesons overleaf).

So for an ideal hadron gas we have that

$$P_{H0}(T,\mu) = \underbrace{P_{M0}(T)}_{Mesons} + \underbrace{P_{B0}(T,\mu)}_{Baryons} \tag{5.50}$$

where

$$\begin{aligned} P_{M0}(T) &= Tg\left(\frac{mT}{2\pi}\right)^{3/2} e^{-m/T}, \text{ and} \\ P_{B0}(T,\mu) &= TG\left(\frac{MT}{2\pi}\right)^{3/2} e^{-M/T}\left[e^{\mu/T} + e^{-\mu/T}\right]. \end{aligned} \tag{5.51}$$

We see that with T fixed, increasing μ increases P_{B0}. Moreover, the growth is exponential. Since the quark-gluon plasma pressure, $P_{QGP}(T,\mu)$, is only polynomial in T and μ there will be no phase transition beyond a certain μ contrary to the expectation that, even at $T = 0$, one can compress nuclear matter so much that nucleons lose their identity and a QGP forms. What suggests itself is, that as μ increases, the neglect of interactions is no longer justified. To see how interactions can be included so as to achieve the expected behaviour, we follow the prescription of Olive [152]. In our interpretation we start with a potential based on the grand canonical potential, but including interactions, by writing it as

$$\Omega(T,\mu;n) = TG\left(\frac{MT}{2\pi}\right)^{3/2} e^{-(M+Kn)/T}\left[e^{\mu/T} + e^{-\mu/T}\right] + \frac{1}{2}Kn^2 \tag{5.52}$$

where Kn is an additional repulsive mean field interaction term proportional to the density, added so that the density, and therefore the pressure, does not rise as fast. Davidson and Miller *et al* [153] have also done work including the Kn term based on the mean-field approach in [152] and [154].

If one starts with the generalised two-body potential

$$V(r) = \sum_i C_i \frac{e^{-m_i r}}{r}, \tag{5.53}$$

and the potential due to all other particles in the system

$$U(\overrightarrow{r}) = \int d^3r' V\left(\overrightarrow{r} - \overrightarrow{r'}\right) n\left(\overrightarrow{r'}\right), \tag{5.54}$$

and, if $n\left(\overrightarrow{r'}\right) = n$, *i.e.*, the system is homogeneous, then

$$U(\overrightarrow{r}) = n\int d^3r V(r)$$

$$
\begin{aligned}
&= n\sum_i C_i \int_0^\infty 4\pi r^2 dr \frac{e^{-m_i r}}{r} \\
&= 4\pi n \sum_i C_i \int_0^\infty r e^{-m_i r} dr \\
&= 4\pi n \sum_i C_i \left[\frac{e^{-m_i r}}{m_i} r \Big|_0^\infty + \int_0^\infty dr \frac{e^{-m_i r}}{m_i} \right] \\
&= \underbrace{\left[4\pi \sum_i \frac{C_i}{m_i^2} \right]}_{K} n \\
&= Kn. \qquad (5.55)
\end{aligned}
$$

Equation 5.52 will be consistent with the thermodynamic identities, *e.g.*

$$n_B = \frac{\partial P_B}{\partial \mu} , \qquad (5.56)$$

iff

$$\frac{\partial \Omega}{\partial n} = 0 , \qquad (5.57)$$

i.e.

$$P_B(T,\mu) = \Omega(T,\mu;n)|_{extremised} \qquad (5.58)$$

with

$$\frac{\partial \Omega}{\partial n} = K \left[n - TG \left(\frac{MT}{2\pi} \right)^{3/2} e^{-(M+Kn)/T} \left[e^{\mu/T} + e^{-\mu/T} \right] \right] . \qquad (5.59)$$

Therefore, n is a solution of the self-consistent equation (after setting Equation 5.59 equal to zero)

$$
\begin{aligned}
n &= TG \left(\frac{MT}{2\pi} \right)^{3/2} e^{-(M+Kn)/T} \left[e^{\mu/T} + e^{-\mu/T} \right] \\
&= n_0 e^{-Kn/T} , \qquad (5.60)
\end{aligned}
$$

where n_0 is the ideal gas number density.

To see the effect we can write the self consistent equation as

$$\frac{n}{n_0} = \exp\left(-\left(\frac{Kn_0}{T} \right) \frac{n}{n_0} \right) , \qquad (5.61)$$

or,

$$x = e^{-yx} \qquad (5.62)$$

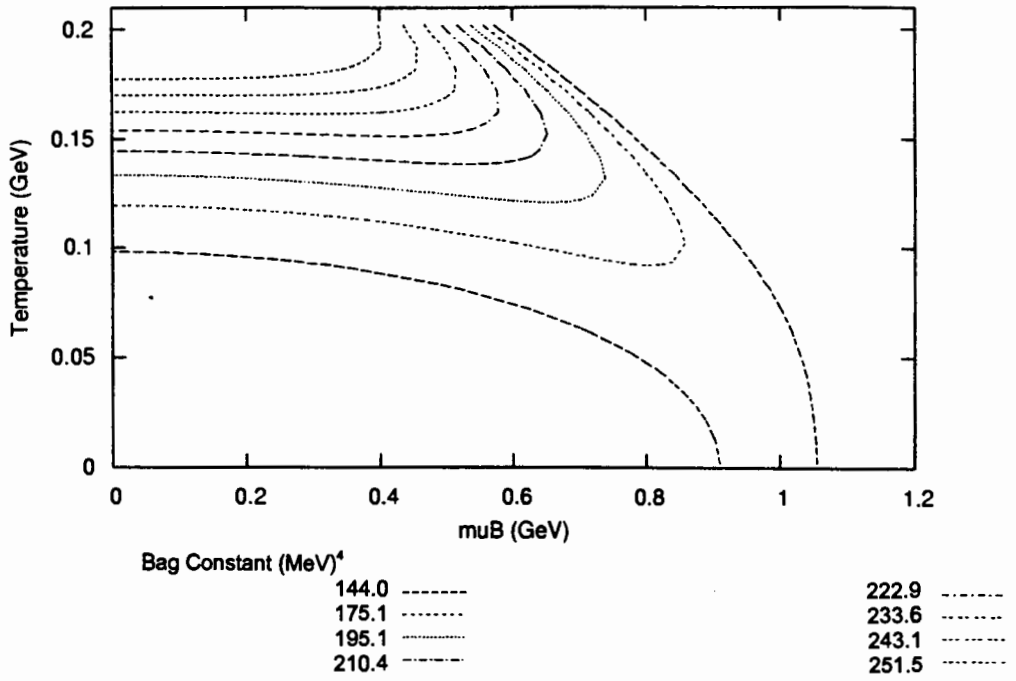

Figure 5.3: *Phase Boundary Curves for different values of B but, with no interaction terms in* P_{HG}.

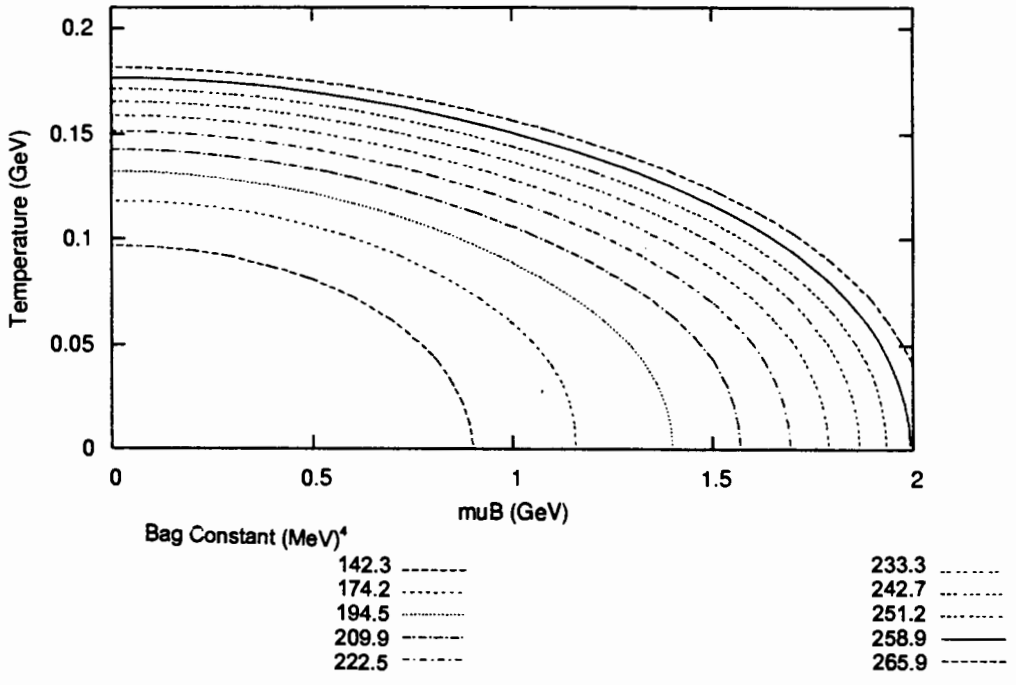

Figure 5.4: *Phase Boundary Curves for different values of B with interaction terms in* P_{HG}, *but not including QCD corrections.*

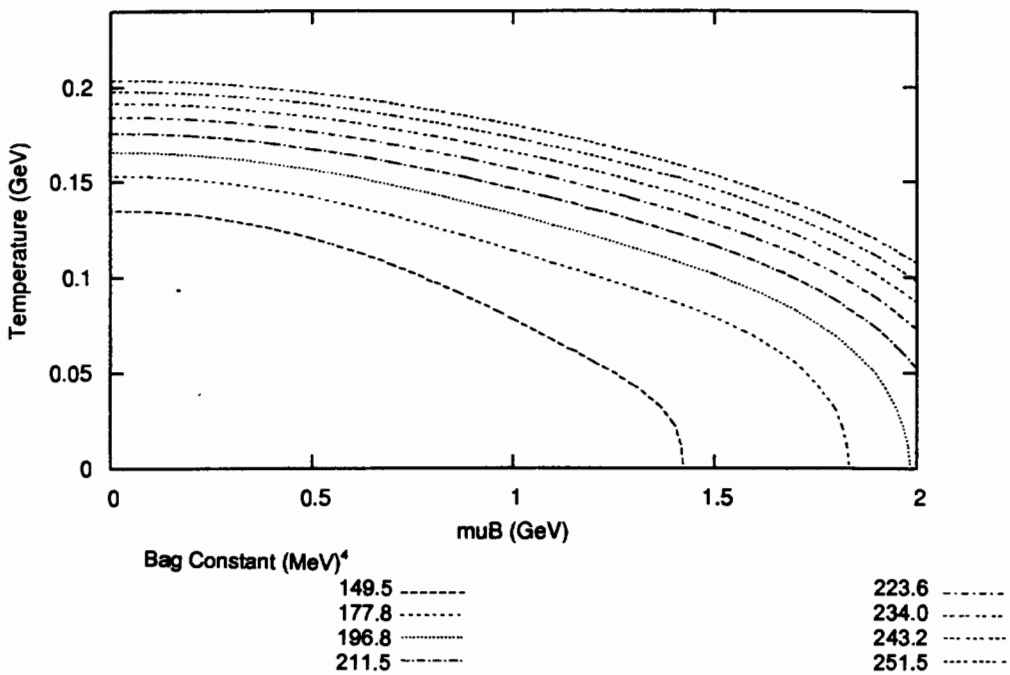

Figure 5.5: *Phase Boundary Curves for different values of B with interaction terms in P_{HG}, and including QCD corrections.*

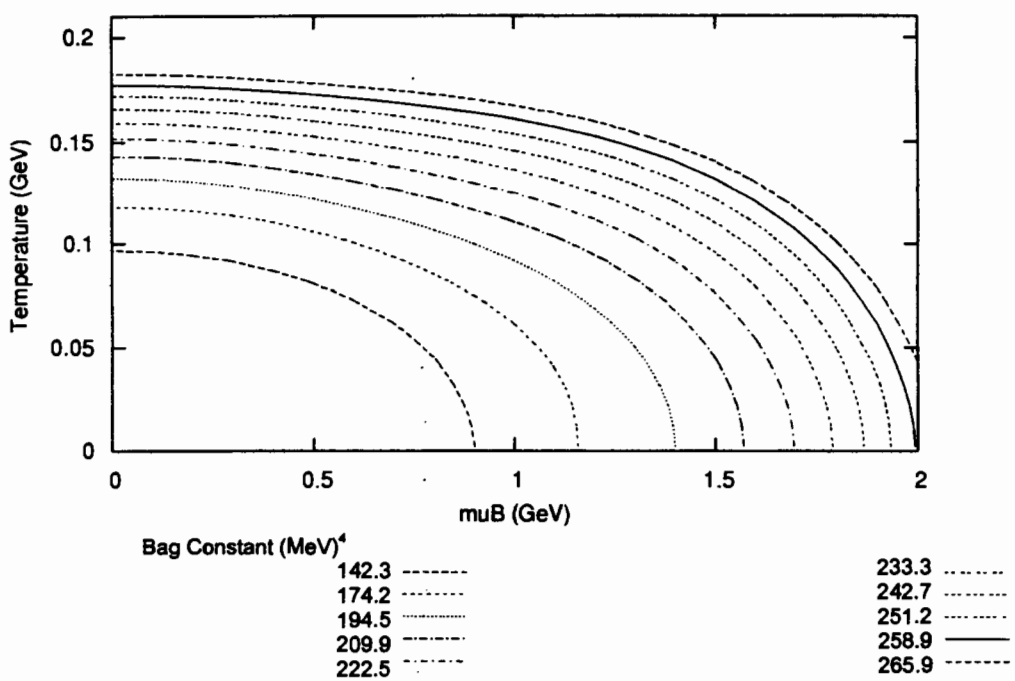

Figure 5.6: *Phase Boundary Curves for different values of B with interaction terms in P_{HG}, but without the $\left(\frac{m_{baryon}}{m_{nucleon}}\right)^2$ factor.*

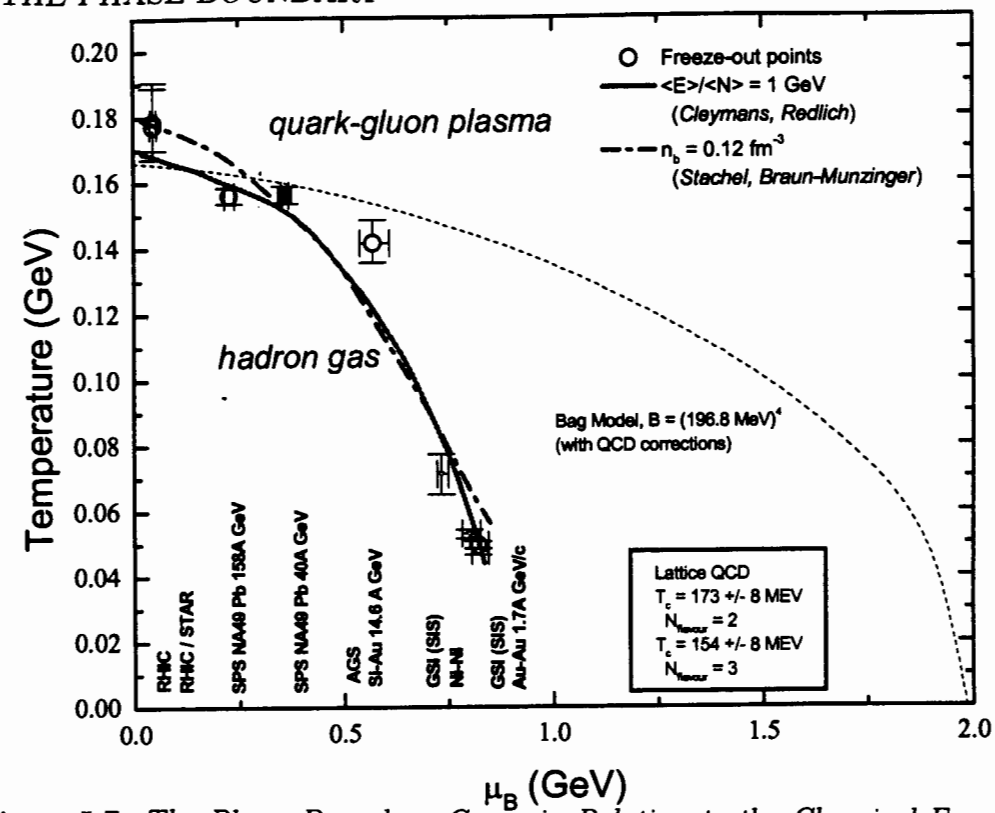

Figure 5.7: *The Phase Boundary Curve in Relation to the Chemical Freeze-Out curve.*

5.3 The Phase Boundary

A comparison of the phase transition curve with the chemical freeze-out curve will reveal whether chemical freeze-out, when the particle abundances are fixed, occurs in the quark-gluon plasma or the hadron gas. It will therefore tell us which phase the freeze-out parameters are conveying information about.

Figure 5.7 shows the phase boundary obtained by using the preceding arguments including QCD corrections to P_{QGP}.

For the phase boundary $T_c\,(\mu_{B_{critical}})$ in the $T-\mu_B$ plane, the critical value for the temperature, $T_{cr}\,(\mu_B = 0) = 166$ MeV, was chosen around $T = 160$ MeV (which corresponds to the universal slope parameter governing transverse momentum spectra in hadronic reactions [24], [156]).

As we see in Figure 5.7, the phase boundary is clearly above the freeze-out curves discussed in Chapter 3, until about the $Pb-Pb$ SPS point. In the region between the phase transition and chemical freeze-out, we find the interacting thermalized hadron gas in which reactions between hadrons are in chemical equilibrium. This forms an intermediate phase between the break-up, or hadronization, of the expanding QGP fireball and, the temperature at which chemical

interactions cease and particle abundances are fixed.

At higher temperature and lower μ_B (that is, lower baryon density) the intermediate region becomes smaller. There is a smaller difference in temperature between hadronization and chemical freeze-out since chemical interactions between hadrons cease faster because of their lower density.

On the plot the $Au - Au$ RHIC points fall in the QGP as well as (within error) on the energy density curve of 1.0 GeV per nucleon and, the total baryon plus antibaryon density curve of $n_b = 0.12/fm^3$. In the regime that the chemical freeze-out curve lies above the phase boundary curve, freeze-out happens in the QGP and freeze-out parameters obtained give us information about the plasma phase.

In this scenario equilibrated chemical reactions take place in the expanding QGP fireball as long as their reaction rates exceed the expansion rate. When the expansion rate becomes greater, chemical equilibrium ceases and chemical freeze-out occurs. Kinetic interactions continue in equilibrium. When the temperature cools below the critical temperature, the fireball undergoes hadronization.

Different mechanisms for hadronization after the QGP cools below critical temperature have been suggested by various authors (for example, see [157], [158]).

5.4 Conclusion

Phase transition curves obtained based on the M.I.T.-bag model including QCD corrections and using exact strangeness conservation, compared to chemical freeze-out discussed previously, has shown that, in the high temperature low μ_B regime of $Pb - Pb$ collisions at SPS energies and beyond, the possibility of producing a QGP and, of chemical freeze-out happening in the plasma phase. Freeze-out parameters obtained in this case using a statistical-thermal model will therefore convey information directly about the quark-gluon plasma phase.

Chapter 6

Summary Review: Perspectives on Particle Production

A summary and review of freeze-out and hadronization in the context of our thermal model follows.

Thermal modelling of particle production has been very successful in reproducing particle ratios in nucleus-nucleus collisions [159]. Since thermal models use statistical weight factors very few parameters are needed to describe the freeze-out stages of the produced system.

In high-energy collisions the interactions of the produced particles in the final state hadron gas determine the dynamical evolution of the system [161]. So, for elementary collisions, few particles are produced compared with $A - A$ collisions, and, therefore, not many final state interactions between the produced particles are likely. The particles decouple or "freeze-out" from the system soon after being produced, whereas for $A-A$ collisions the density of produced particles is sufficiently large over an extended region of space-time such that their mean free path length decreases. The result is that many final state interactions occur which drive the system towards local *thermodynamic* equilibrium, *i.e.*, thermal, mechanical and chemical equilibrium, with freeze-out occurring when microscopic interaction rates become smaller than the macroscopic expansion rate of the system [161].

As pointed out, for example, by Heinz [160] and Rischke [161], at CERN SPS energies and above, it is found that the chemical freeze-out temperature is higher than the kinetic freeze-out temperature. If one considers that chemical equilibrium involves frequent *inelastic* collisions and freeze-out occurs when these collisions cease and particle abundances are "frozen in", we

ratios/abundances determine the temperature at *chemical freeze-out.* This occurs earlier, *i.e.*, at a higher temperature than kinetic equilibrium which only involves *elastic* collisions - *kinetic freeze-out* occurring when these collisions cease. The extraction of a temperature from single-inclusive spectra assumes only kinetic equilibrium [158].

For a system in chemical equilibrium the possible values of μ_i are determined by the overall chemical potentials for: baryon number (μ_B), strangeness (μ_s), and charge (μ_Q).

Global conservation of baryon number, strangeness and charge impose additional constraints - the isospin asymmetry in the initial state fixes μ_Q and strangeness neutrality eliminates μ_s [68]. The abundance of particle species in equilibrium hadronic matter can thus be fully described by only two independent parameters, namely; the temperature, T, and the baryochemical potential, μ_B. Values for T and μ_B are extracted from a thermal model using a χ^2 analysis. Additional parameters which depend on particular strategies of various authors to perform such an analysis, such as; hard-core repulsion between hadrons [159, 160], relaxing the assumption of strangeness equilibration [161, 44], exact strangeness conservation in a canonical ensemble [105] - can be introduced without fundamentally changing the underlying assumptions [158].

At chemical freeze-out all the hadronic resonances decay into the known branching ratios, $N_{j+} = \sum N_i^0 Br\,(i \to j^+)$, and we have to take into account hadronic resonance masses and decay widths.

An interesting question, though, is the possible influence of in-medium effects on hadronic properties as most fits assume that the hadronic masses and decay widths at chemical freeze-out are the same as in a vacuum. Modifications of mass due to in-medium effects have been studied in the context of a chiral model for $Pb - Pb$ collisions at the SPS where it was found that masses generally decrease at high temperature and density [162].

In the broad range of energy from SIS/GSI through AGS/BNL up to SPS/CERN and RHIC/BNL, experimental data on particle yields in nucleus-nucleus collisions are well described within the statistical approach taken in this work. We point out, however, that following convergence difficulties similar to those encountered in [70], we were unable to resolve an additional point, namely, the AGS $Au - Au$ 11.6A GeV point within reasonable bounds. Freeze-out parameters were eventually found in [70] ($T = 121.2 \pm 6.3$, $\mu_B = 558 \pm 21$ and $T = 130.6 \pm 9.4$, $\mu_B = 594 \pm 56$)MeV from two different analyses.

A common feature to all theses points for all combinations of T and μ_B, as noted by Cleymans and Redlich, is that the average *energy/particle* $\simeq$ 1 GeV [110].

This can be intuitively understood as setting the energy scale below which inelastic collisions cease and chemical equilibration becomes impossible [158].

An alternative to this description of the freeze-out trajectory has been given in terms of a constant total baryon plus antibaryon density ($n_b = 0.12/fm^3$) by Braun-Munzinger and Stachel [130]. In this picture chemical freeze-out occurs at a critical density through baryon-baryon and baryon-meson interactions.

Both the above descriptions have been investigated in Chapter 4 and compared with results from our model calculations. This is shown in Figure 4.20 and again in Figure 5.7.

In Chapter 5 we have shown that, in the high temperature low μ_B regime of $Pb-Pb$ collisions at SPS energies and beyond, the possibility of chemical freeze-out happening in the plasma phase using bag model calculations incorporating QCD corrections. Chemical freeze-out parameters obtained in this scenario from statistical-thermal modelling will thus convey information directly about the quark-gluon plasma.

Appendix A

Exact versus Grand Canonical Treatment

The overestimation of anti-He^3 by seven orders of magnitude in proton-proton collisions when using the grand canonical ensemble in its standard form, pointed out by Hagedorn in 1968 [163], is due to the fact that, because of the small volume and small number of particles, one has to take into account the production of three accompanying nucleons with energy, E_N, in order to conserve the baryon number. Instead of the particle abundance being proportional to the usual Boltzmann factor, *i.e.*,

$$N_{\overline{He^3}} \sim \exp\left(-\frac{m_{\overline{He^3}}}{T}\right), \tag{A.1}$$

it is proportional to

$$N_{\overline{He^3}} \sim \exp\left(-\frac{m_{\overline{He^3}}}{T}\right)\left[V\int\frac{d^3p}{(2\pi)^3}e^{-\frac{E_N}{T}}\right]^3. \tag{A.2}$$

Thus, one obtains a cubic volume dependence and a suppression of the production.
In what follows, similar treatments are considered for a p, $\overline{p}$ gas in order to demonstrate the conditions under which the grand canonical approach can be used in its standard form. The same is then considered for heavy-ion collisions at the SIS, AGS, and the SPS.

A.1 In a p, $\overline{p}$ Gas

The effect of imposing exact baryon number conservation in the statistical description of a free point-like proton-antiproton gas is investigated and the results compared with a grand canonical treatment where baryon number holds only as an average over many ensembles.

We begin by constructing partition functions, which tell us how the particles in the gas are partitioned or split between the different energy levels, for the two cases above.

A.1.1 Partition function for the Exact case

The partition function with total baryon number, B, can be written as

$$Z_B = \frac{1}{2\pi}\int_0^{2\pi} d\psi e^{-iB\psi} \exp\left\{Z_1^p e^{i\psi} + Z_1^{\overline{p}} e^{-i\psi}\right\} \text{ (for example, see , [33], [76], [164]).} \quad \text{(A.3)}$$

For vanishing overall baryon number (*baryons* − *antibaryons*), $B = 0$, equation A.3 becomes

$$Z_{B=0} = \frac{1}{2\pi}\int_0^{2\pi} d\psi \exp\left\{Z_1^p e^{i\psi} + Z_1^{\overline{p}} e^{-i\psi}\right\}. \quad \text{(A.4)}$$

where $Z_1(T,V) = V\int \frac{d^3p}{(2\pi)^3} e^{-\frac{E_p}{T}}$ is the single-particle partition function.
We can expand each factor in a power series using

$$\exp\{A+B\} = \sum_{n=0}^{\infty}\frac{A^n}{n!}\sum_{m=0}^{\infty}\frac{B^m}{m!}, \quad \text{(A.5)}$$

and write the partition function (Equation A.3) more explicitly as

$$Z_B = \frac{1}{2\pi}\int_0^{2\pi} d\psi e^{-iB\psi}\sum_{n=0}^{\infty}\frac{(Z_1^p)^n}{n!}\sum_{m=0}^{\infty}\frac{\left(Z_1^{\overline{p}}\right)^m}{m!}e^{in\psi}e^{-im\psi}, \quad \text{(A.6)}$$

or, integrating over ψ

$$Z = \sum_{n=0}^{\infty}\frac{Z_1^p}{n!}\sum_{m=0}^{\infty}\frac{Z_1^{\overline{p}}}{m!}\delta_{(n.m+B)}, \quad \text{(A.7)}$$

where

$$\delta_{(n.m+B)} = \frac{1}{2\pi}\int_0^{2\pi} e^{i(n-m-B)\psi}d\psi. \quad \text{(A.8)}$$

Applying this, Equation A.7 becomes, in terms of the antiproton number,

$$\begin{aligned} Z &= \sum_{m=0}^{\infty}\frac{(Z_1^p)^{m+B}}{(m+B)!}\frac{\left(Z_1^{\overline{p}}\right)^m}{m!} \\ &= \sum_{m=0}^{\infty}\frac{(Z_1^p)^{m+B}\left(Z_1^{\overline{p}}\right)^m}{m!(m+B)!} \\ &= (Z_1^p)^B\sum_{m=0}^{\infty}\frac{\left(Z_1^p Z_1^{\overline{p}}\right)^m}{m!\,(m+B)!}. \end{aligned} \quad \text{(A.9)}$$

Comparing Equation A.6 with the following Bessel function:

$$I_\nu(z) = \left(\frac{1}{2}z\right)^\nu \sum_{k=0}^{\infty} \frac{\left(\frac{1}{4}z^2\right)^k}{k!\Gamma(\nu+k+1)} \tag{A.10}$$

or,

$$I_B(z) = \left(\frac{z}{2}\right)^B \sum_{k=0}^{\infty} \frac{\left(\frac{1}{4}z^2\right)^k}{k!\,(k+B)!}\,, \tag{A.11}$$

allows us to equate the following:

$$\begin{aligned} k &= m \\ \frac{1}{4}z^2 &= Z_1^p Z_1^{\overline{p}}. \end{aligned} \tag{A.12}$$

We thus obtain:

$$z = 2\sqrt{Z_1^p Z_1^{\overline{p}}} \tag{A.13}$$

and,

$$\left(\frac{z}{2}\right)^B = \left(Z_1^p Z_1^{\overline{p}}\right)^{\frac{B}{2}}. \tag{A.14}$$

Making the assumption that $Z_1^p = Z_1^{\overline{p}}$,

$$\left(\frac{z}{2}\right)^B = \left(Z_1^p\right)^B. \tag{A.15}$$

Therefore,

$$Z_B^{Exact} = I_B\left(2Z_1^p\right). \tag{A.16}$$

More generally, if $Z_1^p \neq Z_1^{\overline{p}}$,

$$Z_B^{Exact} = \left(Z_1^p\right)^B \frac{I_B\left(2\sqrt{Z_1^p Z_1^{\overline{p}}}\right)}{\left(\sqrt{Z_1^p Z_1^{\overline{p}}}\right)^B}. \tag{A.17}$$

A.1.2 Partition function for the Grand Canonical case

In the grand canonical case we include the baryonic chemical potentials, μ_p and $\mu_{\overline{p}}$, and write the partition function in the following way:

$$Z^{GC}(T,V) = \underbrace{\exp\left\{V\int\frac{d^3p}{(2\pi)^3}e^{-\frac{E_p}{T}+\frac{\mu_p}{T}}\right\}}_{\text{proton part}\ \left(Z_1^p e^{\frac{\mu_p}{T}}\right)} \cdot \underbrace{\exp\left\{V\int\frac{d^3p}{(2\pi)^3}e^{-\frac{E_{\overline{p}}}{T}+\frac{\mu_{\overline{p}}}{T}}\right\}}_{\text{antiproton part}\ \left(Z_1^{\overline{p}} e^{\frac{\mu_{\overline{p}}}{T}}\right)}. \tag{A.18}$$

A.1.3 Particle Number expressions from Z^{Exact} and Z^{GC}

We find particle abundances by introducing a fictitious chemical potential for the conserved quantum number and projecting out numbers using the standard grand canonical method, namely;

$$\langle N_i \rangle = \frac{T}{Z(T,V)} \frac{\partial Z(T,V)}{\partial \mu_i}\bigg|_{\mu_i=0}, \tag{A.19}$$

In the exact case we obtain the following for the number of protons by using Equation A.16:

$$\begin{aligned} \langle N_p \rangle &= \frac{\partial I_B\left(2Z_1^p e^{\frac{\mu_p}{T}}\right)}{\partial \mu_p} \frac{T}{Z_B} \\ &= Z_1^p \frac{I_{B+1}(2Z_1^p)}{I_B(2Z_1^p)} . \end{aligned} \tag{A.20}$$

For $B = 0$,

$$\langle N_p \rangle = Z_1^p \frac{I_1(2Z_1^p)}{I_0(2Z_1^p)} . \tag{A.21}$$

In the grand canonical case, considering only the proton part and differentiating with respect to μ_p, we obtain

$$\frac{T}{Z(T,V)} \frac{\partial Z(T,V)}{\partial \mu_p} = V \int \frac{d^3p}{(2\pi)^3} e^{-\frac{E_p}{T}+\frac{\mu_p}{T}} . \tag{A.22}$$

Therefore,

$$\begin{aligned} \langle N_p \rangle &= V \int \frac{d^3p}{(2\pi)^3} e^{-\frac{E_p}{T}} \\ &= Z_1^p(T,V) . \end{aligned} \tag{A.23}$$

The expressions for the number of antiprotons can be similarly found.

In the thermodynamic limit the exact and the grand canonical formulations are equivalent. However, for a small system the difference becomes more pronounced. This can be seen in Figure A.1 where $N^{Exact}/N^{GC} \to 1$ as the radius of the interaction volume of the gas increases. We can also see this in the large and small volume limits of the factor, $\frac{I_1(2Z_1^p)}{I_0(2Z_1^p)}$, which, in the exact case, measures the deviation of particle multiplicities from the grand-canonical result. As $V \to \infty$ the argument of the Bessel function $z \to \infty$ so that

$$\lim_{V\to\infty} \frac{I_1(2Z_1^p)}{I_0(2Z_1^p)} \to 1, \tag{A.24}$$

and Equation A.21 tends to the grand canonical case, Equation A.23.

In the limit of a small volume, $V \to 0$, we have

$$\cdot \lim_{V \to 0} \frac{I_1\left(2Z_1^p\right)}{I_0\left(2Z_1^p\right)} \to \frac{2Z_1^p\left(T,V\right)}{2} = Z_1^p\left(T,V\right). \tag{A.25}$$

Therefore,

$$\left\langle N_p^{Exact} \right\rangle \to Z_1^p Z_1^p. \tag{A.26}$$

From this we can see that, at fixed temperature and chemical potential, the volume dependence in the exact and grand canonical ensembles of the number of particles is as follows:

$$\langle N_p \rangle \sim \begin{cases} V : V \longmapsto \infty \ (GC) \\ V^2 : V \longmapsto 0 \ (Exact). \end{cases} \tag{A.27}$$

From the foregoing discussion we can see that in the large volume limit both descriptions are identical and a detailed investigation of small volumes shows that if the radius of the interaction volume of the gas is larger than about 5 fm and/or the baryon number is larger than about 50, finite volume corrections are negligible and it is justified to use the grand canonical ensemble (see Figure A.1).

A.2 In Heavy Ion Collisions

The exact conservation of strangeness can be taken into account analogously to baryon number conservation.

The effect of the (canonical suppression) factor, $\frac{I_1(Z)}{I_0(Z)}$, has been investigated in heavy-ion collisions in [105] assuming $S = 0$, including particles up to $|strangeness| = 1$ and, taking into account all resonance decays. The suppression factor, measuring the deviation of particle multiplicities from their grand canonical result, is written as

$$F_S \equiv \frac{I_1\left(x\right)}{I_0\left(x\right)}, \tag{A.28}$$

where the argument of the Bessel function, x, is given by

$$x = 2\sqrt{K_{+1}K_{-1}}, \tag{A.29}$$

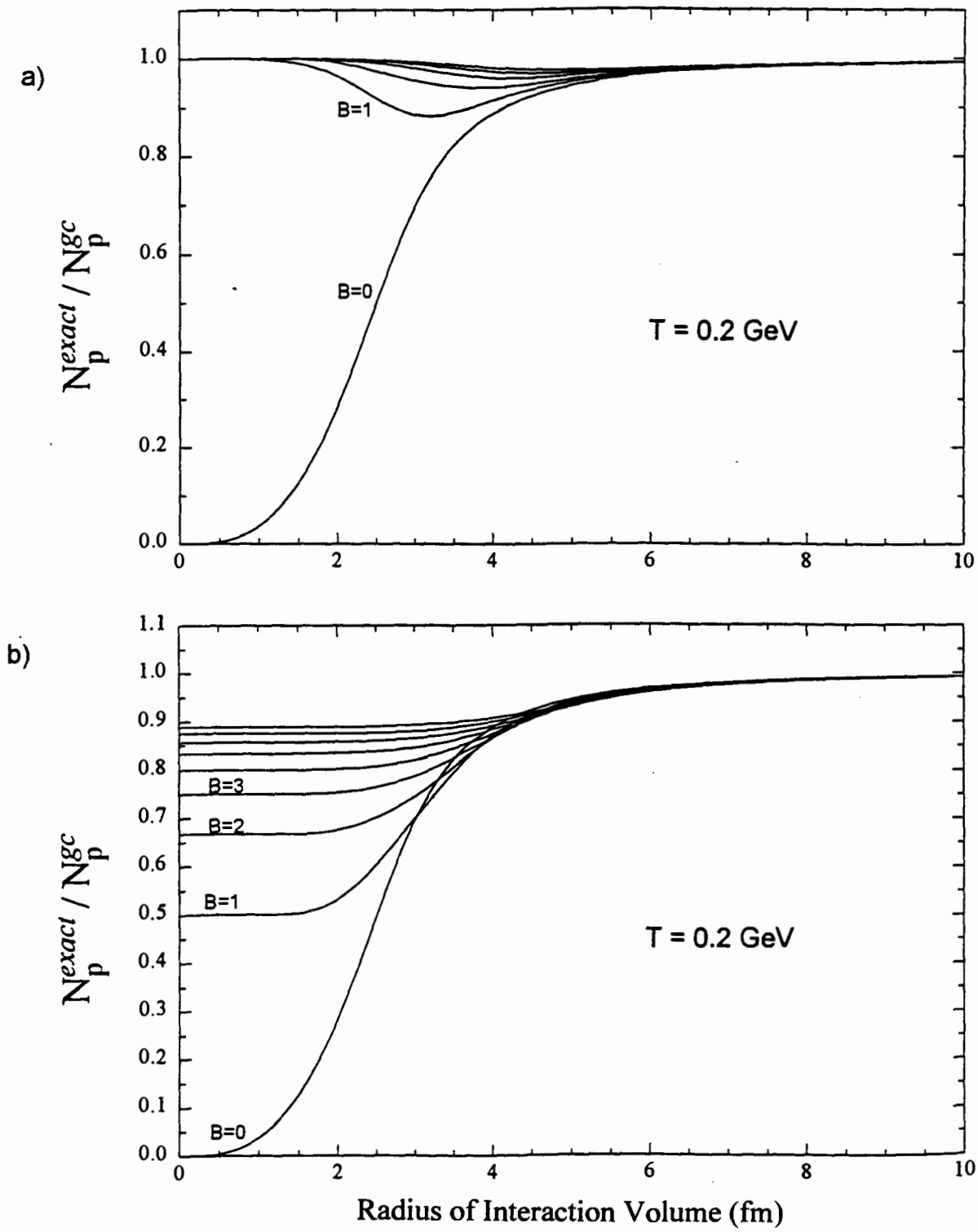

Figure A.1: *a)* N_p^{Exact}/N_p^{GC} *ratio and, b)* $N_{\overline{p}}^{Exact}/N_{\overline{p}}^{GC}$ *ratio as a function of the radius of the interaction volume of a proton-antiproton gas with exact baryon number conservation for different cases of* B.

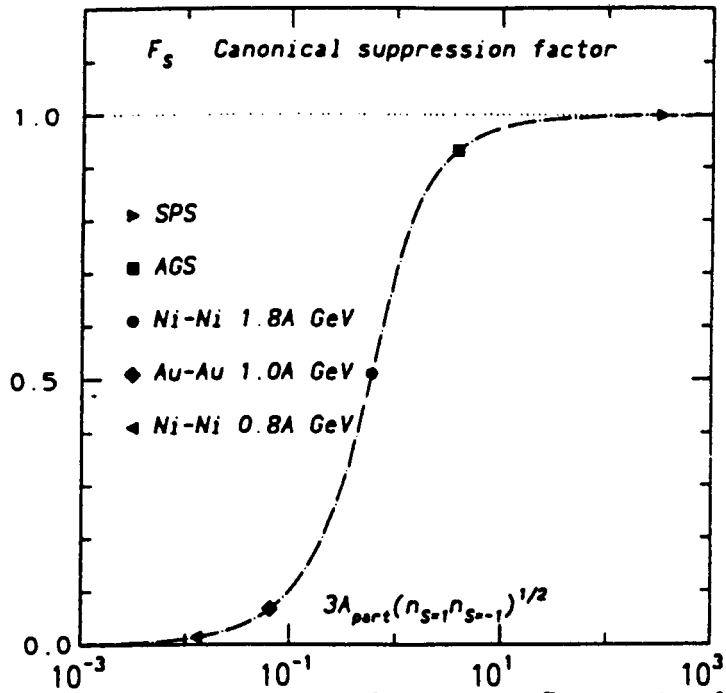

Figure A.2: *Canonical Strangeness Suppression factor [108].*

and K_{+1} stands for the sum of all single-particle partition functions with strangeness plus one:

$$K_{+1} = Z_K + Z_{\overline{\Lambda}} + Z_{K^*} + \cdots, \tag{A.30}$$

while K_{-1} stands for the sum of all single-particle partition functions with strangeness minus one:

$$K_{-1} = Z_{\overline{K}} + Z_\Lambda + Z_{\overline{K^*}} + \cdots. \tag{A.31}$$

The initial volume of the system has been related to the number of participants using the approximate relation $V \sim 1.9\pi A_{part}$. Figure A.2 shows the canonical suppression factor, F_S, as a function of the argument, x, where x has been calculated at SIS, AGS and SPS energies using baryochemical potentials and temperatures extracted from the measured particle multiplicity ratios.

From the figure we see that, at SIS energies, F_S plays a significant role compared with AGS and SPS energies where the suppression becomes less relevant and the grand canonical formulism suffices.

For small systems there will *always* be corrections due to size.

Appendix B

Geometrical Model for calculating B and Q

In collisions of two nuclei of different sizes, where the smaller of the two burrows its way through the larger, we need some way of calculating B and Q in order to fix the value of the charge chemical potential, μ_Q, by giving the neutron surplus, $B/2Q$.
We start by considering Figure B.1 which models the target and projectile by two spheres, and, define the following:

$$\begin{aligned} R_T &= \textit{radius of target} \\ R_P &= \textit{radius of projectile} \\ L &= \textit{length of cylindrical interaction region.} \end{aligned} \tag{B.1}$$

For a central collision the interaction region is taken to be a cylinder of length, L, plus two spherical segments at the ends of the cylinder where

$$L = 2\sqrt{R_T^2 - R_P^2}, \tag{B.2}$$

as illustrated in Figure B.1.
In order to calculate the baryon number contained in the cylindrical path of the projectile through the target, we begin by calculating the volume contained in the cylindrical path.
The method we follow is to place a (projectile) sphere at the centre of the target sphere which fits exactly into the cylinder. Half the sphere and half the cylinder from the centre, and, in the direction of the cylindrical path, are then considered.

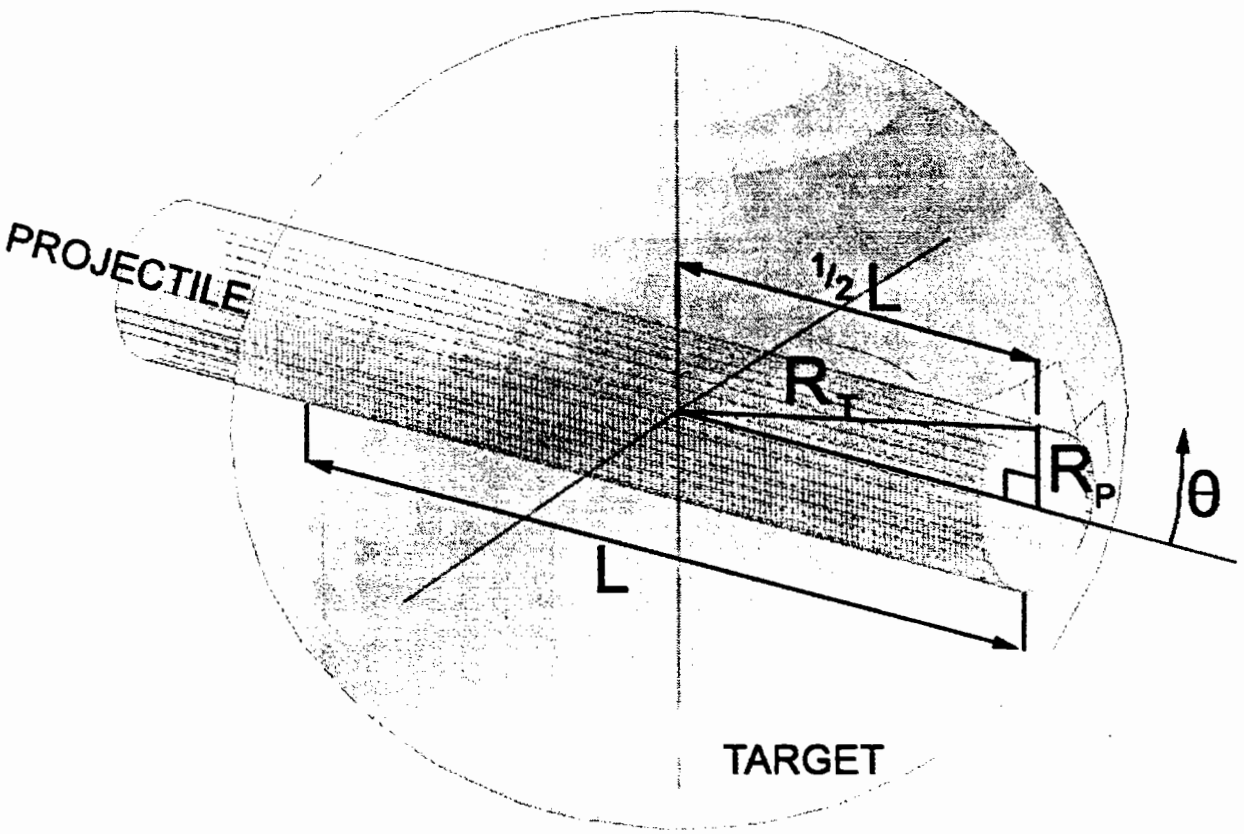

Figure B.1: *Geometrical model of a Projectile nucleus through a larger Target nucleus in a central collision.*

To find the volume of the cylinder we find: *a*) the volume of the sphere at the centre, by integrating over half the sphere and doubling it, *b*) the volume of the cylinder minus the volume of the sphere at the centre, by integrating over half this and doubling it, and *c*) adding the two integrated parts together.

For the sphere, r is integrated over the limits from zero to R_P, and, for the cylinder minus the sphere, from R_P to R_T.

We note that, for $r \geq R_P$,

$$\begin{aligned} \cos\theta &\geq \frac{\sqrt{r^2 - R_P^2}}{r^2} \\ &\geq \sqrt{1 - \frac{R_P^2}{r^2}}\,, \end{aligned} \tag{B.3}$$

to remain in the interaction volume.

The procedure is carried out below.

$$\begin{aligned} V &= \underbrace{2.2\pi \int_0^{R_P} r^2 dr . \int_0^1 d\cos\theta}_{\textit{volume of sphere at centre}} \\ &\quad + \underbrace{2.2\pi \int_{R_P}^{R_T} r^2 dr \int_{\sqrt{1-\frac{R_P^2}{r^2}}}^{1} d\cos\theta}_{\textit{cylinder-sphere at centre}} . \\ &= 4\pi \left[\int_0^{R_P} r^2 dr + \int_{R_P}^{R_T} r^2 dr \left[1 - \sqrt{1 - \frac{R_P^2}{r^2}} \right] \right] \\ &= 4\pi \left[\int_0^{R_T} r^2 dr - \int_{R_P}^{R_T} r\sqrt{r^2 - R_P^2} dr \right] \\ &= 4\pi \left(\left[\frac{1}{3} r^3 \right]_0^{R_T} - \frac{1}{3} \left[\left(r^2 - R_P^2 \right)^{\frac{3}{2}} \right]_{R_P}^{R_T} \right) \\ &= \frac{4}{3}\pi \left[R_T^3 - \left(R_T^2 - R_P^2 \right)^{\frac{3}{2}} \right] \\ &= \frac{4}{3}\pi R_T^3 \left[1 - \left(1 - \frac{R_P^2}{R_T^2} \right)^{\frac{3}{2}} \right] \\ &= \frac{4}{3}\pi R_T^3 \left[1 - \left(1 - \left(\frac{R_P}{R_T} \right)^2 \right)^{\frac{3}{2}} \right] . \end{aligned} \tag{B.4}$$

The final result of can be related to the mass number, A, by the following relationship:

$$R = r_0 A^{\frac{1}{3}}, \tag{B.5}$$

where

$$r_0 = 1.07 \text{ fm [165]}. \tag{B.6}$$

Therefore

$$\begin{aligned} A_P &\propto R^3, \\ A_T &\propto R^3. \end{aligned} \tag{B.7}$$

The total number of participating nucleons or, baryon number, B, can thus be taken as

$$B = A_P + A_T \left\{ 1 - \left[1 - \left(\frac{A_P}{A_T} \right)^{\frac{2}{3}} \right]^{\frac{3}{2}} \right\}, \tag{B.8}$$

and similarly, with the atomic number

$$Z \propto R^3, \tag{B.9}$$

so that the total charge in the interaction region can be taken as

$$Q = Z_P + Z_T \left\{ 1 - \left[1 - \left(\frac{Z_P}{Z_T} \right)^{\frac{2}{3}} \right]^{\frac{3}{2}} \right\}. \tag{B.10}$$

Appendix C

Resonance Widths

The usual single-particle partition function,

$$Z(T,V) = V\int \frac{d^3p}{(2\pi)^3} e^{(-E+\mu_B)/T}, \tag{C.1}$$

assumes stable particles.

To take lifetimes into account we note that

$$\begin{aligned} & \int d^3p e^{(-E+\mu_B)/T} \\ = & \int d^3p e^{\left(-\sqrt{p^2+m^2}+\mu_B\right)/T} \\ = & \int ds\delta\left(s-m^2\right)\int d^3p e^{\left(-\sqrt{p^2+s^2}+\mu_B\right)/T}. \end{aligned} \tag{C.2}$$

and the representation of the delta function

$$\delta\left(s-m^2\right) = \lim_{m\Gamma\to 0} \frac{m\Gamma/\pi}{\left(s-m^2\right)^2+m^2\Gamma^2}\ . \tag{C.3}$$

Relaxing the limit $\Gamma \to 0$, $Z(T,V)$ becomes

$$\begin{aligned} Z(T,V) &= \frac{V}{n}\int ds \frac{m\Gamma/\pi}{\left(s-m^2\right)^2+m^2\Gamma^2}\int d^3p e^{\left(-\sqrt{p^2+s^2}+\mu_B\right)/T} \\ &= \frac{V}{n}\int d^3p\int ds \frac{m\Gamma/\pi}{\left(s-m^2\right)^2+m^2\Gamma^2}\cdot e^{\left(-\sqrt{p^2+s^2}+\mu_B\right)/T} \end{aligned} \tag{C.4}$$

where n is the normalization such that

$$n^{-1}\int_a^b ds \frac{m\Gamma/\pi}{\left(s-m^2\right)^2+m^2\Gamma^2} = 1 \ for\ \Gamma \neq 0. \tag{C.5}$$

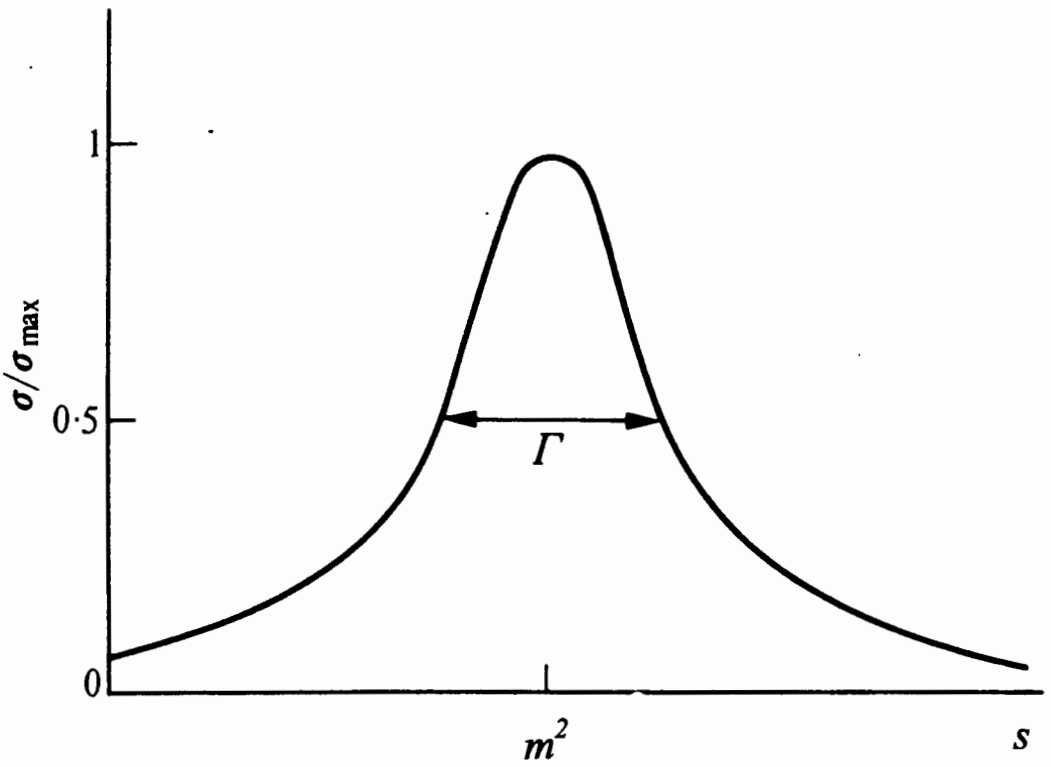

Figure C.1: *Shape of the Breit-Wigner resonance curve.*

Bibliography

[1] White Paper Report of the Special Workshop: *Hadron Physics in the 21st Century*, held at the George Washington Universty Research Campus, editor in chief, J. Comfort, March 27-29, 1998.

[2] RHIC, The Physics of RHIC: http://www.bnl.gov/rhic/QGP.htm

[3] J. Rafelski, M. Danos, Perspectives in High Energy Nuclear Collisions, NBSIR 83-2725, Washington, D.C. (1983).

[4] Workshop on Future Relativistic Heavy Ion Experiments, Proceedings edited by R. Stock and R. Bock, GSI 81-6, Orange Report (1981).

[5] Workshop on Quark Matter Formation and Heavy Ion Collisions, proceedings edited by M. Jacob and H. Satz, World Scientific Publ. Co., Singapore (1982).

[6] H. Satz, Critical Behaviour in Statistical QCD, in *The Quark Structure of Matter*, edited by M. Jacob and K. Winter, World Scientific Publ. Co., Singapore (1986).

[7] R.A. Salmeron, *An Introduction to the Search for the Quark-Gluon Plasma in Ultrarelativistic Heavy Ion Interactions*, lectures delivered at the Winter School on Quark-Gluon Plasma, Puri, Orissa, India, 5-16 December 1989.

[8] J-P. Coffin, talk given in Cape Town, October 2002.

[9] E. Quercigh and J. Rafelski, A strange quark plasma, in Physics World, vol. **13** (**5**), October 2000.

[10] U. Heinz, P. Koch, K.S. Lee, E. Schnedermann, H. Weigert, Dynamical Evolution and Particle Production in Relativistic Nuclear Collisions, in *Phase Structure of Strongly Interacting Matter*, edited by J. Cleymans, Springer-Verlag, Berlin, Heidelberg (1990).

[11] J. Rafelski, M. Danos, Nuclear Matter Under Extreme Conditions, in *Hadrons and Heavy Ions*, edited by W.D. Heiss, Springer-Verlag (1985).

[12] L. McLerran, Quark-Gluon Plasma and Space-Time Picture of Ultra-relativistic Nuclear Collisions, in *Hadrons and Hadronic Matter*, edited by D. Vautherin, F. Lenz and J.W. Negele, Plenum Press, New York (1990).

[13] R. Hagedorn, Suppl. Nuovo Cimento **6**, 311 (1968).

[14] R. Hagedorn, The Long Way to the Statistical Bootstrap Model, in *Hadrons and Hadronic Matter*, edited by J. Letessier, H. Gutbrod and J. Rafelski, Plenum Press, New York (1995).

[15] W. Heisenberg, Z. Phys. **101**, 533 (1936).

[16] B. Anderson, G. Gustafson and Nilsson-Almsquist, Nucl. Phys. B **281**, 289 (1987).

[17] A. Capella and J. Tran Thanh Van, Phy. Lett. B **93**, 146 (1980); Z. Phys. C **38**, 177 (1988).

[18] A. Capella *et al.*, Z. Phys. C **33**, 541 (1987); Phys. Rev. D **35**, 2921 (1987).

[19] S. Daté, M. Gyulassy and H. Sumiyoshi, Phys. Rev. D **32**, 619 (1985).

[20] J. Schukraft, Little Bang at Big Accelerators: Heavy ion physics from AGS to LHC, in *Physics and Astrophysics of the Quark-Gluon Plasma*, eds. B.C. Sinha, D.K. Srivastava, Y.P. Viyogi, Narosa Publishing House (1998).

[21] K. Werner, Phys. Rep. **232**, 87 (1993).

[22] B. Andersson *et al.*, Nucl. Phys. B **281**, 286 (1995).

[23] I. Tserruya, Heavy Ion Collisions, CERN PPE/95 - 185, invited talk at the International Europhysics Conference on High Energy Physics, Brussels, Belgium, July 27 - August 2 1995.

[24] R. Hagedorn, Suppl. Nuovo Cimento **3**, 147 (1965).

[25] P. Braun-Munzinger, J. Stachel, J.P. Wessels and N. Xu, Phys. Lett. B **344**, 43-48 (1995).

[26] F. Becattini, Proceedings of the 33rd Eloisatron Workshop: Universality Features in Multihadron Production and the Leading Effect, Erice, Italy, pp. 74-104, World Scientific (1996).

[27] K. Redlich and L. Turko, Z. Phys. C **5**, 201 (1980).

[28] H. Elze, W. Greiner and J. Rafelski, Phys. Lett., B **124**, 515 (1983).

[29] L. Turko, Phys. Lett. B **104**, 153 (1981).

[30] H-Th. Elze and W. Greiner, Phys. Rev. A **33**, 1879 (1986); K. Redlich and D.E. Miller, Phys. Rev. D **37**, 3716 (1988); Phys. Rev. D **35**, 2524 (1987); D.S. Skagerstam, Z. Phys. C **24**, 97 (1984); J. Phys. A**18**, 1 (1985); Phys. Lett. B **133**, 419 (1985).

[31] R. Hagedorn and K. Redlich, Statistical Thermodynamics in Relativistic Particle and Ion Physics: Canonical or Grand Canonical?, Z. Phys. C - Particles and Fields **27**, 541-551 (1985).

[32] J. Rafelski and M. Danos, Phys. Lett.B **97**, 279 (1980).

[33] J. Cleymans, E. Suhonen, G.M. Weber, Exact Baryon and Strangeness Conservation in Hadronic Gas Models, Z.Phys. C-Particles and Fields **53**, 485-491 (1992).

[34] J. Cleymans, M. Marais, A. Muronga, Talk presented by M. Marais at the 40th Annual Conference of the South African Institute of Physics, University of the Western Cape, July 1995.

[35] H. Meyer-Ortmanns, Phase transitions in quantum chromodynamics, Reviews of Modern Physics, vol. **68 (2)**, 473 - 598, April 1996.

[36] J. Letessier, J. Rafelski and A. Tounsi, Strange Particles from Dense Hadronic Matter, Acta Phys. Pol. B **27 (5)**, 1035 (1996).

[37] F. Staley, talk given in Cape Town, October 2001.

[38] G. Paic, Heavy-ion collisions at the LHC, in *Physics and Astrophysics of the Quark-Gluon Plasma*, eds. B.C. Sinha, D.K. Srivastava, Y.P. Viyogi, Narosa Publishing House (1998).

[39] T. Matsui and H. Satz, Phys. Lett. B **178**, 416 (1986).

[40] J. Rafelski, Phys. Rep. **88**, 331 (1982).

[41] The STAR Physics Handbook: Strangeness, http://www.star.bnl.gov/afs/rhic/star/doc/www/physics/Strangeness.html

[42] U. Heinz, Nucl. Phys. A **566**, 205c (1994).

[43] J. Rafelski and B. Müller, Phys. Rev. Lett. **48**, 1066 (1982); P. Koch, B. Müller and J. Rafelski, Phys. Rep. **142**, 167 (1986); J. Rafelski, Phys. Lett. B **262**, 333 (1991).

[44] J. Letessier and J. Rafelski, Observing Quark-Gluon Plasma with Strange Hadrons, Int. J. Mod. Phys. E **9**, 107-147 (2000).

[45] P. Koch, B. Müller and J. Rafelski, Phys. Rep. **142**, 167 (1986).

[46] S.A. Bass, M. Gyulassy, H. Stöcker and W. Greiner, J. Phys. G **25**, R1-R57 (1999).

[47] C. Greiner, Nucl. Phys. A **698**, 591c-594c (2002).

[48] J-P Blaizot, Nucl. Phys. A **698**, 360c-371c (2002).

[49] G.E. Brown, M. Rho and C. Song, nucl-th/0010008.

[50] K. Redlich, Nucl. Phys. A **698**, 94c-103c (2002).

[51] Proceedings of *Quark Matter '99*, Nucl. Phys. A **661** (1999); F. Sikler *et al.*, NA49 Collaboration, Nucl. Phys. A **661**, 45c (1999) and references therein; H. Bialkowska *et al.*, NA35 Collaboration, Z. Phys. C **64**, 381 (1994); E. Andersen *et al.*, WA97 Collaboration, Phys. Lett. B **449**, 401 (1999).

[52] E802 Collaboration, Y. Miake *et al.*, Z. Phys. C **38**, 135 (1988); P. Vincent *et al.*, Nucl. Phys. A **498**, 67 (1989).

NA35 Collaboration, G. Vesztergomi *et al.*, Z. Phys. C **38**, 129 (1988); A. Bamberger *et al.*, Z. Phys. C **43**, 25 (1989).

[53] C. Blume for the NA49 Collaboration, Nucl. Phys. A **698**, 104c-111c (2002).

[54] M. Gazdzicki *et al.*, Z. Phys. C **65**, 215 (1995); Acta Phys. Pol. B **30**, 2705 (1999).

[55] T. Abbot *et al.*, E802 Collaboration, Phys. Rev. C **50**, 1024 (1994).

[56] E. Andersen *et al.*, WA97 Collaboration, Phys. Lett. B **294**, 127 (1992).

[57] E. Andersen *et al.*, WA97 Collaboration, Phys. Lett. B **327**, 433 (1994).

[58] S. Abatzis, *et al.*, Nucl. Phys. A **566**, 499c (1994); Nucl. Phys. A **566**, 491c (1994); Nucl. Phys. A **566**, 225c (1994).

[59] S. Abatzis, *et al.*, Phys. Lett. B **316**, 615 (1993).

[60] D. DiBari, *et al.*, Nucl. Phys. A **590**, 307c (1995).

[61] J.B. Kinson *et al.*, Nucl. Phys. A **590**, 317c (1995).

[62] H. Helstrup *et al.*, Nucl. Phys. A **610**, 165c (1996).

[63] I. Kralik *et al.*, Nucl. Phys. A **638**, 115c (1998).

[64] M. Venables *et al.*, J. Phys. G **23**, 1857 (1997).

[65] E. Andersen *et al.*, WA97 Collaboration, Phys. Lett. B **449**, 401 (1999).

[66] N. Carrer, for the NA57 Collaboration, Nucl. Phys. A **698**, 118c-126c (2002).

[67] J.C. Dunlop *et al.*, Phys. Rev. C **61**, 031901 (2000); C.A. Ogilvie, Nucl. Phys. A **698**, 3c-12c (2002).

[68] J. Cleymans, H. Oeschler, K. Redlich and A. Tounsi, Acta Phys. Polon. B **33**, 1609-1628 (2002).

[69] P. Braun-Munzinger, J. Cleymans, H. Oeschler, K. Redlich, Maximum Relative Strangeness Content in Heavy Ion Collisions Around 30 *A* GeV, Nuclear Physics A **697**, 902-912 (2002).

[70] F. Becattini, J. Cleymans, A. Keränen, E. Suhonen and K. Redlich, Phys. Rev. C **64**, 024901 (2001).

[71] J-P. Coffin, STAR Collaboration, talk given in Cape Town, October 2002, and private communication.

[72] F. Sikler *et al.*, NA49 Collaboration, Nucl. Phys. A **661**, 45c (1999) and references therein.

[73] H. Bialkowska *et al.*, NA35 Collaboration, Z. Phys. C **64**, 381 (1994).

[74] M.I. Gorenstein, W. Greiner and S.N. Yang, Phase Transitions in the Gas of Bags, J. Phys. G **24**, 725-744 (1998).

[75] J. Cleymans and K. Redlich, Chemical and thermal freeze-out parameters from 1A to 200A GeV, Phys. Rev.C **60**, 054908 (1999).

[76] J. Cleymans, K. Redlich and E. Suhonen, Canonical Description of Strangeness Conservation and Particle Production, Z. Phys. C **51**, 137-141 (1991).

[77] K. Zalewski, Acta Phys. Pol. **28**, 933 (1965); E.M. Ilgenfritz and J. Kripfganz, Nucl. Phys. B **62**, 141 (1973); R. Hagedorn and K. Redlich, Z. Phys. C - Particles and Fields **27**, 541-551 (1985); L. Turko, Phys. Lett. B **104**, 153 (1981).

[78] C. Derreth, W. Greiner, H-Th. Elze, and J. Rafelski, Phys. Rev. C **31**, 360 (1985).

[79] M. Gorenstein, V.K. Petrov, and G.M. Zinovjev, Phys. Lett. B **106**, 327 (1981).

[80] P. Koch, B. Müller and J. Rafelski, Strangeness in Relativistic Heavy Ion Collisions, Physics Reports **142** (**4**), 167-262, p228, North Holland, Amsterdam (1986).

[81] B. Müller, *The Physics of the Quark-Gluon Plasma*, Lecture Notes in Physics **225**, pp. 91-104, Springer-Verlag, Berlin (1985).

[82] J. Cleymans, Strangeness: Theoretical Status, in *Physics and Astrophysics of the Quark-Gluon Plasma*, edited by B.C. Sinha, D.K. Srivastava and Y.P. Viyogi, Narosa Publishing House (1998).

[83] J. Letessier and J. Rafelski, Phys. Rev. C **59**, 947 (1999).

[84] J. Letessier and J. Rafelski, J. Phys. G, Nucl. Part. Phys. **25**, 295 (1999).

[85] J. Rafelski, On the strange-quark-gluon plasma front line, J. Phys. G, Nucl. Part. Phys. **27 (3)**, 723 (2001).

[86] F. James, MINUIT-Function Minimization and Error Analysis Reference Manuel Version 94.1, CERN Program Library Long Writeup **D506**, CERN, Geneva (1994).

[87] Nu Xu and M. Kaneta, Nucl. Phys. A **698** [1], 306c-313c (2002).

[88] R. Stock, Nucl. Phys. A **661**, 282c (1999).

[89] H. Oeschler, in "*Hadrons in Dense Matter and Hadrosynthesis*", Lecture Notes in Physics **516**, eds. J. Cleymans, H.B. Geyer and F.G. Scholtz, Springer, Berlin (1999).

[90] Y. Akiba *et al.*, E802 Collaboration, Nucl. Phys. A **590**, 179c (1995).

[91] T. Abbot *et al.*, E802 Collaboration, Nucl. Phys. A **525**, 455c (1994).

[92] P. Braun-Munzinger, D. Magestro, K. Redlich and J. Stachel, Phys. Lett. B **518**, 41-46 (2001).

[93] J. Cleymans, H. Oeschler and K. Redlich, J. Phys. G **25**, 281 (1999).

[94] J. Harris for the STAR Collaboration, Nucl. Phys. A **698**, 64c-77c (2002).

[95] H. Caines for the STAR Collaboration, Nucl. Phys. A **698**, 112c-117c (2002), and private communication.

[96] N. Xu for the STAR Collaboration, Nucl. Phys. A **698**, 607c-610c (2002).

[1] Nucl. Phys. Rev. **689** - *Proceedings of Quark Matter 2001.*

[97] H.Z. Huang for the STAR Collaboration, Nucl. Phys. A **698**, 663c-666c (2002).

[98] H. Ohnishi for the PHENIX Collaboration, Nucl. Phys. A **698**, 659c-662c (2002).

[99] PHOBOS Collaboration, Phys. Rev. Lett. (May 2001).

[100] I.G. Bearden for the BRAHMS Collaboration, Nucl. Phys. A **698**, 667c-670c (2002).

[101] BRAHMS Collaboration, Phys. Rev. Lett. (April 2001).

[102] R. Caliandro for the WA97 Collaboration, J. Phys. G: Nucl. Part. Phys. **25**, 171-180 (1999).

[103] R.A. Fini for the WA97 Collaboration, J. Phys. G: Nucl. Part. Phys. **27**, 375-381 (2001).

[104] F. Antinori *et al.*, Eur. Phys. J. C **14**, 633 (2000).

[105] J. Cleymans, H. Oeschler K. Redlich, Phys. Rev. C **59**, 1663 (1999).

[106] J. Cleymans, D. Elliot, A. Keränen and E. Suhonen, Phys. Rev. C **57**, 3319 (1998).

[107] F. Becattini, hep-ph/0202071, February 2002.

[108] Particle Data Group, Eur. Phys. J. C **3**, 1 (1998).

[109] W. Florkowski, W. Broniowski and M. Michalec, Acta Phys. Polon. B **33**, 761-769 (2002).

[110] P. Braun-Munzinger, J. Cleymans and K. Redlich, Nucl. Phys. A **697**, 902-912 (2002).

[111] J. Cleymans and K. Redlich, Phys. Rev. Lett. **81**, 5284 (1998).

[112] R.A. Barton for the NA49 Collaboration, J. Phys. G: Nucl. Part. Phys. **27**, 367-374 (2001).

[113] E.L. Bratkovskaya *et al.*, Nucl. Phys. A **634**, 168 (1998).

[114] C. Adler *et al.*, STAR Collaboration, nucl-ex/0205015, submitted to Phys. Rev. Lett., 22 May 2002.

[115] R. Rapp and J. Wambach, Adv. Nucl. Phys. **25**, 1 (2002); R. Rapp, Phys. Rev. C **63**, 054907 (2001).

[116] J. Schaffner-Bielich, Phys. Rev. Rev. Lett. **84**, 3261 (2000).

[117] J. Lettesier *et al.* J. Phys. G **27**, 427 (2001); G. Torrieri and J. Rafelski, Phys. Lett. B **509**, 239 (2001).

[118] Y.J. Pei, Z. Phys. C **72**, 39 (1996), and references therein; P.V. Chliapnikov, Phys. Lett. B **470**, 263 (1999).

[119] A.J. Baltz and C. Dover, Phys. Rev. C **53**, 362 (1996).

[120] Helen Caines, STAR Collaboration, private communication.

[121] C. Adler *et al.*, STAR Collaboration, nucl-ex/0206011, Kaon Production and Kaon to Pion Ratio in Au+Au collisions at $\sqrt{s_{NN}}$ = 130 GeV, to be submitted to Phys. Rev. Lett. 2002.

[122] C. Adler *et al.*, STAR Collaboration, Phys. Rev. Lett. **86**, 4778 (2001).

[123] B.B. Back *et al.*, Phys. Rev. Lett. **87**, 102301 (2001).

[124] J. Castillo, STAR Collaboration, talk given at SQM 2001.

[125] F. Becattini, A. Keränen, Phys. Rev. C **65**, 044901 (2002).

[126] F. Antinori, Nucl. Phys. A **661**, 130c (1999); D. Elia, Nucl. Phys. A **661**, 649c (1999); web page of the WA97 experiment: http://www.cern.ch/WA97/QM99table/TableQM99.html

[127] A. Mischke for the NA49 Collaboration, nucl-ex/0209002 (Sep. 2002).

[128] A. Mischke for the NA49 Collaboration, nucl-ex/0201012 (2002).

[129] J. Cleymans and K. Redlich, Phys. Rev. Lett. **81**, 5284 (1998).

[130] P. Braun-Munzinger and J. Stachel, J. Phys. G **28**, 1971-1976 (2002).

[131] P. Braun-Munzinger, I. Heppe and J. Stachel, Phys. Lett. B **465**, 15 (1999).

[132] P. Koch, B. Müller and J. Rafelski, Strangeness in Relativistic Heavy Ion Collisions, Physics Reports **142** (4), 167-262, p172, North Holland, Amsterdam (1986).

[133] B. Müller, *The Physics of the Quark-Gluon Plasma*, Lecture Notes in Physics **225**, pp. 15-21, Springer-Verlag, Berlin (1985).

[134] R.F. Alvarez-Estrada, F. Fernández, J.L. Sánchez-Gómez and V. Vento, *Models of Hadron Structure Based on Quantum Chromodynamics*, Lecture Notes in Physics **259**, Springer-Verlag, Berlin (1986).

[135] A. Chodos, R.L. Jaffe, K. Johnson, C.B. Thorn and V.F. Weisskopf, Phys. Rev. D **9**, 3471 (1974).

[136] K. Johnson, Acta Phys. Polonica B **6**, 865 (1975).

[137] J. Cleymans, R.V. Gavai, E. Suhonen, Quarks and Gluons at High Temperatures and Densities, Physics Reports **130** (4), 217-292, North Holland, Amsterdam (1986).

[138] W. Greiner, L. Neise, H. Stöcker, *Thermodynamics and Statistical Mechanics*, Springer-Verlag, New York (1995).

[139] A.T.M. Aerts and J. Rafelski, Phys. Lett. B **148**, 337 (1984).

[140] A.T. Aerts and J. Rafelski, Strange Hadrons in the MIT bag model, CERN-TH-4160-85 and UCT-TP-27-2-85, April 1985.

[141] T. deGrand, R.L. Jaffe, K. Johnson and J. Kiskis, Phys. Rev. D **12**, 2060 (1975).

[142] M.A. Shifman, Z. Physik C **9**, 347 (1981).

[143] L.D. Landau and E.M. Lifshiftz, *Course of Theoretical Physics* Vol. 5, *Statistical Physics*, Pergamon Press, Oxford (1978).

[144] B. Freedman and L. McLerran, Phys. Rev. D **16** (1977).

[145] J. Kapusta, Finite-temperature field theory, Cambridge University Press (1989).

[146] S. Hamieh, J. Letessier, J. Rafelski, Quark-gluon plasma fireball, Phys. Rev. C **62** (2000).

[147] Handbook of Mathematical Functions (Abridged), edited by M. Abramowitz and I. Stegun, Verlag Harri Deutsch, Germany (1984).

[148] A. Pershier, B. Kämpfer and G. Soft, Phys.Rev. D **66,** 094003 (2002).

[149] F. Karsch, E. Laermann and A. Peikert, Phys. Lett. B **478**, 447 (2000).

[150] F. Karsch, Nucl.Phys. A **698**, 199-208 (2002).

[151] E.W. Kolb and M.S. Turner, *The Early Universe*, Addison Wesley Longman Inc. (1990/3).

[152] K. Olive, Nucl.Phys. B **198**, 461-473 (1982).

[153] N.J. Davidson, H.G. Miller, D.W. von Oertzen and K.Redlich, Z. Phys. C B **56**, 319-324 (1992).

[154] J. Kapusta, K. Olive, Nucl.Phys. A **408**, 478 (1983).

[155] J. Ellis, K. Olive, Phys. Lett. B **260**, 173-178 (1992).

[156] R. Hagedorn and J. Raft, Suppl. Nuovo Cim. **6** 169, (1968).

[157] J.W. Clark, J. Cleymans, J. Rafelski, Clustered Quark Matter, Phys. Rev. C **33**, 703-708 (1986).

[158] L. van Hove, Z. Phys. C **27**, 135 (1985).

[159] F. Becattini, J. Cleymans, A. Keränen, E. Suhonen and K. Redlich, hep-ph/0011322.

[160] U. Heinz, Nucl. Phys. A **698**, 153c-163c (2002).

[161] D. Rischke, Nucl. Phys. A **661**, 140c (1999).

[162] P. Braun-Munzinger, J. Stachel, J.P. Wessels, N. Xu, Phys. Lett. B **344**, 43 (1995); P. Braun-Munzinger, I. Heppe, J. Stachel, Phys. Lett. B **465**, 15 (1999).

[163] M.I. Gorenstein *et al.*, J. Phys. G **24**, 1777 (1998).

[164] F. Becattini, J. Phys. G **23**, 1933 (1997); F. Becattini *et al.*, hep-ph/0002267.

[165] D. Zschiesche *et al.*, Nucl. Phys. A **681**, 34 (2001).

[166] R. Hagedorn, CERN Yellow Report, 12-71 (1971).

[167] J. Cleymans, E. Suhonen and G.M. Weber, Seminar on Theoretical Physics, Bloemfontein, South Africa (1991).

[168] A.L. Fetter, J.D. Walecka, *Quantum Theory of Many Particle Systems*, p348, McGraw-Hill (1971).

Acknowledgements

My deepest gratitude and many thanks to my supervisor, Prof. Jean Cleymans, for his patience, inspiration and many, many hours of fruitful discussions on physics, life, and everything else. Thanks for being such a good teacher – *Le Génie, c'est la patience. Dōmo arigatō, Jean-san.*

To my folks who really, really wondered whether I'd be done by the next day and could hardly wait. Thank-you for everything (and don't worry, this will have been worth the wait).

I am very grateful to colleagues and friends for useful discussions and correspondence, among whom – Helen Caines, Gene Van Buren, Jean-Pierre Coffin, Nick van Eijndhoven, Antti Keränen, Gary Tupper and Robert Lindebaum.

Thank-you very much Professors Margit Härting and David Britton for all your encouragement, good advice, well wishes and inspiring wisdom.

To my brother, Adrian, for, once again, his artistic appreciation of my thesis and an artist's perception of high-energy collisions and the quark-gluon plasma.

"Frankly, I'd be satisfied now if I could even turn gold into lead."

A cartoon by Sidney Harris

"The time has come", the Walrus said,
"To talk of many things:
Of shoes—and ships—and sealing-wax—
of cabbages—and kings—
And why the sea is boiling hot—
And whether pigs have wings."
Lewis Carroll
Through the Looking Glass

From ghoulies and ghosties and long-leggety beasties
And things that go bump in the night,
Good Lord, deliver us!
Anonymous

Chapter 1

The Fireball: A Quark-Gluon Plasma?

" The structures that can be formed from the interaction of elementary quarks and gluons are, at this time, the most fundamental and represent the frontier of challenges to the human understanding of nature." [1]

1.1 Introduction

The exciting possibility of producing a completely new form of matter and probing key challenges in physics and the evolution of the early universe, has driven the quest to explore nuclear matter under extreme high conditions of energy density and temperature in relativistic high-energy, heavy-ion collisions.

The aim is to create this new state of matter, namely, a quark-gluon plasma (QGP), in the laboratory and thereby recreate the scenario which, according to present theory, occurred in the first few microseconds in the cosmic fireball created in the big-bang.

Hadrons, particles subject to strong nuclear forces, such as protons and neutrons in the nuclei of atoms, are made up of quarks and gluons. By compressing nuclei so that their individual protons and neutrons fuse or overlap, releasing their quark and gluon content, an enormous amount of energy is dumped into a very small volume and it should be possible to create a much greater volume, compared to typical hadron volumes, in which we find a completely new form of matter, namely, a "soup" or plasma of free quarks and gluons. The short time during which this would occur is on the scale of a fermi (3.3×10^{-24} seconds).

The deconfinement or, release of the quarks and gluons and, thus, the phase transition from hadronic matter to a plasma state, is an almost inevitable consequence of quantum chromo-

hadron gas phase (HG) in terms of temperature and baryon density.

In the quest for the QGP key issues of fundamental importance in making, identifying and probing the QGP in the laboratory include: the mechanism whereby quarks are confined in hadrons, understanding the nature of the phase transition, chiral symmetry breaking/restoration, the process of hadronization and, testing the predictions of (lattice) QCD.

1.2 Existence of Fireballs

The idea of a "fireball" - a region in space where, after a collision, the energy of the longitudinal motion is largely transferred to transverse degrees of freedom [11] or, a cluster of highly excited hadronic matter sticking together for a very short period of time and where the hadron gas phases move with collective motion [13, 14], had begun with Heisenberg's claim in 1936 [15] that a single elementary hadron-hadron collision can give rise to multiple secondary particle production (eleven years before the discovery of the pion!). The first Hydrogen bubble chamber pictures proved Heisenberg correct. Thus, in a single nucleus-nucleus collision a domain in space will arise from which many secondary particles will emanate. This region of production can be thought of as the "fireball".

The fireball can be characterized by the following physical variables:

- energy density,
- baryon number density and,
- total volume.

1.3 Relativistic Collisions

In a nucleus-nucleus collision in the centre-of-mass (c.m.) system the two colliding nuclei approaching each other with relativistic velocities are highly Lorentz contracted ("pancake-shaped"). They overlap either partially as in a peripheral collision or, totally as in a central collision.